UNIVERSITÉ DU LUXEMBOURG

PhD- FSTC-2019-37
The Faculty of Sciences, Technology and Communication

DISSERTATION

Defence held on 10/05/2019 in Luxembourg
to obtain the degree of

DOCTEUR DE L'UNIVERSITÉ DU LUXEMBOURG

EN PHYSIQUE

by

MD Asiqur RAHMAN
Born on 25 June 1988 in Chittagong, (Bangladesh)

ALIGNED MULTI-WALL CARBON NANOTUBE SHEETS FOR LIQUID CRYSTAL DISPLAYS

Dissertation defence committee

Dr Giusy Scalia, dissertation supervisor
ADR, Université du Luxembourg

Dr John Roy Sambles
Professor, University of Exeter, UK

Dr Andreas MICHELS, Chairman
Professor, Université du Luxembourg

Dr Yuko Inoue
Professor, Shizuoka University, Japan

Dr Philippe Poulin, Vice Chairman
CNRS Research Director DR1, Centre de Recherche Paul Pascal in Bordeaux, France

Abstract

The great interest in carbon nanotubes (CNTs) was triggered by their discovery by Iijima and has led to significant research efforts finding exceptional electrical and mechanical properties. The extraordinarily high anisotropy is not just limited to the shape of CNTs, but it is also reflected in their properties that show strong orientational dependence. However, a crucial step involves the incorporation of CNTs into macro-size devices while keeping the nanotubes perfectly aligned in a single direction with a high degree of nanotube straightness. It has been an additional challenge to produce CNT assemblies that meet all these requirements until Kaili Jiang et al introduced a solid state method to produce highly aligned multi-wall CNTs pulled from a forest. They reported that it is possible to pull continuous strings of nanotubes from vertically-aligned CNT forests, forming parallel arrays aligned along the pulling direction. Due to their high alignment, transparency, flexibility, conductivity and optical anisotropy, sheets formed by aligned CNTs are promising as optical polarizer, heaters, sensors, energy devices and aligning and electrodes layers in displays.

The alignment of a liquid crystal (LC) on a CNT surface was first realized by Giusy Scalia et al. Later, Russel et al. showed that surfaces with aligned CNTs align LCs unidirectionally, followed by Fu et al. demonstrating that coated CNT sheets can also act as transparent electrodes for switching LC. Thus, aligned CNT sheets show promise as attractive multifunctional systems for LC displays, being able to simultaneously serve diverse functions by replacing both polyimide (PI) and indium tin oxide (ITO) layers, thus, minimizing costs and simplifying the fabrication process. The mechanical properties of CNTs offer also better performance than ITO when used on flexible substrates. However, the optical anisotropy of MWCNT sheets in the range of visible wavelengths remains almost unexplored. There is thus an urgent need to investigate and fundamentally understand the interaction of light with CNT sheets in order to accurately realize CNT-based liquid crystal optical devices.

Abstract

In LC displays, the modulation of light is based on the use of polarized light, and the introduction of an optically anisotropic layer can affect the modulation; thus, it is important to acquire fundamental knowledge on the interaction between aligned MWCNT sheets and light. We followed the technique reported by Kaili Jiang and Ray Baughman to produce highly aligned CNT sheets by pulling CNTs from a spinnable CNT forest. We further deposited the aligned CNT sheets on a glass substrate and characterized them in the visible wavelength range, finding that the aligned CNT sheets anisotropically absorb light. Furthermore, the linearly polarized light travelling through the CNT sheets is rotated and the polarization of the light is affected by the presence of even a single layer of CNTs. Moreover, the magnitude of rotation of polarization increases as the layer thickness increases. We performed theoretical investigations which closely fit the experimental data, suggests that the origin of the rotation is mainly due to the anisotropic absorption. However, other contributions, such as from birefringence, cannot be ruled out. By optical investigations, the dependence of the optical behavior on thickness of CNTs was also established.

Moreover, the average orientational order parameter of the CNT sheets was evaluated from the anisotropic absorption of aligned CNT sheets. A high value of orientational order parameter in CNT sheets is needed since the alignment of the CNT sheets translates to LC alignment. The order parameter of free-standing CNT sheets was found to be ~0.6; however, it decreases once deposited on a substrate.

The adhesion between the CNT sheets and the substrate is an additional problem and was studied using different strategies correlating the adhesion to the final alignment of the CNTs on a substrate. Parts of this research effort were devoted to investigating CNT sheets on various polymer surfaces, leaving the surface of CNTs almost free from polymer, for a direct investigation of the LC alignment on the CNT graphitic surface. The general goal was to improve the adhesion while keeping the alignment of the CNTs intact as pulled from the forest. We found a tradeoff between the adhesion of the CNTs and their alignment on a substrate; however, achieving highly-ordered CNTs and perfect adhesion on the surface is an issue. A second approach was based on complete coverage of CNTs by coating the nanotube films with inorganic dielectric layers (SiO_2 or Al_2O_3). We found that SiO_2 coating preserved the freely-suspended CNT alignment while

improving the film flatness. These inorganic coatings help to obtain good electrical performance of LC in cells made with the CNT-based substrates. The alignment of the liquid crystal 4-cyano-4'-pentylbiphenyl (5CB) in the cells was generally planar and unidirectional, with differences in the quality depending on the type of coating layer and on the value of the order parameter of the CNT sheets. We investigated both the uniformity of the LC alignment as well as the switching voltages and times and compared this to the performance of the LC in commercial cells.

Integration of aligned CNTs with LC requires the understanding of the interactions of CNT layers with light to realize CNT devices. Aligned CNTs from forests can be obtained easily; sequentially depositing CNT layers, however, while maintaining control of the degree of alignment when integrating them into devices is an open issue. This work shows the occurrence of unexpected interactions with polarized light due to the intrinsic properties of CNTs and due to their alignment. By exploring and optimizing the optical performance of CNT sheets, through their orientational order, it can be possible to use them as optical films for producing, among other optical devices, variable rotation of polarization, polarizers and transparent electrodes that also can align LCs integrated into LCDs.

Acknowledgments

I would like to deeply thank all those people who have taught, helped, and guided me throughout my three-year journey, exploring this fascinating and exciting research area.

Firstly, my greatest gratitude goes to my supervisor, Dr. Giusy Scalia, for providing me with the opportunity to become a scientist. Life is an endless learning process, and I am still on my way to learning to become a successful scientist. She has offered me guidance on the ethics of science, on how to carry out systematic analysis, from identifying problems to designing the experiment, and to communicate the results, whether in the form of a poster, presentation, or in a subsequent grant proposal. With her persistent patience, encouragement, and continuing support, she helped me overcome many difficulties. I especially would like to thank Dr. Scalia for her generous help during my first year, when she taught me a lot of fundamental concepts of optics, carbon nanotubes and liquid crystals, that helped me succeed and thrive in my project. From the LC Nano group, I would also like to thank Dr. Ji-Hyun Park and Dr. Hakam Agha for our many discussions and hands-on teaching experience.

Secondly, I would like to thank Prof. Roland André Sanctuary and Dr. Philippe Poulin for serving as members on my PhD committee and providing insightful comments and suggestions on my research. Many thanks to our collaborator Prof. Dongseok Suh for providing us carbon nanotube (CNT) forest and very fruitful discussions and comments on our findings. I am very grateful to one of his PhD student Thuy-Kieu Truong for teaching me the fabrication techniques and providing me a lot of samples that I characterized and studied in this thesis. I am also thankful to Prof. Jun Yamamoto for both his feedback and discussions throughout the course of my research here and for affording me the opportunity to visit and work with him in his labs in Kyoto University.

I am also grateful to Prof. Jan Lagerwall for providing me with access to his laboratory and equipment. I am truly lucky to have been able to work with Prof. Lagerwall and his group (ESMP); not only the assistance but also the discussions with his group members were always inspiring, particularly with Dr. Anshul Sharma and Larry Honaker. I am grateful that they have been always eager to help when I encountered difficulties. I would also be remiss not to thank the technical and administrative staff in the Physics and Materials Science research unit, especially Astrid Tobias, Vanessa Schmidt-Barbé, and Robert Wagener.

Funding during my studies was also provided by the University of Luxembourg and the Luxembourg National Research Foundation, which enabled me to travel extensively during my degree program and attend conferences and workshops in places I never imagined visiting.

Last but not least, I would like to express my gratitude and admiration to my mother Mazeda Begum and my siblings for their everlasting support and love. They have sacrificed so much for me throughout my life. I am very grateful to my uncle Mr. Shafiqul Islam, without whose continuous encouragement I would not be able to make it here. I am very lucky that they have trusted me and supported me which kept me motivated. I would also like to thank my friends for their care, love and suggestions. I am very lucky to have them around and I cannot imagine my PhD life without them.

I dedicate this thesis to my mother.

Table of Contents

Table of contents

Table of contents

List of Figures

List of figures

List of figures

List of figures

List of figures

List of figures

List of figures

List of Tables

Chapter One

Introduction

Individual carbon nanotube possess unique highly anisotropic properties that have stimulated much interest in diverse disciplines. However, there is still no technique available to produce large-scale architectures of highly aligned CNTs. One of the biggest challenges in the field of nanoscience and nanotechnology is how to create macroscopic/microscopic devices by assembling nanomaterials while preserving their extraordinary properties. Due to their anisotropy, CNTs have the additional challenge that their properties change with their degree of orientational order but controlling their alignment is still an issue which limits their applications. Different strategies have been explored for obtaining the alignment of CNTs at a large scale. Here, we use sheets formed by aligned CNTs in extremely long bundles produced in a dry, solvent free and surfactant free process. One of the objectives of this work is to investigate the anisotropic optical and other properties of the CNT sheets relevant for the implementation of the CNT sheets in liquid crystal displays (LCDs). In fact, they have been recently proposed as multifunctional layer (alignment and transparent layer) in LCDs.

Thanks to Kaili Jiang et al. [1] and Ray Baughman et al. [2] for their innovative idea to align CNTs, we were inspired by their work to produced CNT sheets. However, in order to use CNTs in the application, there are fundamental questions that need to be addressed and one of them is how aligned MWCNT sheets interact with light. One of the main findings of this work is the rotation of polarization from aligned MWCNTs which means when a linear polarized light travel through a CNT with its polarization at a certain angle with the alignment direction of CNT it rotates the initial polarization. The output rotation angle depends on the initial angle between light and CNT. However, there is no rotation of polarization when the linear polarized light is either parallel or perpendicular to the CNT alignment. We then further investigated the origin of the rotation of polarization theoretically. Our experimental and theoretical studies suggest that the rotation of

polarization is mainly due to the anisotropic absorption which will be explained in detail in this thesis.

Furthermore, we investigated the order parameter of aligned CNT sheets. Since one of the main objectives is to produce highly aligned CNT sheets, therefore, high value in the orientational order parameter is indeed crucial. We further discussed the influence of the surface of the substrate on the orientational order parameter of CNT sheets and the adhesion of the CNT films on the substrate. According to our findings, there is a tradeoff between the order parameter and adhesion of the CNT sheets in the process that we have used. The order parameter decreases as adhesion improves. The highest order parameter was found for free standing CNTs film and it reduces as it deposited on the substrate after we improved the adhesion. Thus, we investigated the surface interaction between the tubes and the surface of the substrate in order to understand the influence of the substrate on the alignment of the CNTs.

The CNT sheets we produced are promising in the field of liquid crystal research. The LC molecules anchor parallel to the CNTs long axis hence providing planar alignment to the LCs. Therefore, the aligned CNT sheets can be used as an aligning layer for LC. Moreover, aligned CNT sheets are transparent and conductive which can be used as a transparent electrode in liquid crystal devices. Thus, we proposed the aligned CNTs as a multifunctional layer for liquid crystal display. The proposed aligned CNT sheets not only align the LCs planarly but are also used as an electrode to reorient/switch the LC molecules. We studied the interaction between CNTs and LC, the CNTs not only electrically conductive but also transparent which can replace transparent conducting film indium tin oxide (ITO) in LCDs.

Furthermore, from an application point of view other than LC display, aligned CNT sheets can be used as a polarizer. Due to the anisotropic absorption of light, aligned CNTs can produce linear polarization. We characterized our aligned CNT sheets in the visible spectrum and we successfully produced linear polarized light. However, improvement of the alignment is needed to boost the performance of the CNT polarizer.

The ultimate goal of this Ph.D. thesis work is to understand the interaction between CNTs and light, since we proposed aligned CNTs in optical devices in particular in LCDs. The anisotropic absorption and realization of rotation of polarization will help the integration of CNTs in optical devices. Furthermore, the overall alignment of the LCs depends on the alignment of the CNTs, therefore, the studies of orientation order of CNTs is important.

The thesis is structured as follows:

Chapter two reviews the structures, properties, and applications of CNTs, and discusses the alignment and growing technique of CNTs in the literature. It also discusses the basic understanding of the liquid crystal and their optics.

Chapter three introduces the fabrication and experimental procedures used in this work. I will explain all the steps from CNT sheets fabrication to the preparation of the substrate with a single or multiple layer. I will describe the preparation of our LC cells based on CNTs and then the characterization methods of anisotropic absorption, the detection of the rotation of polarization for a single and multiple layer, the experimental setup for the electro-optic behavior and opto-thermal investigation of LC will be explained in this chapter.

In chapter four, we analyzed the data obtained from the characterization. We explained the origin of rotation of polarization, performed numerical analysis and compared theoretical and experimental results. We also established the dependence of rotation of polarization on layer thickness and how it depends on the wavelength of light. We studied the order parameter of aligned CNT sheets and how the alignment of the CNTs changes the interaction between CNTs and light. Finally, we discussed the performance focusing on the response time and heating effect of the CNT sheets in LC display and then use as a polarizer.

Chapter five summarizes the outcomes of the research in this work.

Chapter Two

Background

In this chapter, I will explain the fundamental knowledge on the topic of my research which includes relevant history, theory, other researchers' views on solving the problem and brief discussion on necessary optics.

2.1 What are carbon nanotubes?

Carbon nanotubes (CNTs) are allotropes of carbon and one-dimensional (1D) hollow cylindrical structures formed only by carbon atoms. For a significant period of time, the only known carbon allotropes were diamond and graphite. In1985, the discovery of C60 [3] opens the research field of nanotechnology. Later in 1991, carbon nanotubes were reported by Sumio Ijima [4]. Graphene is a two-dimensional (2D) system, formed by a single layer of carbon atoms, one atom thick, bonded together in a hexagonal lattice pattern. Graphene can be viewed as the fundamental compound of fullerenes, carbon nanotubes, and graphite. These materials can be derived from 2D graphene as shown in Figure 1Figure 1 making tailored cuts and eventually folding it [5].

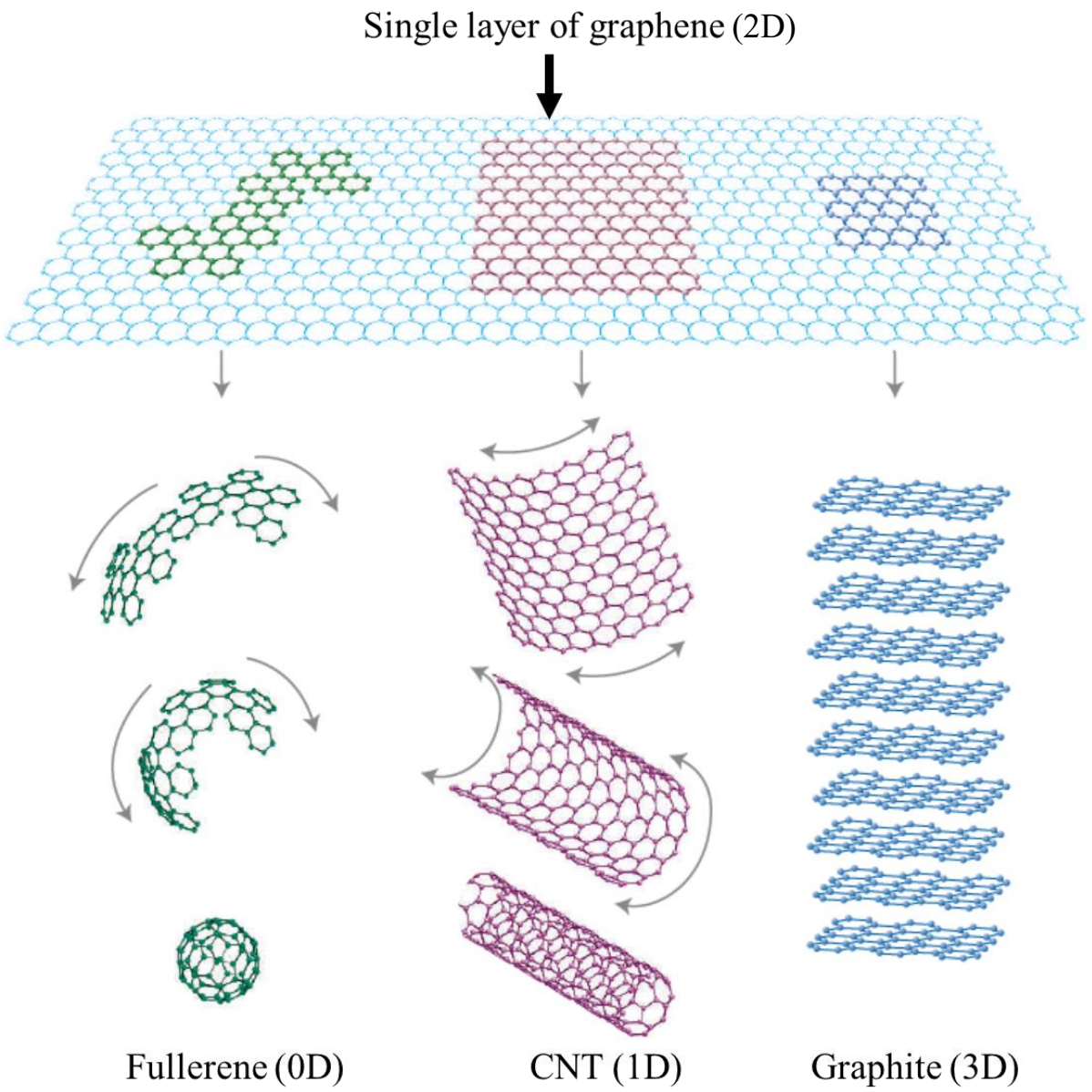

Figure 1: Schematic of graphene (2D), fullerene (0D), carbon nanotubes (1D) and graphite (3D). showing the basis of these three materials is graphene. Adapted from Ref. [5].

The structural arrangements of the carbon atoms determine the distinct electronic, mechanical, thermal, and optical properties of the carbon materials [6] that can substantially differ from material to material. For example, while the electrical conductivity is low in diamonds, the thermal conductivity is very high. Graphite is conductive although anisotropically different in and out of the plane, and graphene is highly conductive but also transparent. As shown in Figure 1, a CNT can be visualized as a rolled-up graphene sheet into a seamless cylinder. Therefore, depending on

the number of layers of rolled graphene sheets, CNTs can typically be classified as single-walled carbon nanotubes (SWNTs) and multi-walled carbon nanotubes (MWNTs) [7]. A schematic of the SWCNT and MWCNT is presented in the Figure 2. The diameter of the SWNTs can vary from 0.4 to 3 nm and in the case of MWCNTs, from 5 to 20 nm (can be greater). The length of the tube can be less than a hundred nm to several centimeters [8-10], resulting in high aspect ratio up to ~10^7 [11, 12]. The unique nanostructure of the CNTs makes them exceptionally strong, with high flexibility, transparency and great conductivity both electrically and thermally [10, 13].

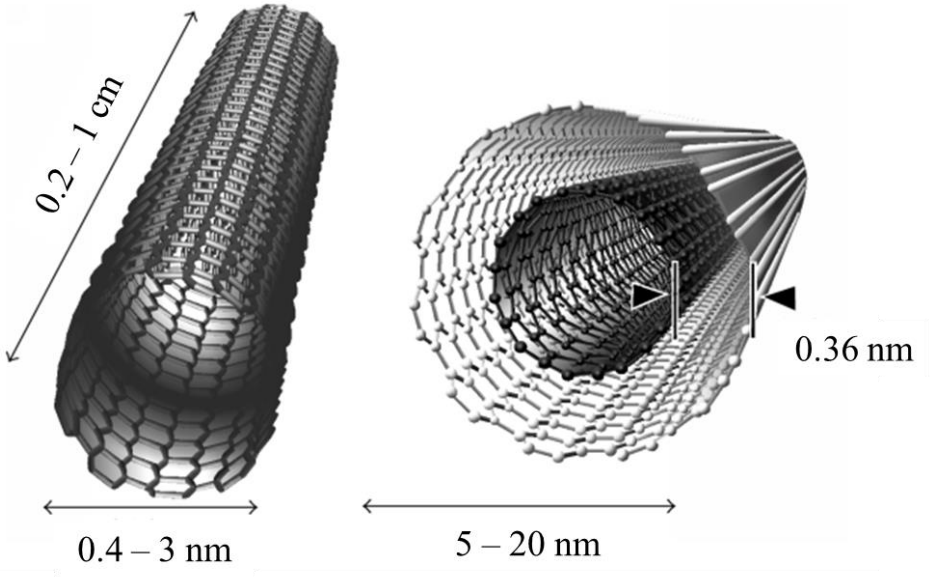

Figure 2: Schematic of SWNT and MWNT adapted from Ref [14]

SWCNTs can be either metallic or semiconducting, and the character of the band structure is dependent on how graphene sheet is rolled up. The way the graphene sheet is wrapped is represented by a pair of indices (n, m), positive integers, the coefficient of the chiral vector $\vec{C} = n\overrightarrow{a_1} + m\overrightarrow{a_2}$, where $n \geq m$. If n = m, the CNTs are called "armchair" and they have metallic properties. The name refers to the shape of the edges of the CNTs after an ideal cut perpendicular to the elongation direction. If m = 0 and n > 0, they are called "zigzag" still from the shape of the edges after an ideal perpendicular cut. They can be either metallic or semiconducting. If the difference between the indices (n – m) is a multiple of three, tubes are metallic otherwise they are semiconducting. Finally, other than above mentioned combination of n & m, nanotubes are called "chiral". Chiral SWCNTs can be either metallic or semiconducting [15-17]. A schematic

representation is shown in Figure 3. It is hard to identify the chirality of MWNTs because of their nested layers; however, most of them exhibit metallic properties. The behavior of MWCNTs is metallic if, at least, one sheet has a metallic chirality [18].

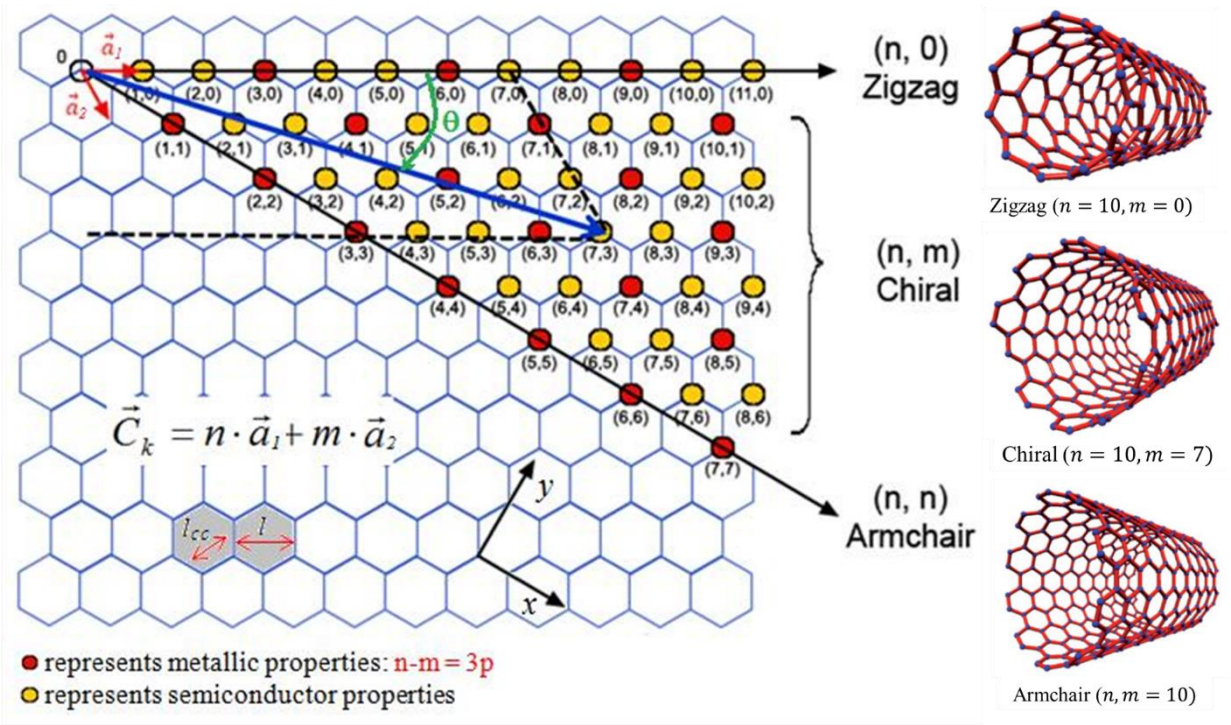

Figure 3: Representation of a rolled up CNT (n, m) from a 2-D graphene sheet with chiral vector $\vec{C}$, and unit vector $\overrightarrow{a_1}$ and $\overrightarrow{a_2}$ [19]. An example of a zigzag, chiral and armchair SWCNT structure [20] are shown on the right.

The growth of CNTs is of great importance since it determines the properties of the nanotubes, and then the final performance of CNT products. It has been shown that given the right conditions, CNT synthesis can occur in a wide range of environments. There are mainly three techniques for growing CNTs: arc discharge, laser ablation, and chemical vapor deposition (CVD) [21]. Chemical vapor deposition is a chemical process resulting in deposits a solid material on a heated surface which occurs from a chemical reaction in the vapor phase [22]. It is widely used to produce high-purity and high-performance solid materials. CVD growth of CNTs is the most often used technique nowadays, often based on iron catalyst deposited on a substrate exposed to a carbon feedstock disassociated by e.g. temperature. The technique is very promising for industrial

production due to its easy setup and operation, easy scale-up at low cost and capability of growing CNTs directly on the desired substrate [23]. The technique used to grow CNTs in this work is CVD and details of the growth are explained in ref [24]. More details about CNT forest is in chapter 3, section 3.1.

2.1.1 Alignment of CNTs

Typically, CNTs produced in bulk have a random order. The unorganized CNT architecture limits not only the investigation of the fundamental properties but also potential applications of CNTs. For instance, very high optical anisotropic absorption [25-28] and anisotropic conductivity [29, 30], achievable with CNTs, rely on the alignment of the tubes. In general, randomly oriented CNT networks have poorer performance compared to the aligned CNTs [31]. Moreover, there are numerous applications such as display devices [32-36], polarizers [37-40], sensors [41], optoelectronic device (TFT transistor) [42, 43], energy devices (solar cells, transparent electrodes) [44-46], heaters [47, 48], actuators [49] and fibers [45, 50] that are dependent on the alignment of the CNTs. Since the extraordinary properties of the CNTs are maximized when they are aligned, then, a controlled and uniform alignment of CNTs is desirable.

The alignment of CNTs has been an issue since their discovery. One of the most extreme challenges in CNTs is aligning them while preserving their properties. Various methods have been reported to produce large scale aligned CNTs. Efforts are in progress to align CNTs either directly during growth [51-53] and/or post growth [54, 55]. Notable techniques include mechanical stretching in a polymer film [43, 56, 57], filtration method [28, 58], Langmuir-Blodgette method [59-61], dispersion of CNTs in LCs [62-65], magnetic alignment [66-69], inject printing [70, 71], dip coating [72, 73]. However, the performance of the reported aligned CNTs is still on average lower than the individual CNT. None of the above-mentioned methods meet the industrial performance due to the limitation of the techniques such as low CNT densities, poor local alignment limiting micro devices, the degree of the final alignment low, inability to control chirality hence type of the tube, complicated process, poor purification, and no control on the thickness of the film. Twenty-eight years since CNT was invented, and there is still no simple and

easy fabrication method available which can produce large scale, defect free and highly oriented CNTs for next generation devices.

2.2 What are liquid crystals?

In general, most of the substances change their state at different temperatures. For example, below 0°C, water is a solid, a liquid between 0°C and 100°C, and a gas over 100°C. These three phases- solid, liquid and gas - exhibit different characteristics since the molecules in each phase possess different degrees of order. There is an intermediate phase between the solid and the liquid called liquid crystal phase which is characterized by some degree of long range orientational order, some case also positional, as shown in Figure 4.

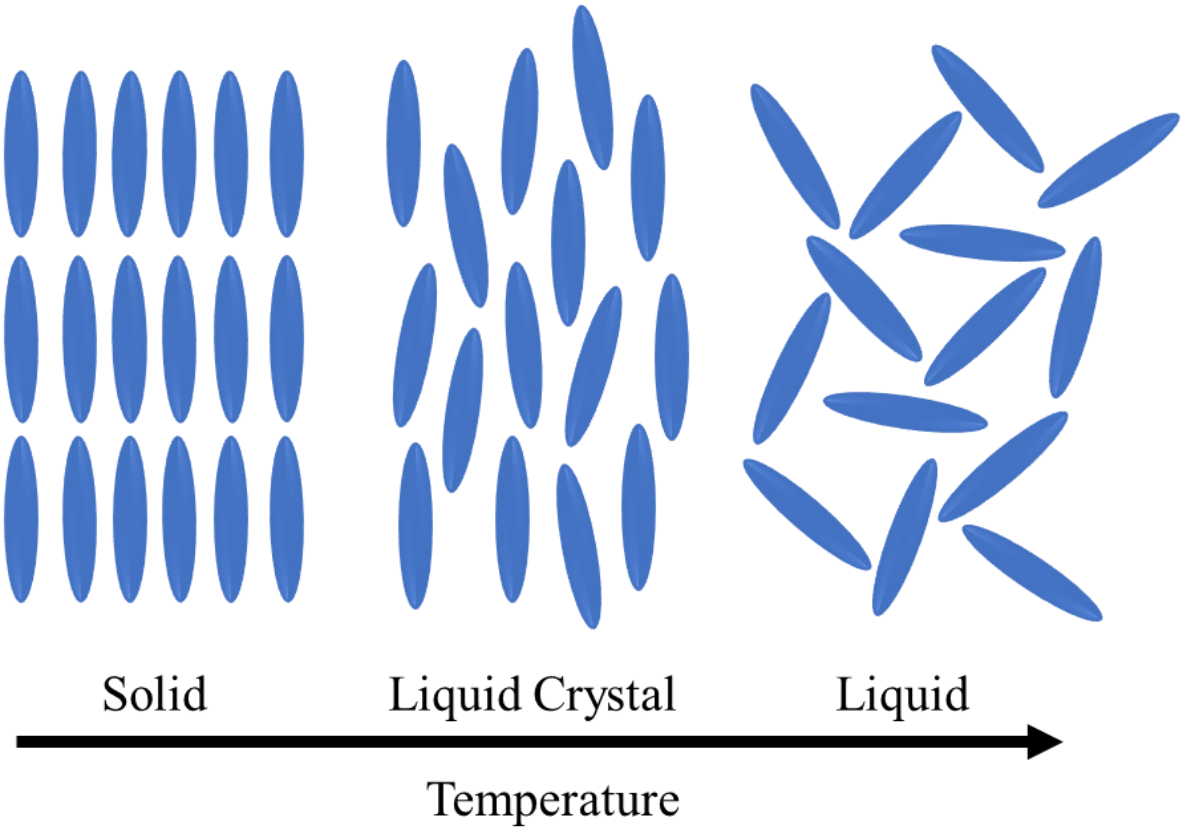

Figure 4: Molecular structure of solid, liquid crystal and liquid as a function of temperature

The discovery of the liquid crystal is attributed to Friedrich Reinitzer in 1888 [74][75]. It was first observed in cholesteryl benzoate; however, liquid crystalline properties can also be found in a common substance such as soapy water. Liquid crystal materials are typically categorized into two types: disc-like molecules (molecules consisting of e.g. a core of adjacent aromatic rings forming rigid parts extended in two dimension) and rod-shaped molecules (one molecular dimension is much longer than the other two). For display applications, rod-like LCs with the physical properties that vary as a function of temperature, thermotropic LCs, are used. Figure 5 shows the basic structures of the most commonly occurring rod-like liquid crystal molecules.

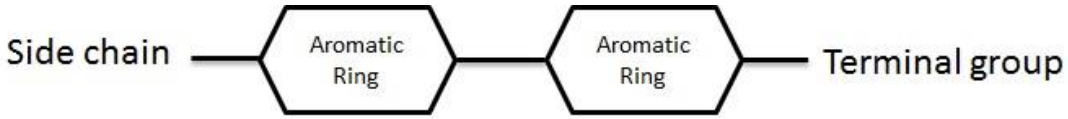

Figure 5: Molecular structure of a typical liquid crystal

Examples of the side chain and terminal groups are –CN, -NO_2, and others such as alkyl, alkoxy groups connected by linkage groups such as stilbene, ester, Schiff base and tolane. The majority of liquid crystals are benzene derivatives.

Nematic phase is the simplest liquid crystal phase that possesses only orientational order, typically with orientational order parameter (S) introduced properly later, assuming values between 0.3 to 0.7. For example, the very common and widely used nematic phase liquid crystal in research is 4-cyano-4'-pentylbiphenyl (5CB). The molecular arrangement of 5CB is shown in Figure 6.

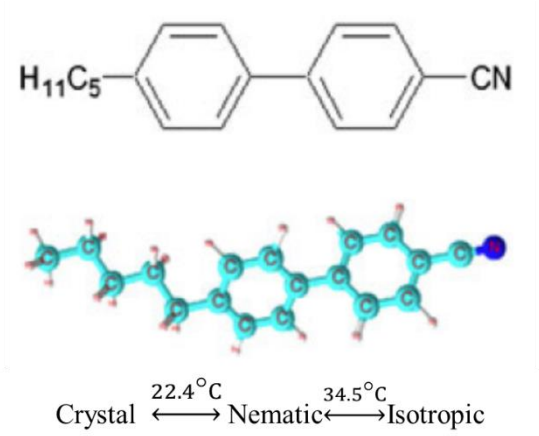

Figure 6 : Molecular arrangement of 5CB Adapted from Ref [76]

The order parameter is an important parameter for liquid crystals and it may be defined through the orientational order parameter S as follows:

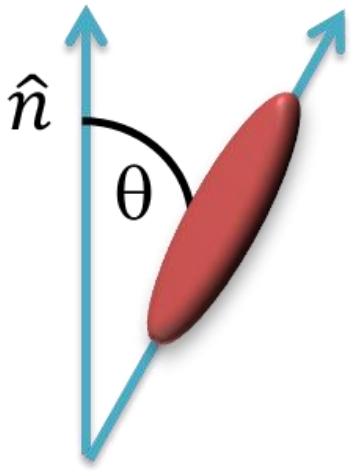

$$S = \frac{1}{2}\langle 3cos^2\theta - 1\rangle \quad \ldots\ldots\ldots (1)$$

In the equation (1), θ is the angle between the LC director ($\hat{n}$) and the symmetry axis of molecules, along their long dimension. The axis along which the molecules are oriented, is called the director and is denoted by the unit vector $\hat{n}$. The equation (1) is an average of all the molecules in the sample. For example, the average of the 3 times cosine square minus one term is zero for an isotropic liquid. Therefore, the order parameter of an isotropic liquid is zero. In contrast, the order parameter equals one for a perfect crystal. The order parameter of a liquid crystal is in between 0.3 and 0.9. In the nematic phase the LC molecules are free to move, but over an average direction along which the molecules tend to orient their long axes. In the nematic phase the LC molecules have long range orientational order but no positional order as shown in Figure 7.

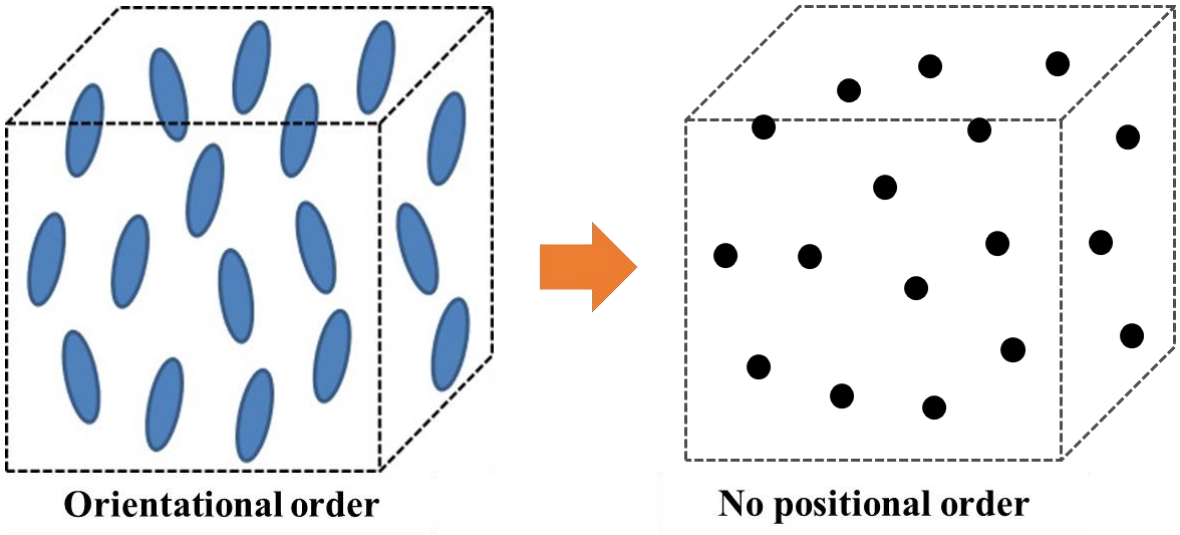

Figure 7: Nematic liquid crystal phase illustration with molecular order. Left image showing the orientation order and right image showing lack of positional order of nematic LC.

The general director orientation can be maintained/reoriented through a magnetic or electric field in order to control the optical properties of the sample. Today, at the heart of modern display technology, the orientational dynamics of the LC director in an applied electric field acts as a fundamental physical phenomenon, which drives the optics of display. The field-induced director reorientation of LC change at surfaces is known as the Fréedericksz effect [77]. Figure 8 explains the LC switching in an electric field.

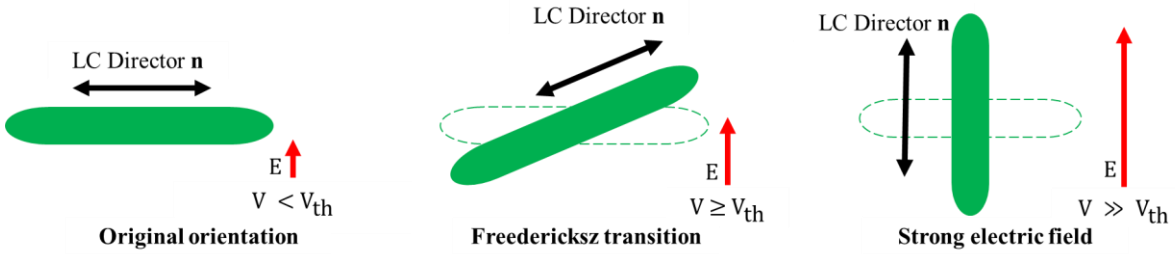

Figure 8 : Schematic of nematic LC orientation under an electric field. Voltage higher than threshold ($V \gg V_{th}$), reorient the LC director parallel (right image) to the electric field direction (in case of positive dielectric LC)

Due to the anisotropic nature of the LC molecules in nematic phase, the physical properties (such as dielectric permittivities $(\varepsilon_{\parallel}, \varepsilon_{\parallel})$, refractive indices $(n_{\parallel}, n_{\perp})$) along and perpendicular to the director differ, thus, giving rise to anisotropy. For example, optical anisotropy defined by $\Delta n =$

$n_{\parallel} - n_{\perp}$ is shown in Figure 9. Light at normal incidence with the optic axis of aligned LC would experience the extraordinary refractive index (n_e) for polarization parallel to the optic axis but the ordinary refractive index (n_o) if the polarization is perpendicular. For polarization directions at intermediate orientations there will be two rays propagating through the LC, since both n_o and n_e are experienced by the light. Regardless of the polarization direction light will experience n_o when propagating along the optic axis.

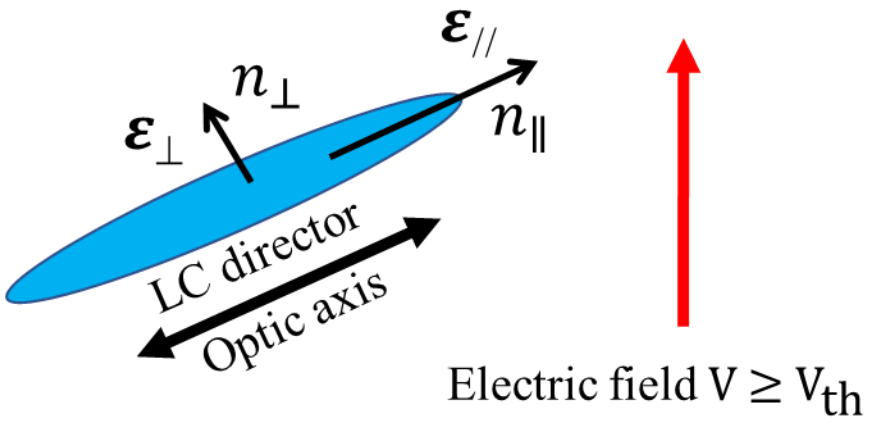

Figure 9 : Liquid crystal with a positive dielectric anisotropy ($\varepsilon_{//} > \varepsilon_{\perp}$) placed inside an electric field.

2.2.2 Alignment of LC

The alignment of the liquid crystal can be obtained by the surface treatment of the substrate which is influenced by both the liquid crystal and the surface's nature [78]. Generally, there are two surface alignments; planar and homeotropic/vertical alignment depending on surface treatment. Figure 10 shows the planar and homeotropic alignment of LC sandwiched between two glass substrates. In the planar aligned liquid crystal cell, the liquid crystal director is consistently parallel to the surface of the substrate. In the homeotropic alignment liquid crystal cell, liquid crystal director is perpendicular to the surface. Homeotropic alignment on substrates is typically achieved by treating the surface with surfactants [79]. In case of planar alignment, the surface of the substrate is coated with a polymer (typically teflon, polyimide or PVA) and then rubbed with a velvet cloth, which creates a grooved surface. The distortion energy of nematic molecules in macroscopically disordered state is reduced by the grooved surface, which increase their

macroscopic anisotropic order. The polymer mainly plays the role of a template to achieve planar alignment [80, 81].

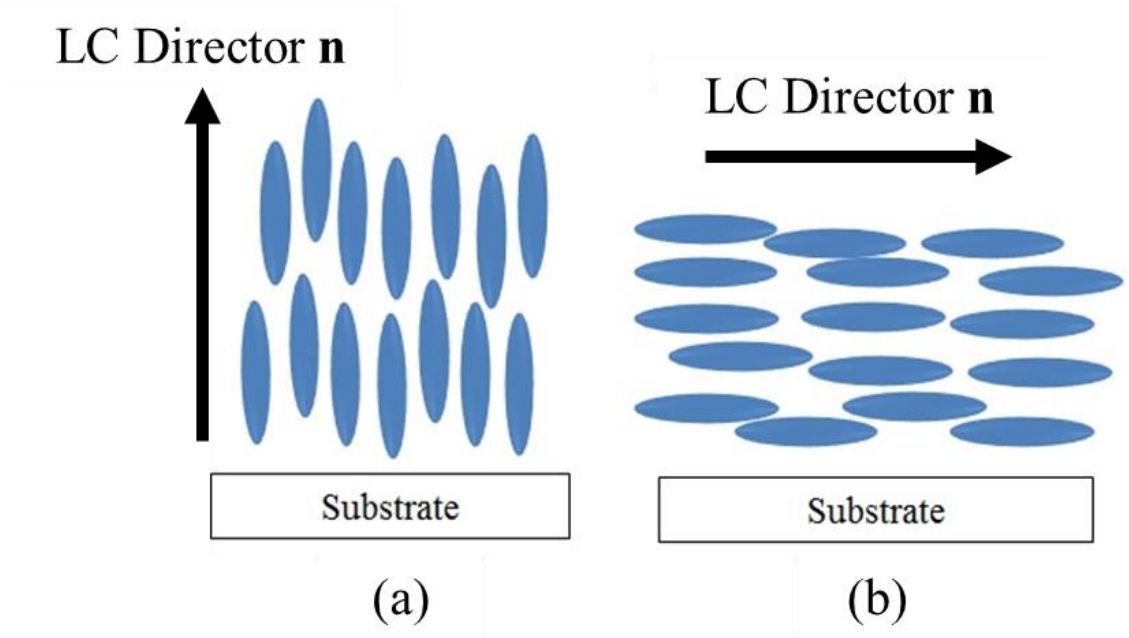

Figure 10 : Schematic representation of liquid crystal alignment inside a cell (a) Homeotropic (vertical) and (b) Planar

2.3 The interaction between CNTs and LCs

Nowadays, LCD technology has been well established and found in many aspects of daily life [82]. Even though using advanced technology, an essential part (the alignment layer), in such displays mainly depends on the mechanical rubbing of a polyimide polymer, done simply by a piece of cloth. This method was invented more than ten decades ago [82-84] and extensively employed in the large scale industry [82, 84]. By rubbing the spin coated polyimide, the generated parallel micro-grooves as well as the production of a large number of similarly oriented bonds on the polyimide surface align the liquid crystal (LC) well in macroscopic scale [82, 84, 85]. However, such a technique has many drawbacks, such as the creation of debris and surface electrostatic charges, contamination, and damage in polymer film that are associated with the mechanical contact [33, 82, 84]. As a result, rubbing induces faulty pixels [82]; therefore, a non-contact aligning method has been expected for the next generation of the large and high resolution LCDs [86]. Several alternative methods have been demonstrated such as photo-induced surface

alignment [87-90], plasma beam alignment [91, 92], and ion–beam alignment (IB) [93-96]. Moreover, improvement of the alignment and the performance of LC devices have been attempted by using nanoparticles as alignment layer [97-99]. However, the improvement in device fabrication and performance was limited.

Carbon nanotubes can be aligned by liquid crystals (LCs) when dispersed in them [62, 100, 101] [102]. However, when CNTs are deposited on surfaces with uniform alignment, they can align liquid crystals even isolated [32] or as sheets [33, 35]. In fact, LC molecules can anchor planarly on the graphitic surface and the orientation of the nanotubes can give the directionality to LC molecules. These molecules at the interface transfer their alignment to the bulk LC molecules producing films with macroscopic monodomains. This easiness of achieving aligned films is one of the most attractive properties of liquid crystals at the base of their successful implementation in displays, together with their electro-optic characteristics. In fact, LCs can induce modulation of light by changing their molecular orientation under electric fields and returning to a steady state, upon removal of the field. The steady state configuration is very important for a reversible and reproducible light modulation process and it can be simply achieved by ensuring strong molecular interaction of the LC molecules with suitable surfaces. Carbon nanotubes films can be an attractive alternative since they can still be deposited in a quick and easy way not needing potentially contaminating steps [32, 33, 35, 103]. They are flexible, strong and optically transparent which made them attractive as transparent electrodes in flexible and stretchable electronics. CNT sheets can then serve several functions for LCs. The quality of the alignment of carbon nanotubes is clearly a key parameter for the uniform alignment of LCs. Additionally, the surface interactions are of tremendous important since it determines the anchoring strength of the molecules that dictate the electro-optic switching of LCs.

2.4 Optical properties of CNTs and LCs

2.4.1 Absorption

The propagation of light in a medium or matter (solid, liquid and gas) is affected in two ways. First, the intensity of the beam decreases as the light travels further into the medium. Second, the

velocity will be less in the medium than in free space. The loss or reduction in intensity is mainly due to the absorption (energy of a photon taken up by the matter) and/or sometimes scattering. In Figure 11, a beam with an intensity I_0 enters into an absorbing medium. The fraction of the intensity (dI) absorbed by the medium depends on the thickness (dx) and the absorption coefficient (α), therefore,

$$dI = -\alpha I dx \text{ [In the linear regime]}$$

$$\frac{dI}{I} = -\alpha dx$$

$$\int_{I_0}^{I} \frac{dI}{I} = -\alpha \int_{0}^{x} dx$$

$$[\ln I]_{I_0}^{I} = -\alpha x$$

$$\ln I - \ln I_0 = -\alpha x$$

$$\ln \frac{I}{I_0} = -\alpha x$$

$$I = I_0 e^{-\alpha x} \ldots \ldots \ldots (2)$$

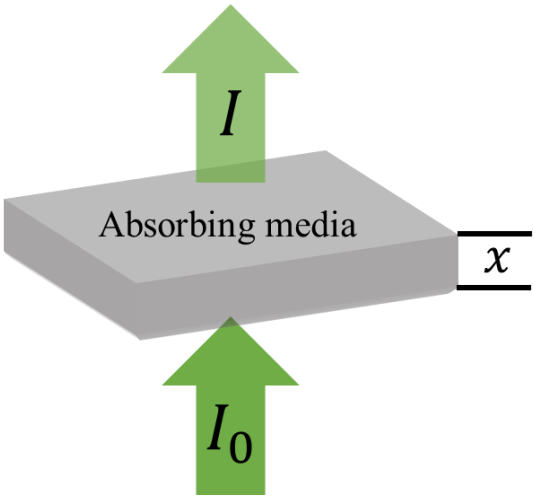

Figure 11: Light travelling through the absorbing medium

Equation (2) is known as Beer Lambert law, here I is the intensity of the beam emerging from the other side, I_0 is the incident beam, *x* is the thickness of the medium, that is the light path in the medium that incident beam travelled through and α is the absorption coefficient.

When light travels in absorbing anisotropic media, there are unequal optical properties, in particular absorption, as a function of the direction of propagation of light in the medium and its polarization. Such characteristic is known as optical anisotropy or anisotropic absorption. A dichroic polarizer is a perfect example of anisotropic absorption. Light is a transverse electromagnetic wave, which contains the electric and magnetic fields perpendicular to each other. Figure 12 shows the electric field in the XY plane, the magnetic field in the XZ plane and the propagation of the wave in the X direction.

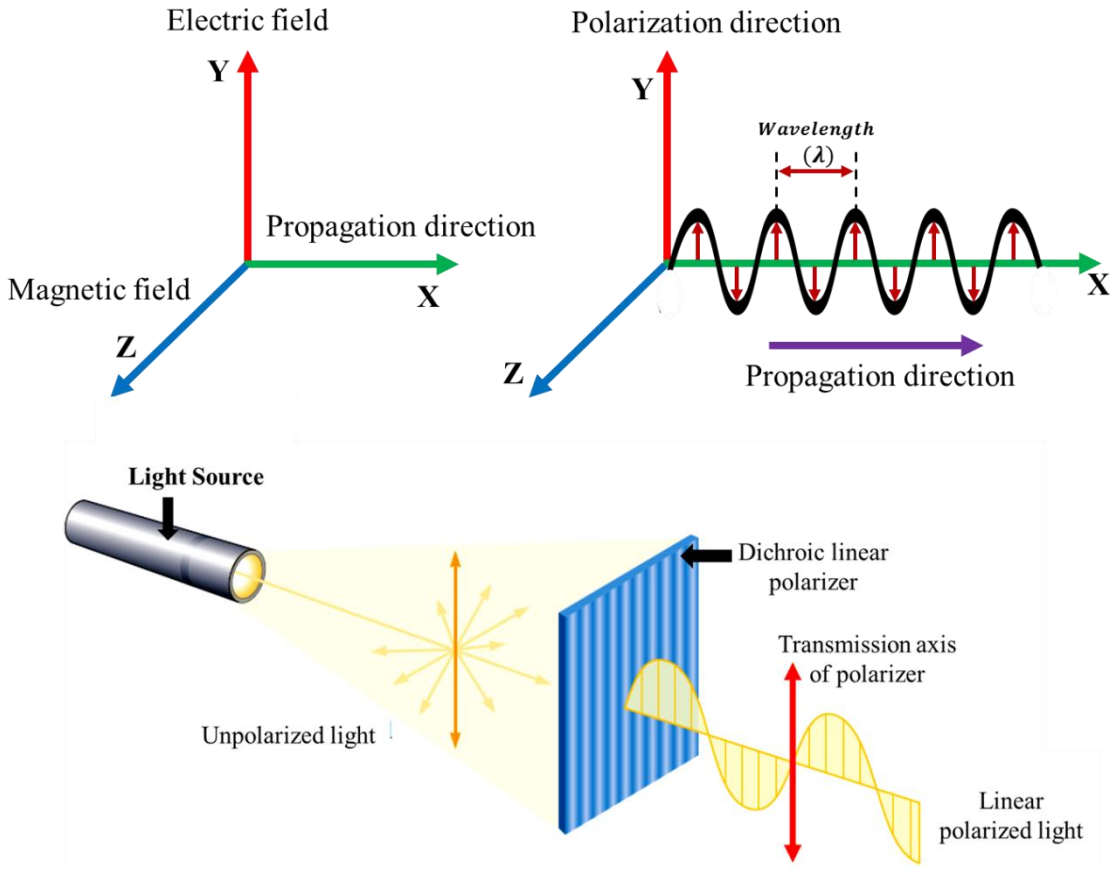

Figure 12 : Illustration of the transverse electromagnetic wave (top). Linear polarization by dichroic medium (bottom) adapted from Ref [104]

Unpolarized light consists of waves that oscillate at all possible angles from the Y direction, still perpendicular to the X axis, in Y-Z plane. Linearly polarized light is defined as the optical wave

that only fluctuates in one specific plane during its propagation and in time. This means that the electric and magnetic field oscillates in a fixed plane. A dichroic polarizer is a plate/material that allows only specific direction of light polarization to pass through (it is worth mentioning that the output intensity is lower than the input/original light due to the absorption of the polarizer). This axis of the polarization is called "transmittance axis" and its perpendicular to the "absorption axis". Typically, the transmitted light is linearly polarized in the direction of transmission axis. The polarization of the light can be tested by another polarizer often addressed as analyzer. Figure 13 (a) shows a generic configuration with two polarizers. If the transmittance axes are set at 90° (crossed), the polarized light from the first is absorbed by the second polarizer as shown in the Figure 13 (b). However, if two polarizers (transmittance axes) are parallel, the light passes completely through the analyzer. The light transmittance decreases as the analyzer's transmission axis rotate from 0 to 90 degrees. The intensity of the light after the second polarizer can be calculated by using Malus' law, which states that the output intensity I for any given relative angle θ between the transmission axes of two polarizers is given by:

$$\boldsymbol{I = I_0\, cos^2\, \theta} \ldots\ldots\ldots (\mathbf{3})$$

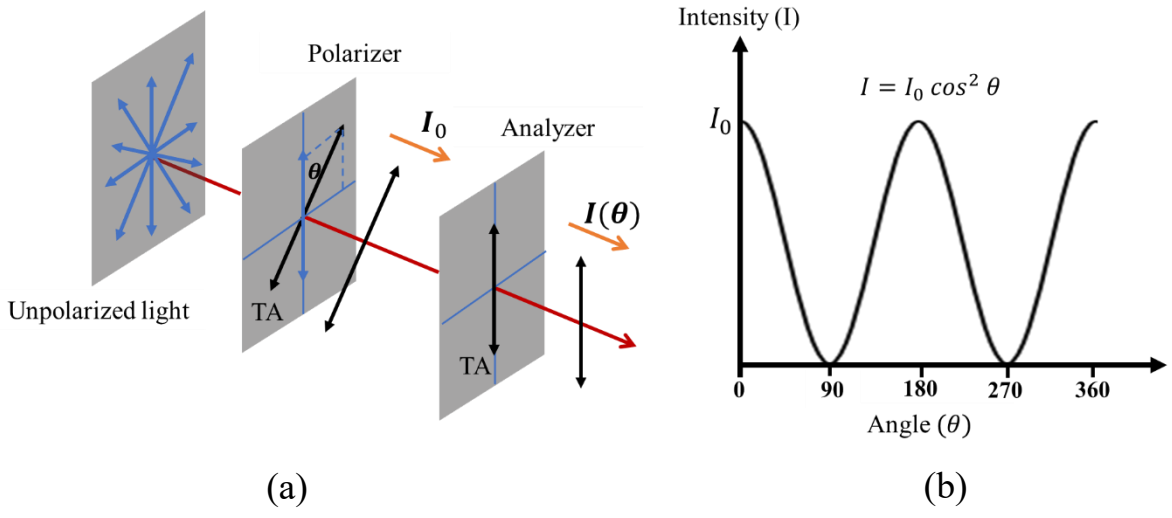

Figure 13 : Intensity profile of parallel and crossed polarization with Malus' law

2.2.4 Birefringence

The previous section introduces the concept of polarized light, absorption and polarizers. This section will describe one of the major optical characteristics of liquid crystals. Due to their anisotropic nature, liquid crystals are found to be birefringent. In other words, they have two indices of refraction in different directions (perpendicular to each other). The light polarized parallel to the director has a different refractive index to the light polarized perpendicular to the director. As seen in Figure 14 (a), the polarized light with the electric field parallel to the LC director experiences the refractive index n_e as it passes through the sample. However, in Figure 14 (b), the polarized light which is perpendicular to the director feels a different refractive index n_o as it passes through the sample. Therefore, the polarized light with 45° to the director will have a refractive index n_{eff} [see in Figure 14 (c)] whose value is between n_e and n_o. The original wave is split into two beams experiencing n_e & n_o respectively.

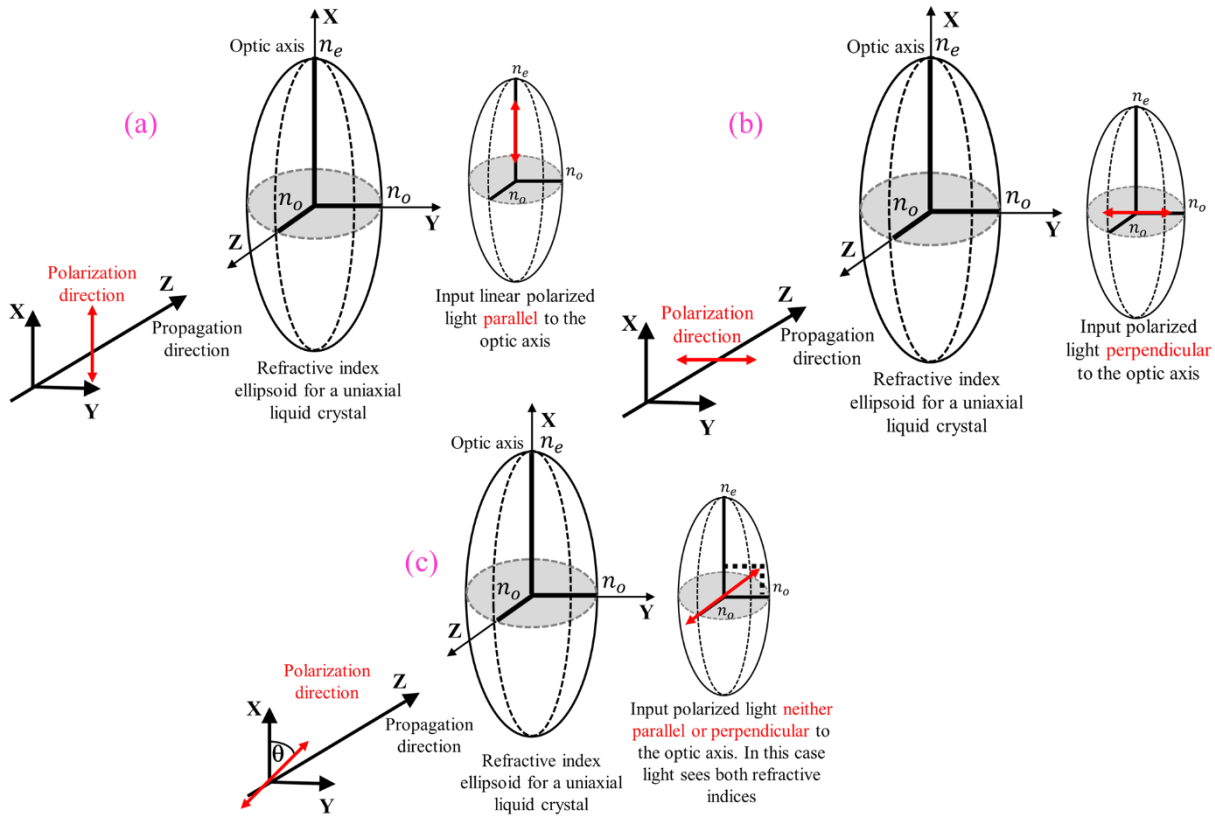

Figure 14 : Linear polarized light travelling (a) Parallel, (b) Perpendicular, and (c) 45° to the LC directors.

When light enters a nematic liquid crystal sample, the process is modeled in terms of the light being broken up into the fast (called the ordinary ray) and slow (called the extraordinary ray) components as shown in Figure 15.

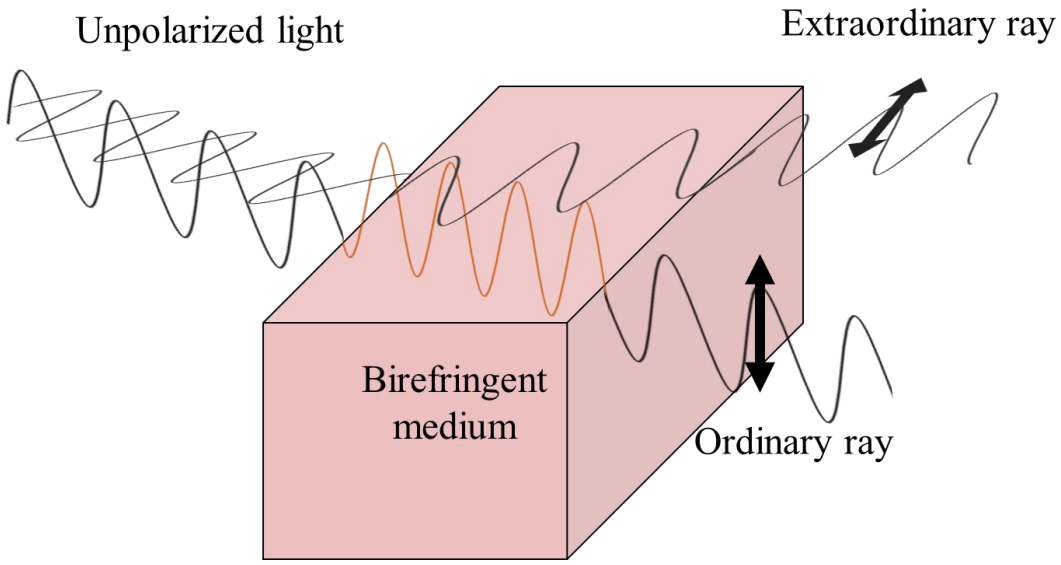

Figure 15 : Light traveling through a birefringent medium breaks into two linearly polarized light beams which travel with polarization perpendicular to each other.

Since the two components encounter different refractive indices, they travel at different speeds resulting in phase shift as they exit the LC sample. As a result, the polarization state will change according to the phase retardation accumulated in the LC layer. Two indices of refraction (ordinary and extraordinary indices of refraction respectively) and their differences are defined, n_o, n_e and $\Delta n = n_e - n_o$ respectively. The ordinary and extraordinary refractive indices can also be written in term of the relative permitivities,

$$n_e = \sqrt{\varepsilon_{\parallel}}, \quad n_o = \sqrt{\varepsilon_{\perp}},$$

The birefringence of a material is defined as:

$$\Delta n = n_e - n_o \dots\dots\dots (4)$$

The phase retardation of LC in a cell is defined as:

$$\delta = \frac{2\pi d \Delta n}{\lambda} \dots\dots\dots (5)$$

Here d is the distance in LC travelled by light, typically corresponding to the cell gap and λ is the light wavelength. Since the optical path is defined as $\Lambda = d.n, \Delta\Lambda = d.\Delta n,$ birefringent media are characterized by anisotropy in the optical path. The phase retardation accumulates as long as the light propagates in the birefringent material. This results in a change of the polarization state of the transmitted light.

2.5 Electro-optic setup for liquid crystal

As mentioned earlier (section 2.2), the optic axis of the nematic phase LC is parallel to the director and the rotation of the director can be controlled by an electric field. By controlling the voltage, continuous phase retardation change can be obtained. The output polarization state can then be manipulated. The birefringence of the liquid crystal can be characterized by placing the sample between the crossed polarizer and by looking at the output intensity. The output intensity is given by the following equation:

$$I = I_0 \sin^2(2\theta) \sin^2\left(\frac{\pi \Delta n d}{\lambda}\right) \dots\dots\dots (6)$$

Where I_0 is the initial intensity of the light and θ is the angle between the LC director/LC optic axis and polarizer. The maximum light transmission/phase retardation from a LC sample between crossed polarizers is given for $\theta = 45°$ and minimum when $\theta = 0$ or $90°$. The minimum voltage needed to reorient the nematic LC in the homogeneously planar alignment i.e. with the director of the LCs are parallel to the surface and electric field perpendicular to the substrate as shown in Figure 16. The threshold voltage is connected to the elastic constants and dielectric anisotropy, therefore,

$$V_{th} = \pi \sqrt{\frac{k_{11}}{\varepsilon_0 \Delta\varepsilon}}$$ [Splay type Fréedericksz-transition is considered] …… (7)

Below threshold voltage, the LCs in a cell remain undeformed. Then at a threshold voltage, the deformation initiates and increases as the voltage increases. This transition of LC molecules at a certain voltage is the Fréedericksz-transition, as explained earlier. It's worth to mention that strong anchoring to the boundaries dominates. Therefore, the LCs on the surface remains and does not undeformed and does not orient parallel to the electric field until very high field strength.

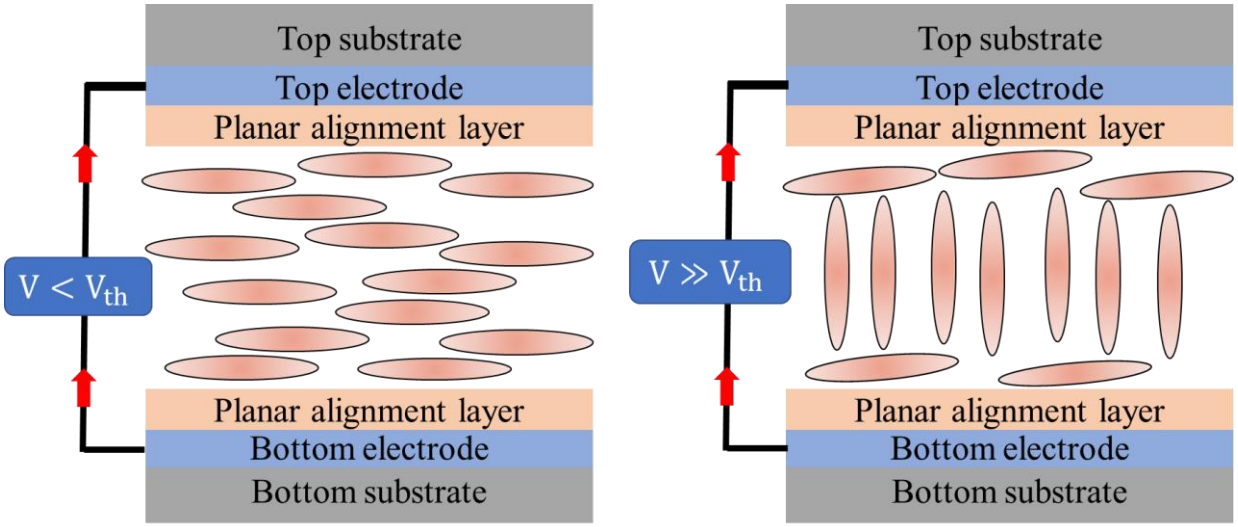

(a) (b)

Figure 16 : The Fréedericksz -transition. Applied voltage (a) below the threshold voltage, (b) above the threshold voltage.

Figure 17 shows a voltage vs transmission curve of a planar alignment LC cell between crossed polarizer. When the applied voltage exceeds the Fréedericksz transition threshold, the director of LC tilt further from the aligning surface. The transmittance decreases and becomes zero at sufficient voltage where the bulk LC is parallel to the electric field.

The response time which includes rise time and decay time mainly depends on the rotational viscosity, the elastic coefficient, applied voltage and anchoring on the surface and is given by:

$$\tau_{rise} = \frac{\gamma_1 d^2}{\varepsilon_0 \Delta\varepsilon V^2 - k_{11}\pi^2} \quad \ldots\ldots\ldots (8)$$

$$\tau_{decay} = \frac{\gamma_1 d^2}{k_{11}\pi^2} \quad \ldots\ldots\ldots\ldots\ldots\ldots\ldots (9)$$

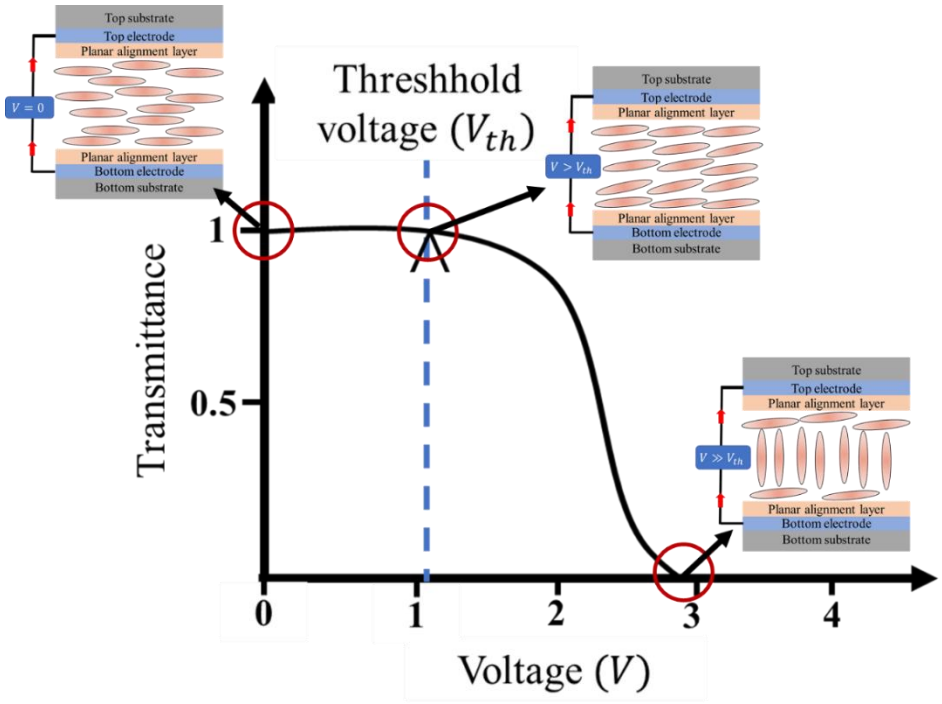

Figure 17 : Typical voltage vs transmission curve of a planar aligned LC cells at 45° between crossed polarizer.

The rise time, the time for the director to reorient parallel to the applied electric field, is represented by equation (8). On the other hand, equation (9) gives an estimation of decay time also known as relaxation time of LC in zero electric field. It's the time that LC molecules take to reach their equilibrium configuration after the applied electric field is switched off. The response time of the LC directors is governed by two torques, the elastic torque and the electric field induced torque. At $V \gg V_{th}$, the electric torque is stronger than the elastic torque and at $V = 0$, the electric torque is zero, then the elastic torque is most relevant, which dominates the relaxation process, therefore τ_{rise} is longer than τ_{decay}. Moreover, τ_{rise} can be externally controlled unlike τ_{decay} [105].

Chapter Three

Fabrication and Characterization Techniques

In this chapter, I will explain the fabrication process of the alignment of the CNTs. I will also discuss the assembly of CNT-LC cell. Moreover, the equipment, the characterization techniques, the preparation of the substrates and detailed information of the materials will be discussed in this chapter.

3.1 Preparation and fabrication

3.1.1 Preparation of CNT sheets

CNT sheets can be produced by either dry or wet methods. Motivated from the ancient art of paper manufacturing, nanotube sheets are produced by dispersion of the tubes in solution of surfactant in water, followed by filtration and drying process and finally peeling them from the filter obtaining a CNT sheet [106, 107]. Even though an ultra-thin and highly conductive and transparent CNT film [108, 109] was produced through modifying the filtration process; however, within the plane CNTs were isotropic. The alignment of the CNTs in CNT sheets produced by filtration was improved by mechanical rubbing of CNTs [110] and applying magnetic field during the filtration process [68]. Wet methods for the dispersion of CNTs also include dip coating [111], Langmuir-Blodgett technique based on the CNT's hydrophobicity [112] and biomolecular self-assembly

[113], all allow wafer-scale fabrication of CNT sheets. However, good alignment is still an issue. Moreover, removing the solvent or surfactant molecules is not easy and there is a possibility that chemical residuals may affect the properties of CNTs. Therefore, the post treatment can be expensive, complicated and it can limit the CNTs applications. In case of dry method, CNT film and/or fiber was produced from CNT aerogel by Li et al. using a floating catalyst method [114]. The CNT film/fiber was continuously spun directly from the CVD machine. The advantage of this technique is the alignment, length and thickness of the film that can be controlled. However, this method is favorable for producing CNT fibers rather than CNT thin films and generation of the CNT aerogel and removing the product from reaction zone make this technique complicated [115].

Alternatively, in order to eliminate the use of dispersions, post treatment and complicated steps; a solid-state method was introduced by Zhang et al. in 2005 to produce highly aligned CNT sheets from CNT forest [116]. This technique was developed from the prior breakthrough in the production of CNT yarns from the vertically aligned CNT forest [117] which was further improved in strength by the twist of the sheet during spinning process [118].

Inspired by their dry drawing method, our MWCNT sheets were produced from a vertically aligned CNT forest also known as CNT array. In a CNT forest, CNTs are standing on a silicon substrate and they are aligned vertically parallel to one another. Due to the van der Waals interaction between the tubes, they are held together and form a bundle. We used single edge metal razor blade to pull the tubes from the CNT forest. In practice, we made contact between the sharp edge of the blade and the side wall of the CNT forest and then gently pulled the tubes with an angle between 30 to 60 degree from the silicon substrate. The pulled CNT sheets were then attached to a glass capillary which was connected to a homemade rotatable stage (see Figure 18). Then, we pulled further by rotating the stage until we obtained stretched and uniform aligned CNT sheets. The free-standing aligned single layer CNT sheets were then deposited on a cleaned glass substrate, as shown in Figure 19. The deposition of the CNT sheets is actually done by pushing the substrate towards the sheets, and then folding those on the sides aiming at maximizing the surface contact. After the deposition, we tilted the substrate and dropped a couple of drops of ethanol (from VWR chemicals, 96%) and let them to flow along the tubes in order to improve the adhesion. We named it ADES treatment. More details on ADES treatment will be found in chapter

four, section 4.3. To evaporate the ethanol quickly, we placed the sample on a hot plate with the temperature of 90°C for 5 min.

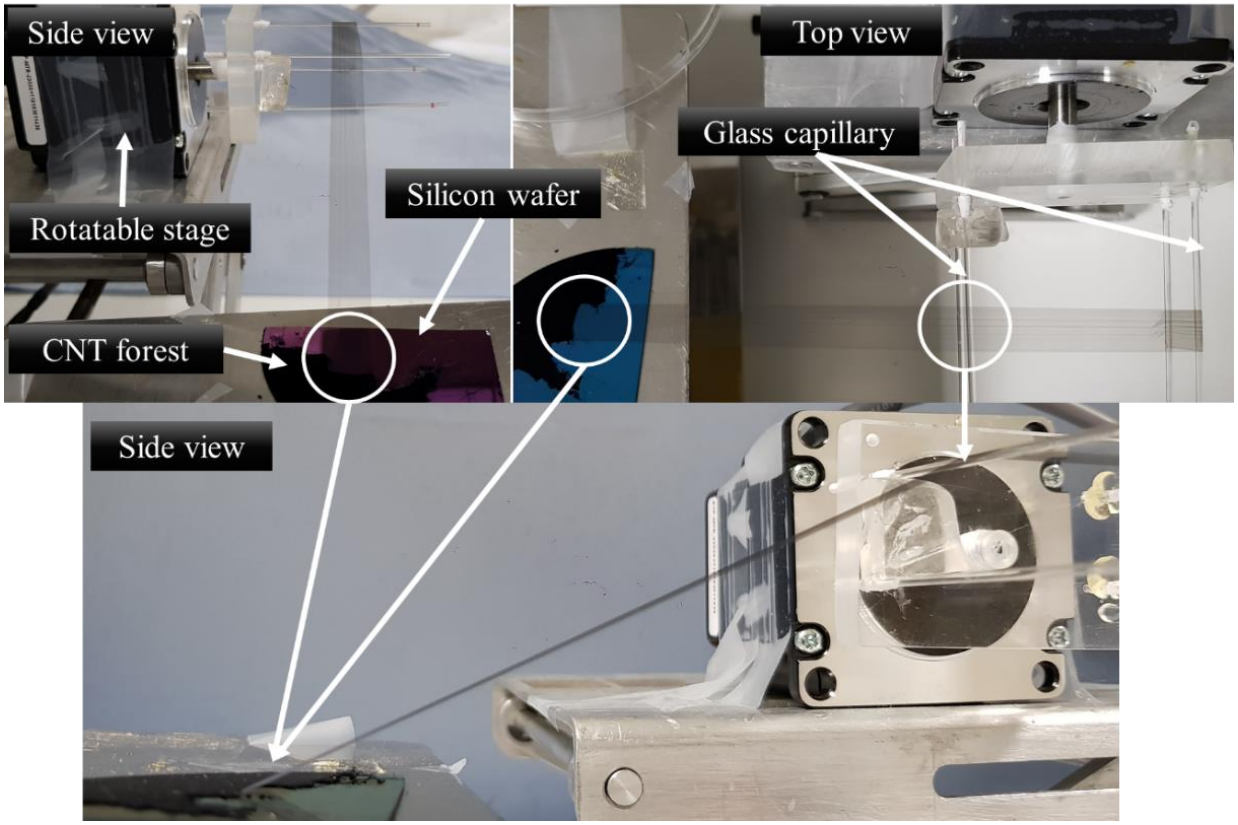

Figure 18 : Side and top view of a CNT sheets (pulled from the forest) attached to the glass capillary connected to the rotatable stage.

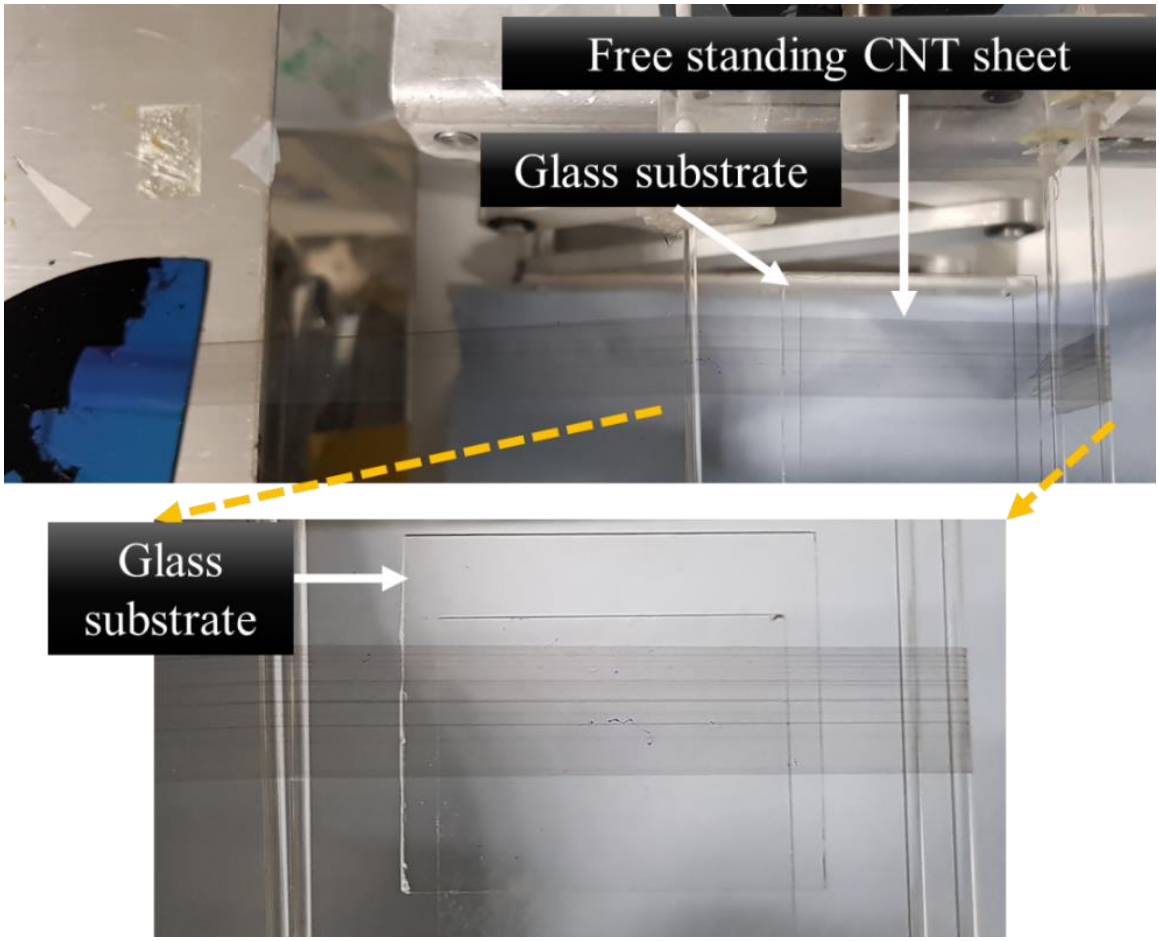

Figure 19 : Transferring free standing CNT sheets to a substrate. The substrate approached from bottom and pushed outward.

3.1.1.1 Pulling mechanism of CNT sheets from CNT forest

There is a broad range of conditions to produce CNT forest that can be spinnable i.e. able to produce sheets that can be eventually twisted in yarn [119-121]. Huynh et al. made comprehensive investigation to understand the growth mechanism and identify the key parameters on the growth of spinnable CNT forest [122]. According to their findings, the catalyst material, the substrate, carbon source gas, catalyst thickness, growth temperature, reaction time and gas flow rate determine the spinnability. However, the interaction of the CNT with each other plays a vital role on spinnability. Later in 2011, Kuznetsov et al. presented a model not only for describing the principle mechanism behind the transformation of CNT forest into CNT sheets but also to explain

the fundamental reasons behind the CNT forest that are not drawable [123]. The model concludes that the drawability depends on the height of the CNTs in the forest and the special interconnections between the CNT bundles which unzip during the drawing process. A possible mechanism of drawing CNT sheets from forest is shown in Figure 20 through graphic representation adopted from ref [123].

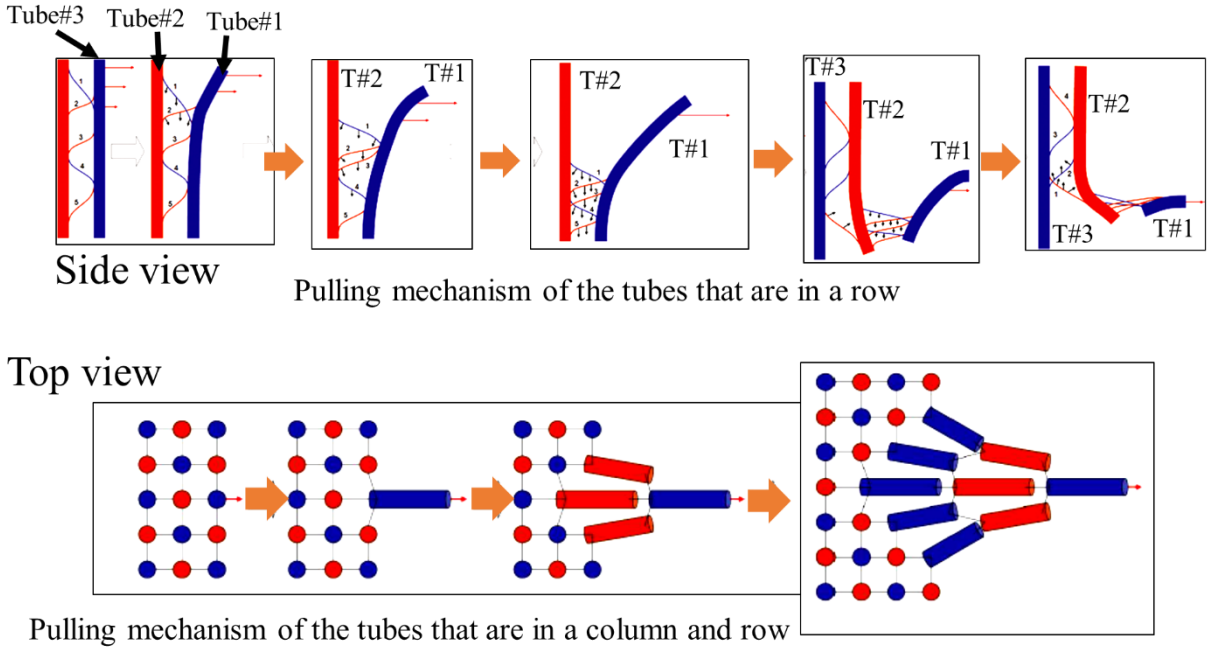

Figure 20 : Top: Pulling process of CNTs from forest. Red and blue bars represent either single tube or bundles of CNTs on the forest. The pulling force and direction are denoted by the red arrows. Bottom: 3D model of the structural arrangement of the big bundles in a spinnable CNT forest. Adopted from ref [123]

3.1.1.2 Characteristics of CNT forest

The MWCNT forest used in our experiment was produced by A-Tech system CO. Ltd, Incheon Korea. The spinnable CNT forest was synthesized by the traditional way to grow CNTs, known as CVD technique. The forest was grown on iron-coated silicon wafer using acetylene gas (C_2H_2) as carbon source. The average height of the individual CNTs in the forest is about 150 µm (as shown in Figure 21) and diameters from (inner) 10 to (outer) 20 nm [24]. However, we used two different batches of forests to make CNT sheets sample to study the reproducibility of the properties and

the effect of the characteristic of the forest on the performance of the CNT sheets. The differences between the two forests are the height (Figure 21), width and presumably the densities of CNTs in the forest. We will label the samples from the two forests as Batch 1 and Batch 2, respectively.

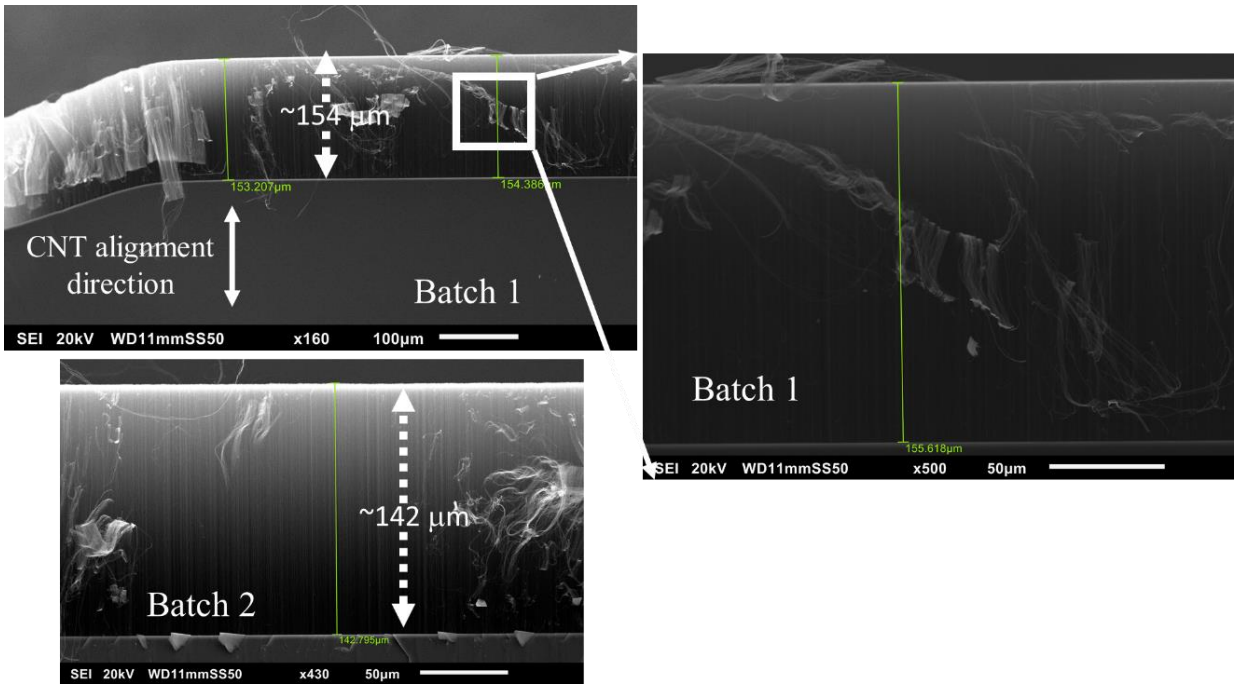

Figure 21 : SEM images of the two forests showing the height of the tube.

3.1.2 Substrate preparation

We used microscope glass slides (made of Soda-Lime, Refractive index 1.517 @ 546 nm) as a substrate. At first, the glass slides were cut into 25 x 30 mm size. The substrate was then cleaned by ultrasonic bath (15 minute in each solvent) with acetone, isopropyl alcohol (IPA) and at the end distilled water, respectively. Finally, the substrate was dried with the air flow by air gun followed by heating with the hotplate for 5 min in 100°C. Figure 22 shows the preparation & cleaning process of the substrates that we used in our experiment.

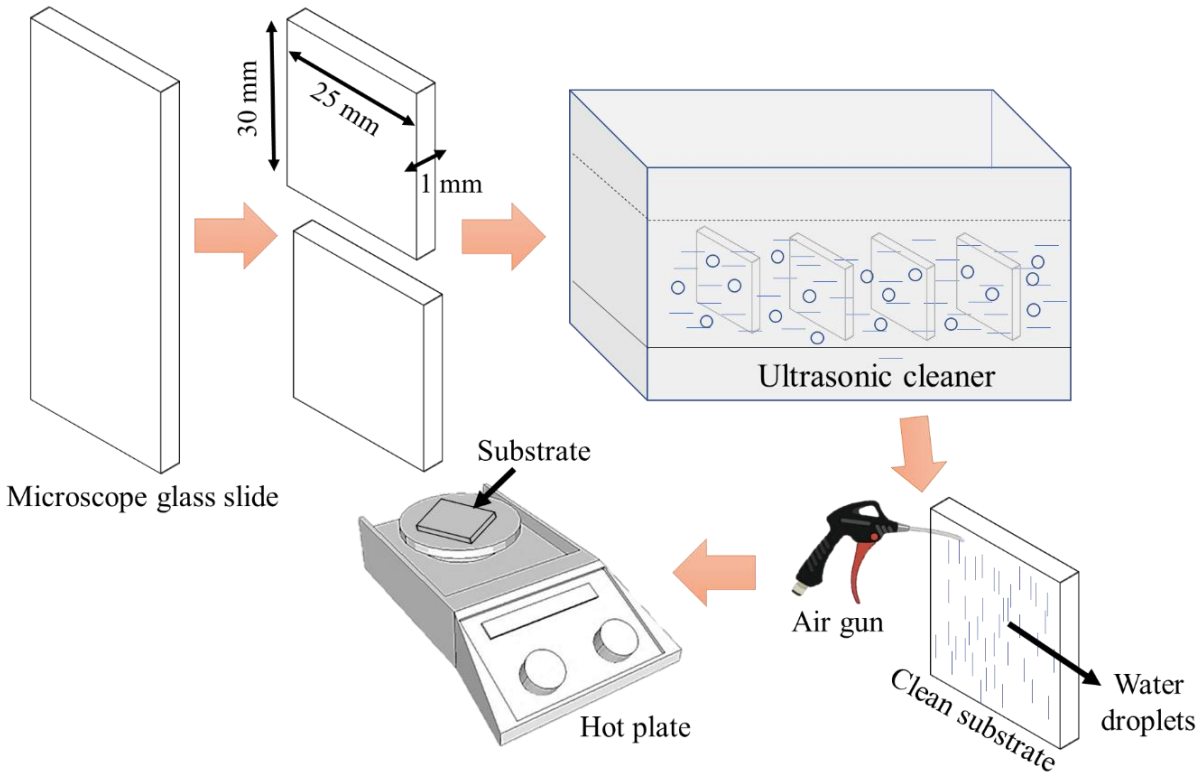

Figure 22 : Preparation of substrate before depositing CNT sheets

3.1.3 Preparation of Multilayer CNT sheets

We made samples with multiple layer of CNT sheets by repeating the deposition process multiple times. It's worth to mention that when we refer to single layer for CNT sheets, we do not necessarily mean that the film contains monolayer of multiwall tubes on the substrate. In fact, the thickness for a single layer CNT sheet is not homogeneous and ranges from 6 nm to 100 nm, due to CNTs bundling as shown in atomic force microscopy (AFM) image (see Figure 23). From the AFM measurement we have calculated, some of the bundled tubes have thickness more than couple of hundred nm and some have lower than 10 nm. According to the TEM analysis, the minimum thickness of a single MWCNT is 10 nm [24] which means the lowest possible thickness of the CNT sheets cannot go below 10nm. However, our AFM analysis indeed shows tubes less than 10 nm thick which is not clear to us yet.

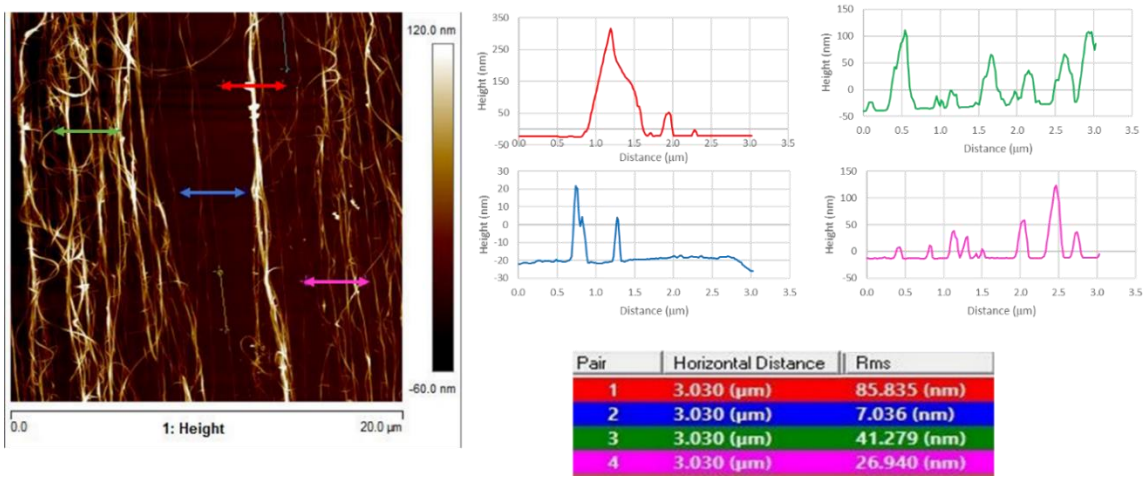

Figure 23: AFM analysis of a single layer CNT sheets. The profiles on the top right correspond to sections on the AFM scan done along the lines of the same color as the plot of the profiles.

"One-layer" CNT sheet means that there is only one sheet pulled from the CNT forest that was deposited. Multiple layers of CNT sheets samples were made by rotating the stage (pulling a longer sheet, thus, more tubes) and then depositing a layer on top of another layer. The schematic in Figure 24 explains the mechanism of the multiple layer.

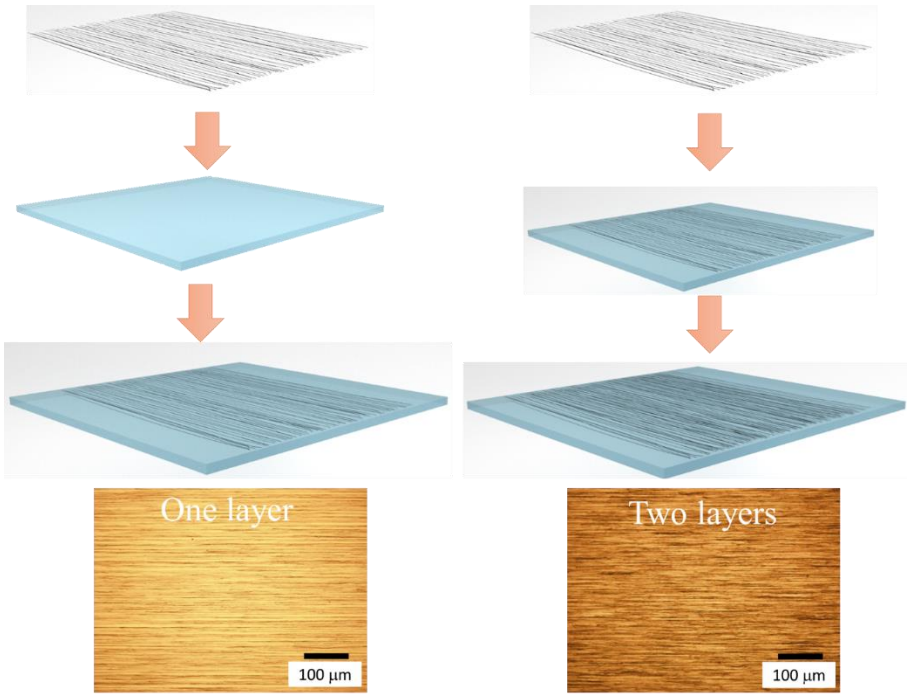

Figure 24 : Preparation of single and multilayer CNT sheets

3.1.4 Preparation of substrate with polymer layer using spin coater

We used spin coater (Laurell technologies, WS-650MZ-23NPPB) to coat a polymer layer on a glass substrate. Polyvinyl alcohol (PVA) (Mw ≅ 13,000-23,000, 87-89% hydrolyzed), Polyvinylpyrrolidone (PVP) (Mw ≅1,300,000), and Poly (methyl methacrylate) (PMMA) (Mw ≅350,000), purchased from sigma Aldrich, are the three polymers we used in our experiments without further purification. PMMA was chosen for using a hydrophobic surface to compare with the hydrophilic PVA and PVP. Toluene, ethanol and distilled water are used as solvents to dissolve the PMMA, PVP, and PVA respectively. The polymer concentration was kept constant (2.5 wt%) in each case, and the solutions were then spin coated on top of clean glass substrates of dimensions of 25x25 mm^2. The substrates were cleaned using the method mentioned earlier before coating the polymer layer.

Spin coating was performed by depositing the solution drop-wise onto the substrates, making sure the solution covers it completely prior to spinning. The process was done in two steps; a pre-spinning phase for 15 seconds at 500 rpm to ensure complete surface coverage, and then with the acceleration time less than 2 seconds, the final spinning speed being reached with a total spinning time of 60 seconds. The spinning speed was optimized in such a way that each polymer will attain a final layer thickness of approximately 100 nm. It is worth noting that the spinning speeds had to be different for each polymer due to the different viscosities of the solution. After spin coating, the substrates were post baked on the hotplate at 100°C for at least 12 hours to insure the removal of any solvent residue and annealing the polymer layer.

3.1.5 Preparation and assembly of liquid crystal cell

Typical LC cell needs two glass surfaces coated with alignment layer for uniform alignment of LC and two transparent electrodes under the alignment layers for the application of the electric field. The cell is then fabricated using the two substrates placed at a fixed distance from each other with glass spheres of several micrometers of diameter (in our case we used 10 μm) used as spacer. By capillary action, the liquid crystal was inserted in the cell gap obtaining a LC film sandwiched between the two substrates. In our investigation, we have used three types of LC cells. Commercial

cells purchased from EHC, cell with glass substrates coated with unidirectionally rubbed polymer for inducing planar alignment layer to the LC. As electrode layers the cells have transparent indium tin oxide (ITO) then was coated on the glass below the alignment layer. The schematic of the commercial cell is shown in Figure 25.

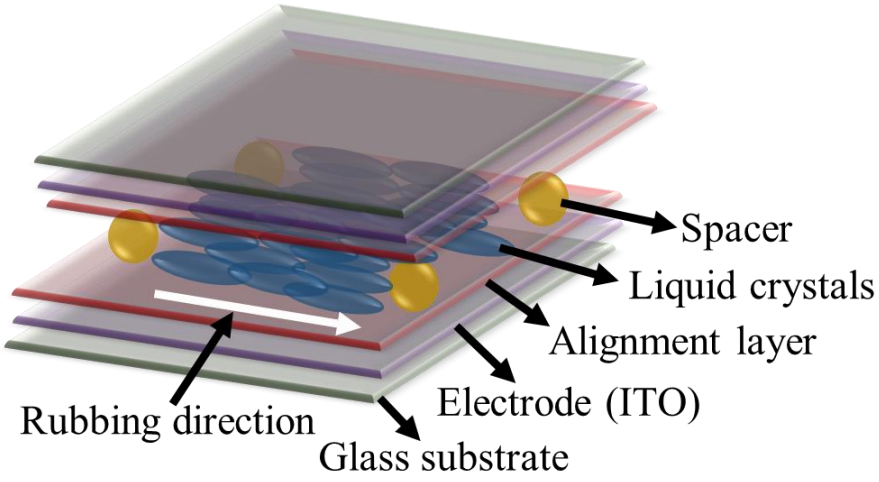

Figure 25 : Schematic of a typical commercial planar LC cell with alignment layer and transparent electrode.

The CNT- SiO_2/Al_2O_3 substrates were produced by a PhD student (Thuy-Kieu Truong) in Sungkyunkwan University, Korea (SKKU) and assembled in University of Luxembourg, Luxembourg (Uni.lu). The glass substrate was cleaned as mentioned earlier, and then it was treated with hexamethyldisilazane (HMDS). The HMDS layer was used to increase the adhesion between CNTs and the substrate by providing hydrophobicity on the surface (substrate), thus, promoting the tendency of nanotubes to lie on the surface. A single layer of CNT sheets was then deposited followed by ADES treatment to induce flattening of the CNTs. However, both HMDS and ADES treatments are not enough for being CNT sheets perfectly adherent to the substrate. Even with these treatments, there are CNTs outside of the main plane and parts of the CNTs strings detached from the substrate. Those dangling nanotubes are long enough to create short circuits which results in lack of stability in LC display cells. (More details are in chapter four, section 4.7).

Therefore, in order to ensure the electrical insulation and smooth out the macroscopic alignment disorder on the CNTs surface, a layer of SiO_2/Al_2O_3 was deposited by atomic layer deposition. Different thicknesses of SiO_2/Al_2O_3 layer have been investigated. However, 100 nm for SiO_2 and

60 nm for Al_2O_3 provided the best performance. In fact, thinner would still leave hairy CNTs out of the main plane while too thick would cover the unidirectionally aligned features of the CNT sheets reducing the alignment transfer on LCs. The schematic of the cell preparation is shown in Figure 26.

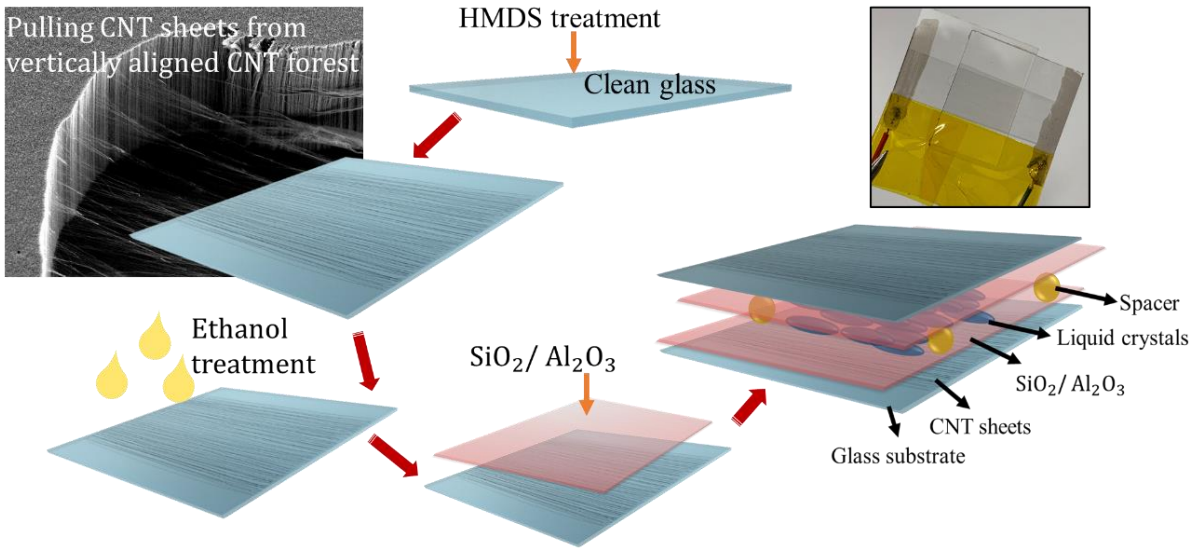

Figure 26 : Fabrication of the LC cell with CNT- SiO_2/Al_2O_3 substrate

To investigate the electro-optic behavior of LC cells, two copper wires were connected to the cell. The electric connection was made by soldering two wires (one on the top substrate and the other on the bottom substrate). The edge of the CNT- SiO_2/Al_2O_3 substrates were first coated with silver paste to obtain uniform/good connection between the wire and the CNTs as shown in Figure 27.

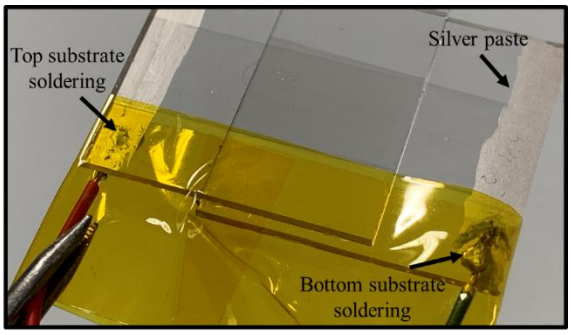

Figure 27 : A CNT- SiO_2 cell with wires solder on both top and bottom substrate.

3.2 Properties of liquid crystals and Azo Dye

The liquid crystal that has been used to fill the cell is 5CB from Synthon Chemicals, which is a room temperature nematic LC (Crystal ⇔ Nematic phase transition temperature 22.5°C and Nematic ⇔ Isotropic 35°C) [124]. The refractive indices are $n_{\parallel} = 1.71$ and $n_{\perp} = 1.53$ and birefringence, $\Delta n = 0.18$ (at 25°C) [125].

For order parameter calculation we used E7 liquid crystal (a mixture of 5CB, 7CB, 8OCB and 5CT LC) from sigma Aldrich and Azo dye (AZO1, the dye has anisotropic absorption and peak absorption 487 nm) from Nematel.co. The purpose of using E7 over the 5CB is that E7 has wider nematic temperature range (-10°C to 61°C) which we believe important in order parameter investigations since the dye-doped LC mixture might get heated up from the light source also absorption from the dye. Additionally, the Azo dye has better dispersion in E7 as reported in the datasheet.

3.3 Characterization

3.3.1 Polarizing optical microscopy

Polarizing optical microscope (POM) was used not only to capture images but also for optical characterization. In our experiments, we used two microscopes; Olympus BX-51 and Nikon Eclipse LV200ND. Both microscopes are equipped with two linear polarizers, the one in the bottom referred as polarizer and the one at the top referred as analyzer. The analyzer in both microscopes is rotatable and can be rotated from 0° to 180°. Other than the polarizers, the microscopes have all the typical components such as condenser, rotatable stage and objectives between polarizers. It's worth to mention that in all our experiment we used linear polarized light. However, the advantage of the Nikon microscope is that the polarizer can be easily removed which was not possible with the Olympus microscope. The polarizer was removed during the characterization of CNT as polarizer. Both microscopes have halogen light sources. For all experiments, the light source was turned on for at least 10 min before conducting any experiment in order to stabilize the source. For order parameter experiment we used another light source, LED

(from CoolLED) lamp besides the halogen. For all the optical characterization we kept the objective of the microscope fixed at 10x.

3.3.2 Spectrophotometer

3.3.2.1 Local spectrophotometer

To measure the light intensity and characterize the absorption/transmission spectrum, we used a local spectrophotometer from Avantes (AvaSpec-2048). The local spectrophotometer was connected on top of the microscope column using a C-mount adapter through an optic fiber as shown in Figure 28.

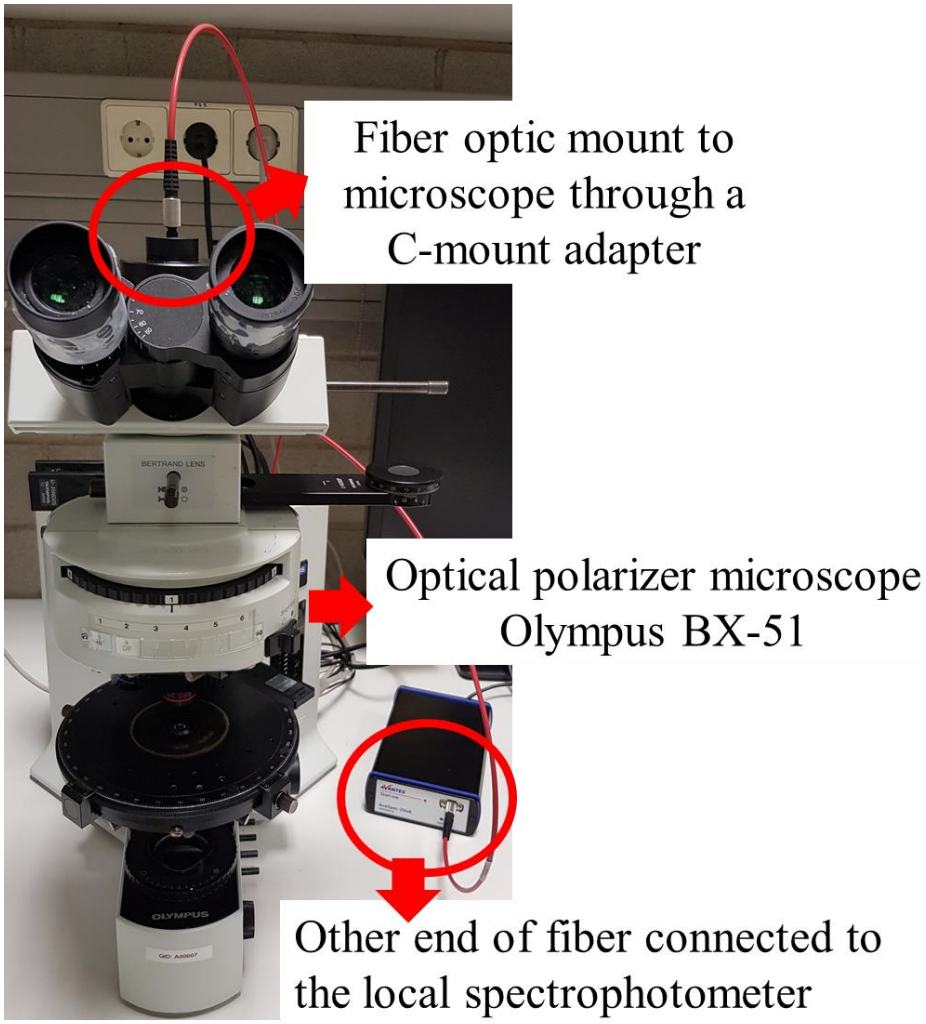

Figure 28 : Spectrophotometer connected through fiber and C-mount adapter with microscope.

3.3.2.2 Standard spectrophotometer

To study the optical anisotropy, we also used a standard UV spectrophotometer (Ultrospec 2000 pro), later repeating the same type of measurements with the spectrophotometer (Avantes) in order to compare the optical spectra from areas of different dimension. In fact, the standard spectrometer that we used probes areas in the order of 0.5 cm^2. Instead, the spectrometer (Avantes) connected to the microscope analyzes much smaller parts of dimensions dependent on the chosen objective magnification, in our case an area of 0.38 mm^2.

3.3.3 Electro-optic setup for liquid crystal

We studied the optical behavior and response of LC cell by applying electric field to the sample. In order to understand different properties of LC, two types of setup were used for electro-optic characterization. One is to observe the switching behavior of LC under the microscope. In this setup, the LC cell (on the microscope stage) was connected to a voltage amplifier (FLC electronics, A400) which was connected to a waveform generator (National Instrument, VirtualBench). The maximum output voltage from the waveform generator was limited to 12 V (amplitude), therefore, an amplifier was used to apply higher voltage. An alternating current (AC) square wave was applied to the LC cell and the behavior of the LC reorientation observed through microscope imaging. This setup was also used to investigate the heating effect from CNT sheets.

The second setup was used to study response time (rise and decay time) of LC. The schematic of the setup is shown in Figure 29. In this setup a diode laser from Thorlabs (LDM635) used as a light source. Linear polarizer film and a photodiode (Thorlabs) were used additionally. The cell was kept between two crossed polarizers. We used National Instrument (NI) as a waveform generator and oscilloscope. NI was connected to the computer and was controlled by an interface made by LabVIEW. We made arbitrary square waves by LabVIEW in which a certain voltage was ON for half a second and OFF for half a second. The change in the transmission was recorded simultaneously when the electric field was ON and OFF. The rise time was calculated by estimating the time needed for changing the transmission (from 10% to 90%) when voltage was ON (above the threshold value) and decay time (transmission change from 90% to 10%) when voltage was OFF.

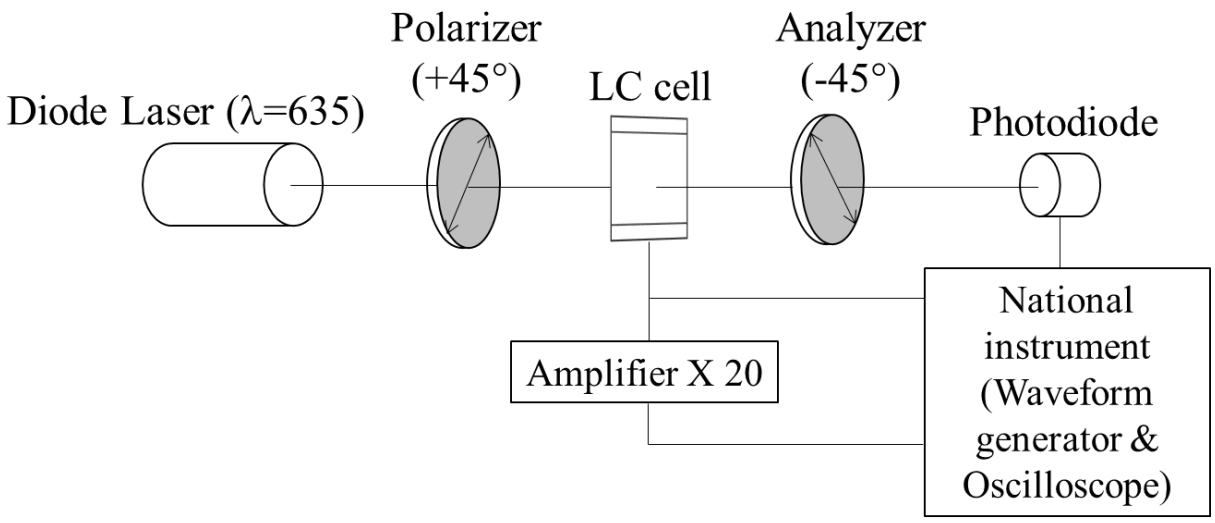

Figure 29 : Schematic of electro-optic setup that was used to investigate response time of LC

Chapter Four

Analysis

4.1 Optical characterization of aligned CNT sheets

To understand the interaction between CNTs and light we used linear polarized light. The polarizer was kept fixed in all our measurements and the sample was rotated. We carefully studied the interaction between linear polarized light and aligned CNT sheets. The schematic of the aligned CNT sheets with the light propagation direction at normal incidence is shown in Figure 30 (a). We found that linear polarized light with E field parallel to the CNTs, absorbs more light than if it's perpendicular to it as shown in Figure 30 (b). Therefore, we named CNT alignment direction 'absorption axis' and the axis perpendicular to it is the 'transmission axis'. The difference in absorbance in parallel and perpendicular to the CNTs is known as anisotropic absorption. It has been reported that a single-wall carbon nanotube would not absorb any light when the linear polarized light parallel to the single-wall carbon nanotubes (SWCNTs) transmission axis and would have strong absorption (depending on the intensity and wavelength) in case of parallel to the absorption axis [37].

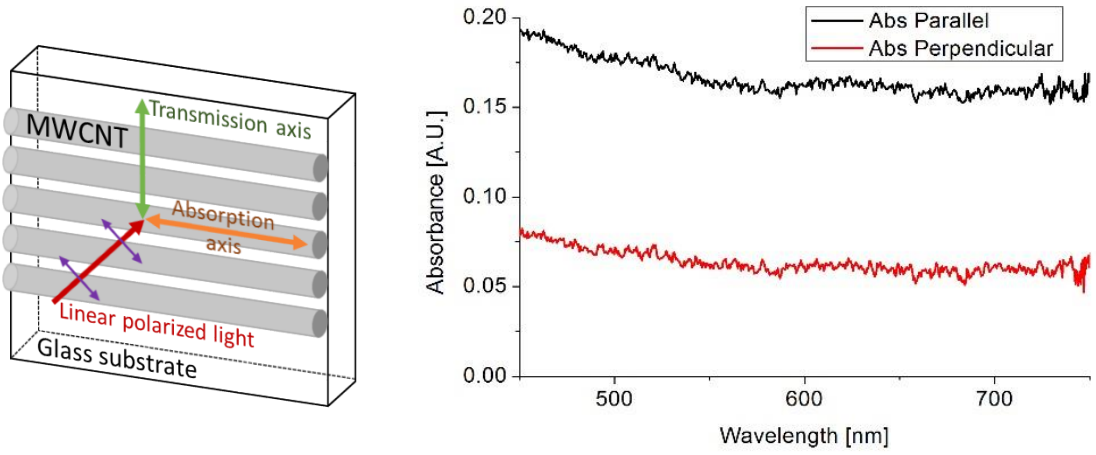

(a) (b)

Figure 30 : (a) Schematic of CNT sheets on the substrate. The axis along the length of the tube is the absorption axis and the perpendicular axis along the diameter is the transmission axis. (b) The absorption spectrum in the visible wavelength of the CNT sheets parallel and perpendicular to the CNTs absorption axis

For a single layer of aligned CNT sheets, the transmittance achieved ~85% at wavelength 520 nm. Moreover, over the visible spectrum (from 450 nm to 750 nm) the transmittance was more or less constant ~83% - 85% as shown in Figure 31. We then increased the thickness of the layer of CNT sheets by depositing one layer on top of another. For each layer, we made two samples. For layer one, three, five and seven we studied multiple locations and recorded the transmission values. The idea is to study multiple locations on the same sample to monitor the possible inhomogeneity. We studied the variance between those locations and used for the calculation of the error bar. However, looking at the POM image, microscopically the sample looks very homogeneous. Nevertheless, locally, the order parameter varies as well as the absorbance.

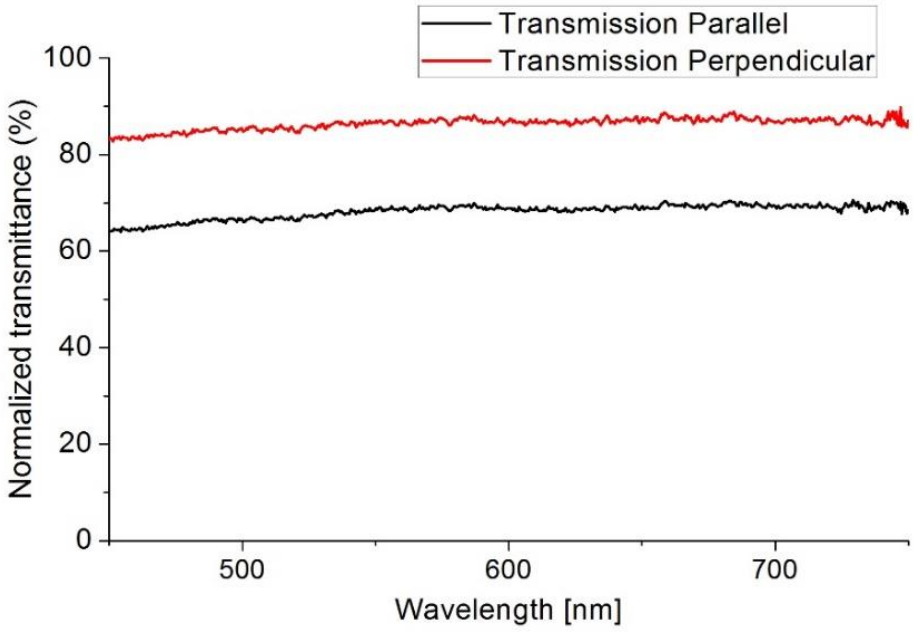

Figure 31 : The transmittance spectrum in the visible wavelength of the CNT sheets parallel and perpendicular to the CNTs absorption axis

The transmission decreases as the CNT layer thickness increases. Transmission level remained over 20% up to seven layers of CNT sheets. From layer one to layer three the transmission decreases greatly which we believe is due to the coverage. POM image (see Figure 32) of the one-layer CNT sheets studies suggested that there are gaps between the CNTs. It is worth to mention that in the experiment, the deposition of a layer on top of another layer is in the air. Thus, we assume that by putting a layer on top of another layer, the CNTs, rather than sitting on top of CNTs, they tend to go between the CNTs strings (since there are spaces between the CNTs and there is a pulling down action during the deposition). From POM images studies we assume that until layer four a new layer prefers to fill in the gaps between CNTs and after layer four a new layer of CNT sheets increases the thickness. We validate our hypothesis through POM images. The change in the brightness from layer two to three is very pronounced unlike layer four to five as shown in Figure 32.

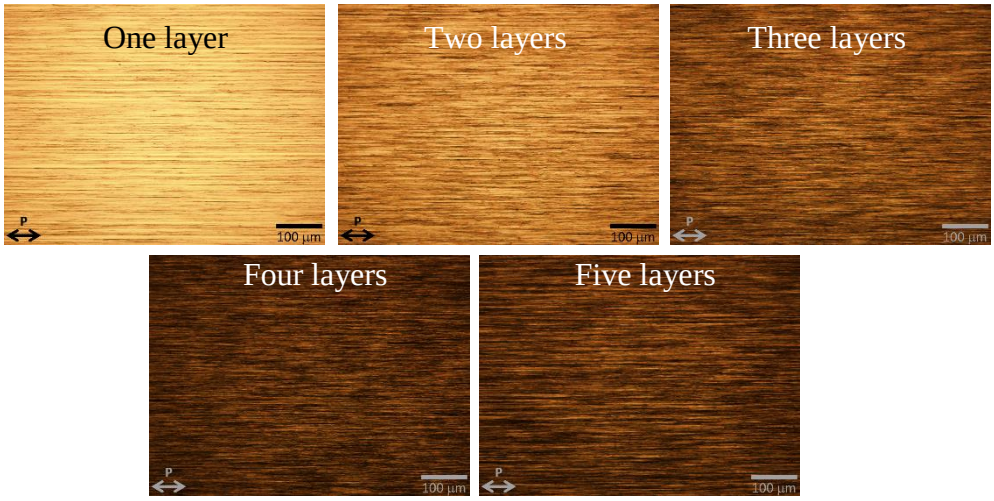

Figure 32 : Optical polarizing microscope images of CNT sheets from layer one to five

Figure 33 shows the measurement of transmittance (λ = 520 nm) by increasing the CNT sheets layer. Both parallel and perpendicular transmittance are showing a decrease, as they are plotted in the graph to understand how the transmittance decreases in both configurations. The transmittance decreases fast from layer one to three both in parallel and perpendicular configuration. From layer three to five, the decrease is more gentle than reaching a plateau. As discussed earlier, layer one to three CNTs goes between the CNTs, and the tubes going on top of the other tubes are still producing a thickness low enough to follow the linear parts of the Beer-Lambert law, consequently, transmission decreases greatly. However, from layer four the CNT sheets get thicker, which means the absorption is getting towards the saturation according to the Beer-Lambert law. As a result, we see a plateau starting from layer four. In other words, from layer four, we expect an increase in the layer number, an increase in the thickness, which means going over the CNTs rather than lying between the tubes, thus, the change in transmission is lower.

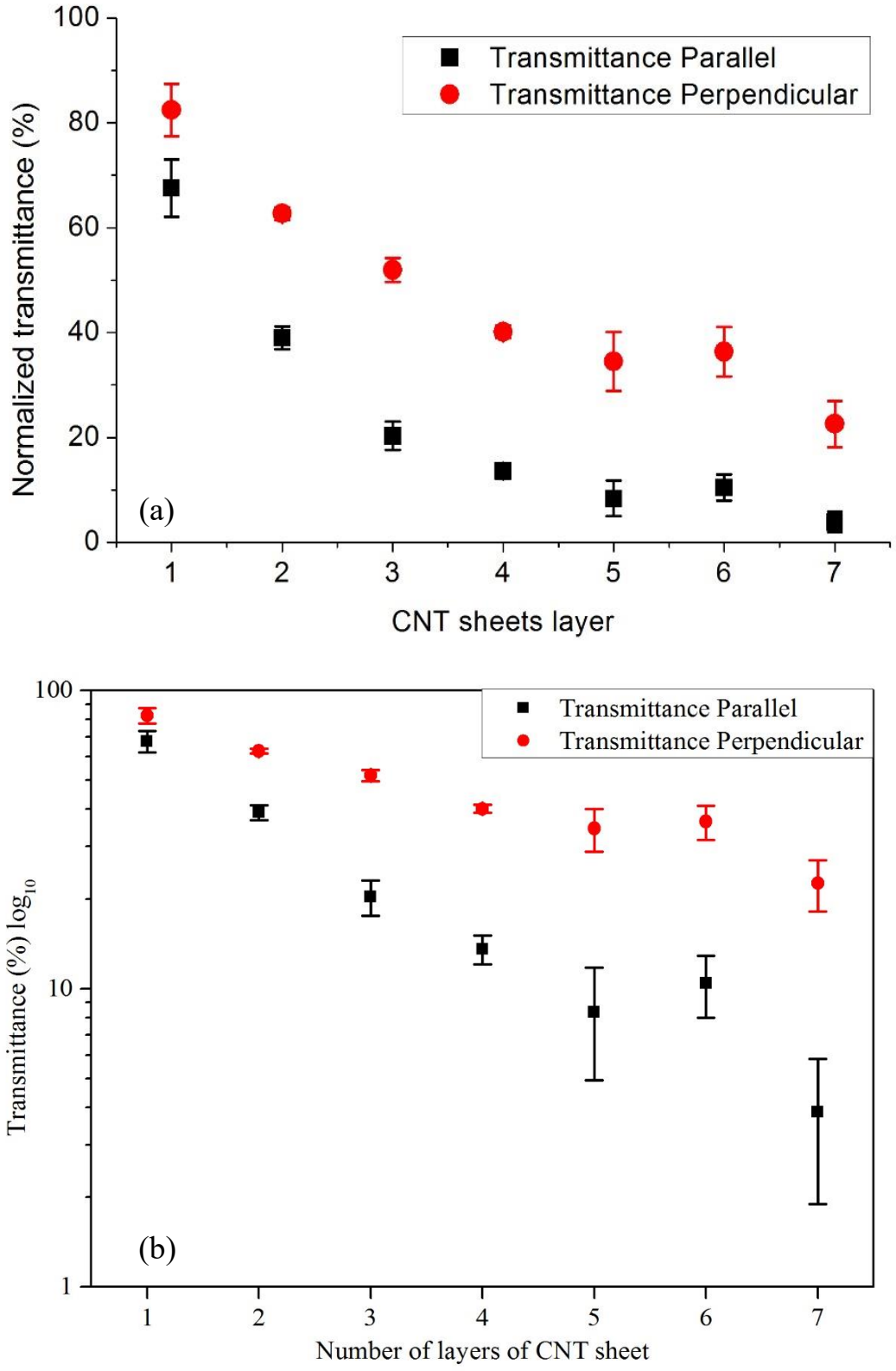

Figure 33 : Transmittance (λ = 520 nm) parallel and perpendicular to the CNTs absorption axis (a) normal and (b) logarithmic scale

The anisotropic transmittance calculated by the following equation:

$$\Delta T = T_{\perp} - T_{\parallel} \dots \dots \dots (10)$$

The anisotropic transmittance defines the difference in transmittance between perpendicular and parallel directions of light polarization. Figure 34 shows how the anisotropy changes by increasing the number of CNT sheets layer. The anisotropy increases linearly from layer one to layer three. Indeed, the highest anisotropy was found in layer three and decreases as layers increase, as shown in Figure 34.

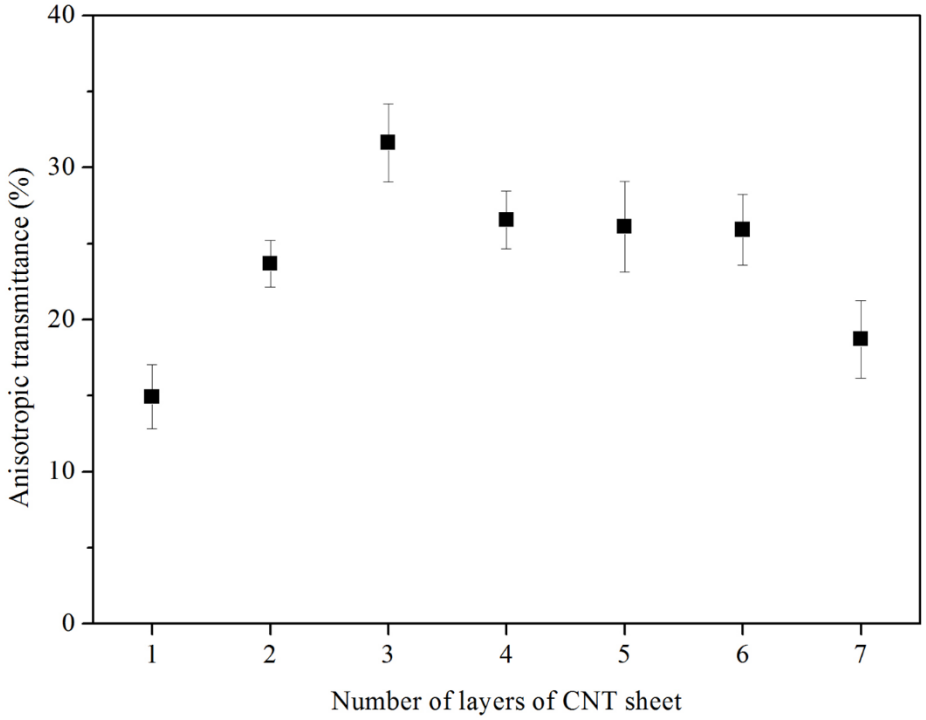

Figure 34 : Anisotropic transmittance as a function of CNT sheets layer

4.1.1 Image analysis vs spectrophotometer

We studied the POM images of the CNT sheets using image J software. We recorded the aligned CNT sheets images parallel and perpendicular configuration as shown in Figure 35. Through image J software, we calculated the mean grey value of the image. This is the sum of the gray values of all the pixels divided by the number of pixels. Typically, mean grey value (MGV) window is 0 to 255. If the image is 100% black, then the MGV is 255. If the image is white, then the MGV is 0. Depending on the image and on how much it is covered with tubes, Image J provides

the grey values. Then, we converted the mean grey value into percentage, which in return provides the value of the transmittance. We compared the values from image analysis with our experimental results from UV-VIS spectrophotometer. The comparison is plotted in Figure 36. The results from image analysis have the same trend as found using spectrophotometer. However, the transmittance value from image analysis is higher than what measured with spectrophotometer, which is observed in both cases (parallel and perpendicular). We believe that this is due to the area of the measurement. With a spectrophotometer, we analyzed local transmission (which is a portion of the area of the POM image) due to the dimension of the optical fiber; however, with image analysis it is an average of the full image. Therefore, with image analysis, the average gives a higher transmission value.

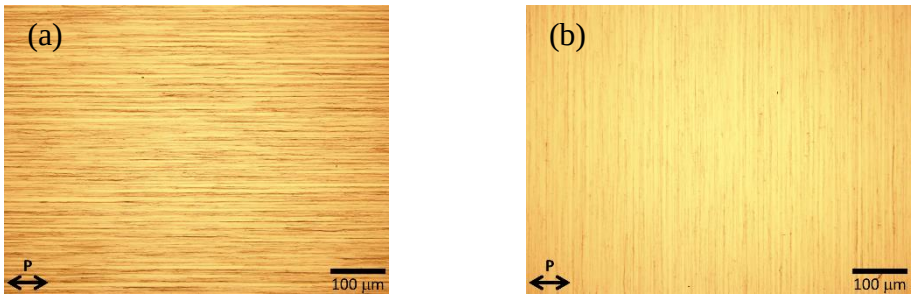

Figure 35 : Optical polarizing microscope image of layer one. Polarizer (a) Parallel and (b) Perpendicular to the CNT absorption axis.

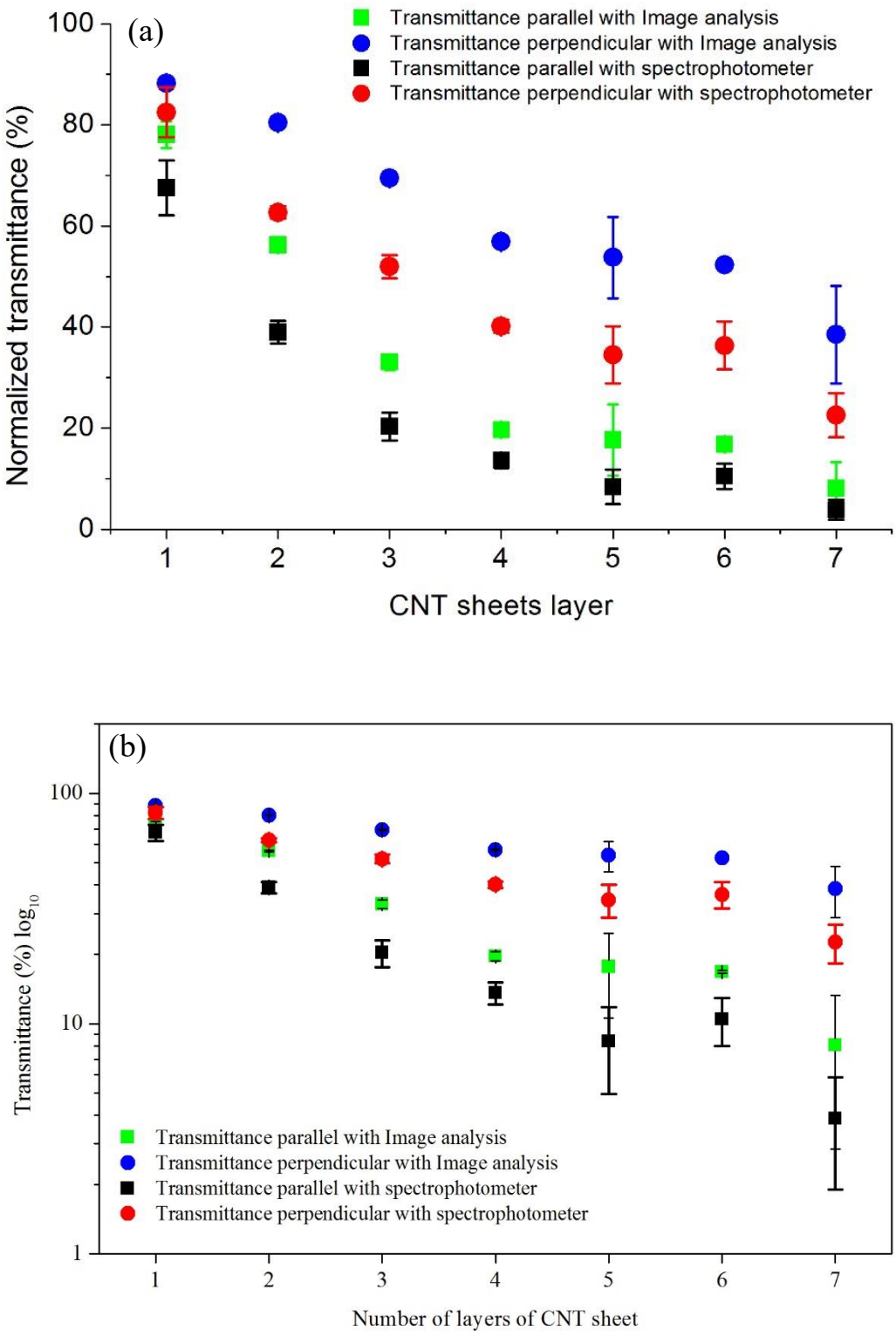

Figure 36 : Transmittance as a function of CNT sheets layer. Comparison between the image analysis and spectrophotometer (a) normal and (b) logarithmic scale.

4.1.2: Comparison between CNT sheets made from different forest

Another set of samples were made from a different forest to study the reproducibility. The differences between the batch one and batch two samples of the CNT sheets is the source of the CNTs, which in this case is the forest. We believe the batch two forest has the different density than the forest of batch one. This is because the transmission is higher in batch two in both directions, while the anisotropy is lower (in case of one layer), hence excluding an effect due to alignment but rather to lower amount of tubes. We characterize the sample from the batch two same way as we did for the batch one samples. The transmittance vs CNT sheets layer results show a similar trend as batch one samples with a minor difference in absolute value as shown in Figure 37. We believe this difference is coming from the local alignment of the sample. Due to the limitation of the CNT forest, we could not prepare the same number of samples as we did for batch one. We made layer one, two, three, five and ten from the batch two forest. The samples from batch two (layer ten) and batch one (layer six) shows close to same transmission in value ($T_{\parallel} = \sim 40\%$ & $T_{\parallel} = \sim 10$). We believe this is due to the density, height and thickness of the batch two forest.

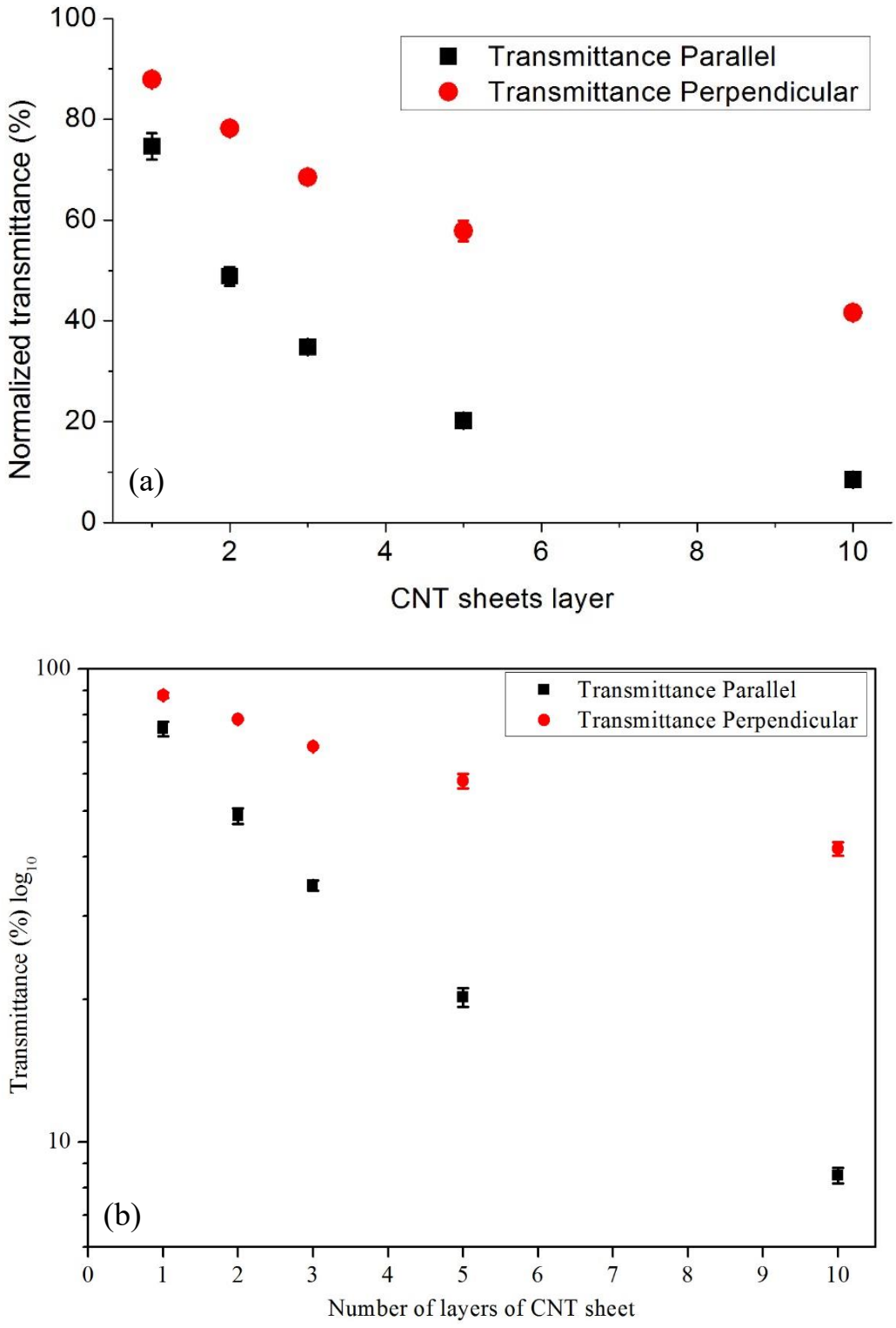

Figure 37 : CNT sheets from batch two. Transmittance as a function of CNT sheets layer (a) normal and (b) logarithmic scale.

Figure 38 shows the comparison of anisotropy between the samples from batch one and batch two. Both batches have a similar trend in anisotropic transmission. From layer one to three, the anisotropy increases. In the case of batch two, the anisotropic transmittance increases up to layer five. However, the anisotropic transmittance slightly decreases at layer ten.

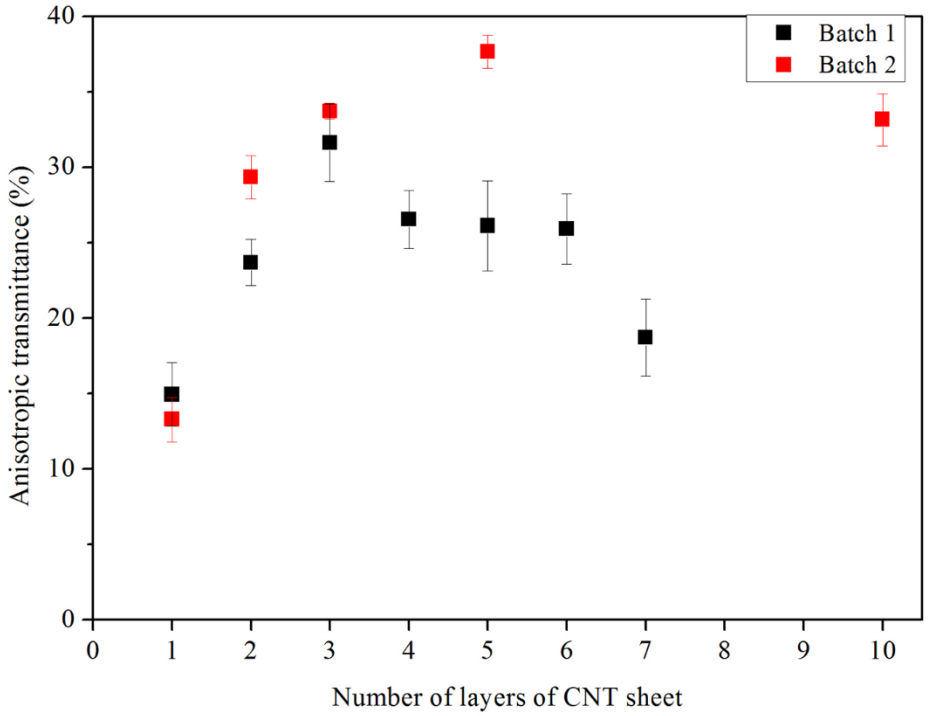

Figure 38 : Anisotropic transmission comparison between batch one and batch two samples as a function of CNT sheets layer

4.2 The degree of orientation order of aligned CNT sheets

To quantify the degree of orientational order of aligned CNT sheets, we adopted the technique which typically use to calculate the order parameter of the liquid crystal in a planar alignment cell. In a nematic liquid crystal system, the nematic order parameter is calculated by the following equation, as mentioned earlier (in section 2.2):

$$S = \frac{1}{2} < 3\cos^2\theta - 1 > \cdots (11)$$

This equation is for a 3D system where θ is the angle between the local director and the molecular axis, where S=1 (i.e., θ = 0) would indicate a perfectly aligned system. Since CNT films have a thickness below 100 nm and cm in width, therefore, we considered two-dimensional configuration for our aligned MWCNT sheets (see Figure 39). Therefore, the above equation became:

$$S = < 2\cos^2\theta - 1 > \cdots (12)$$

However, for dichroic molecules (having anisotropic shape), the orientational distribution can be calculated from the molecular transition dipole moment and can be expressed as a function of the absorbance parallel and perpendicular [126].

$$S = \frac{\boldsymbol{A_{\parallel} - A_{\perp}}}{\boldsymbol{A_{\parallel} + 2A_{\perp}}} (\boldsymbol{for\ 3D\ system}) \ldots\ldots\ldots (13)$$

$$S = \frac{\boldsymbol{A_{\parallel} - A_{\perp}}}{\boldsymbol{A_{\parallel} + A_{\perp}}} (\boldsymbol{for\ 2D\ system}) \ldots\ldots\ldots (14)$$

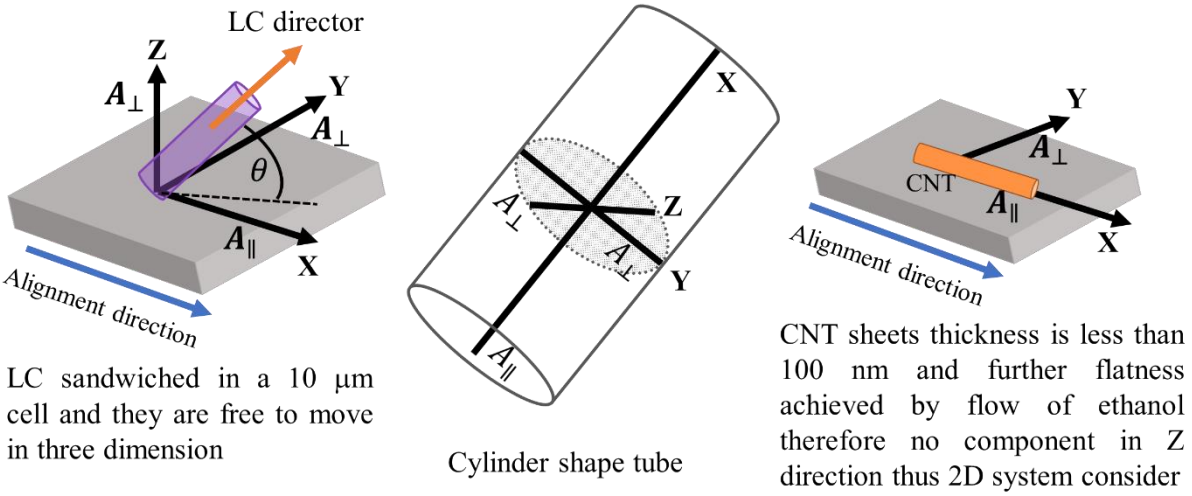

Figure 39: Order parameter in 3D vs 2D

4.2.1 Orientational order parameter of liquid crystal (E7)

Dyes are used to measure the order parameter of LC [127]. In a system with LC and dichroic molecules, one can measure the order parameter of dye by absorption, which gives the overall

order parameter of liquid crystal molecules. We studied a planar aligned LC in a commercial cell made by rubbed polyimide coated and have 10 μm of cell gap. E7 (Sigma Aldrich) liquid crystal mixed with the Azo dye (1 wt% of AZO1, Nematel.co) and filled the cell in capillary action (Figure 40 (a)). The maximum absorption of the AZO1 dye is at 487 nm, as reported and shown in Figure 40(b). A polarizing microscope coupled with a local spectrophotometer (Avantes) used to characterize the absorption peak of the prepared mixture in LC cell. Figure 41 (a) shows the spectrum of the halogen light which was used in the experiment. Since it's a white light source, it has a broad spectrum from 400 to 850 nm. The parallel (along with the LC alignment. e.g. maximum absorption) and perpendicular (e.g. minimum in the absorption) absorption were recorded and used to calculate the order parameter of the LC cell. The absorption spectrums for parallel (red) and perpendicular (black) absorption are shown in Figure 41 (b).

We used the equation (13) to calculate the order parameter. The peak parallel and perpendicular absorptions (487 nm) of the mixture are reported in Table 1 and then used to calculate the order parameter in Table 2. The order parameter 0.62 is found for the commercial cell with E7 and AZO1 mixture.

(a)

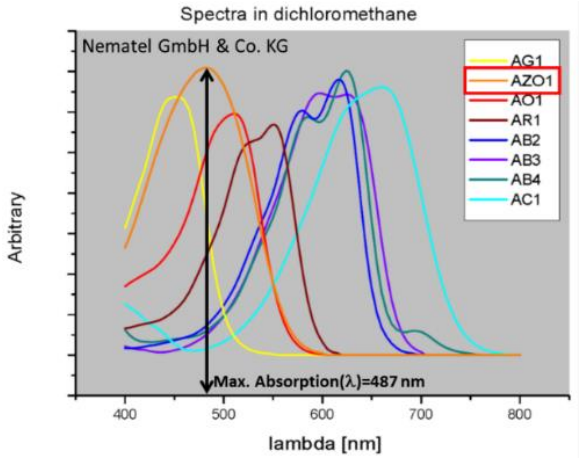

(b)

Figure 40 : (a) 10 μm planar commercial LC cell filled with E7 and 1wt% of AZO1 dye. (b) The specific absorbance of the AZO1 dye reported by Nematal.co (in a solution of 1 g dye in 100 ml of toluene in a 1 cm cuvette)

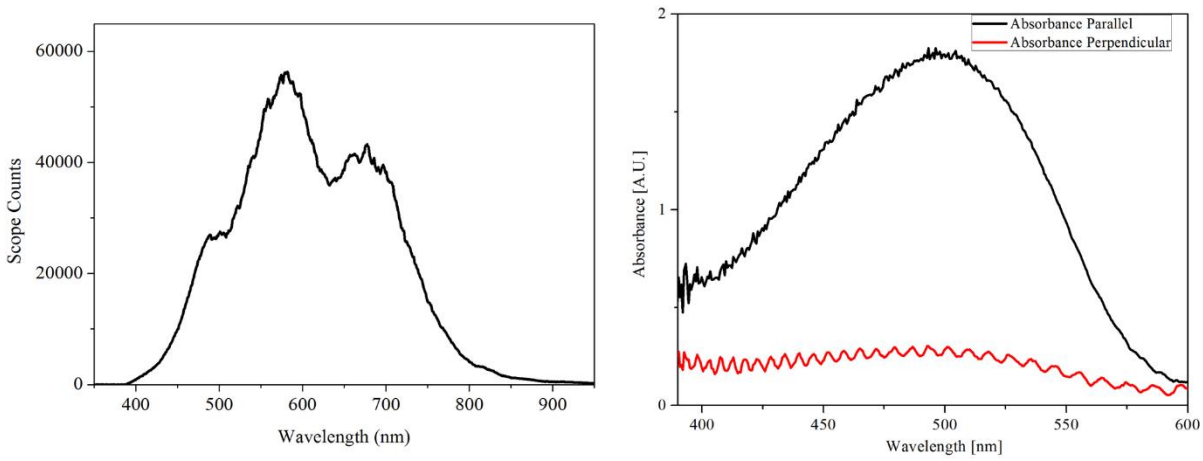

(a) (b)

Figure 41 : (a) The spectrum of the halogen lamp (b) The parallel (black) and perpendicular (red) absorption of the mixture under halogen light source (excluding the reference spectrum, spectrum in (a)).

The same experiment was done with the LED light source in order to confirm that there is no heating from the halogen light source which can influence the order parameter measured for the dye. The LED source used in this experiment has narrow bandwidth with a peak at 490 nm. The spectrum of the LED light is shown in Figure 42 (a). Figure 42 (b) shows the absorption peak of the mixture (LC+AZO1) parallel (polarizer transmission axis parallel to the dyes maximum absorption direction, parallel to the LC director - black curve) and perpendicular (polarizer transmission axis perpendicular to the dyes maximum absorption direction, perpendicular to the LC director - red curve) configuration. We found that similar absorption peak and values compare to the halogen light reported in Table 1. Moreover, the order parameter is also close to the value calculated with halogen light. Therefore, we believe there are no heating effects from the halogen light source which can affect the order parameter of liquid crystal during the experiment.

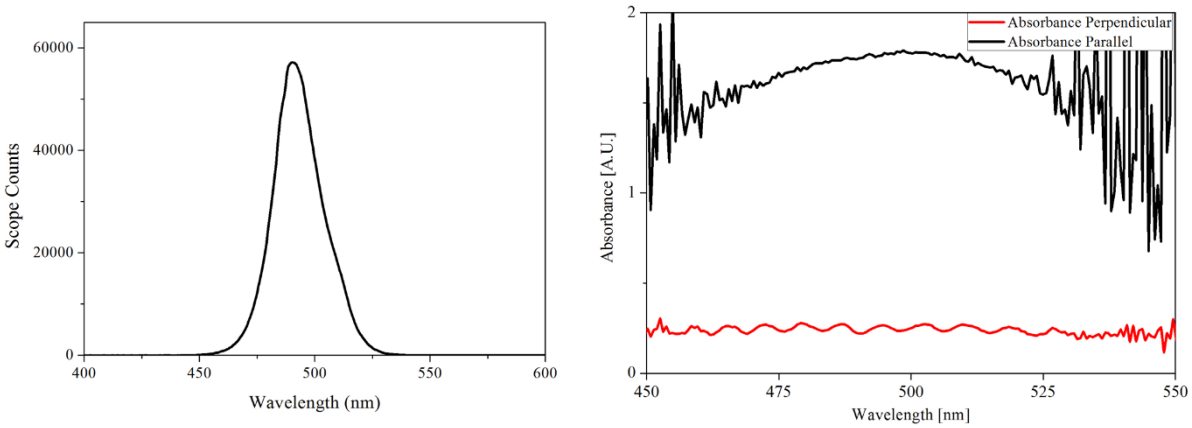

(a) (b)

Figure 42 : (a) Spectrum of the LED lamp (b) parallel (polarizer transmission axis parallel to the dyes maximum absorption direction, parallel to the LC director - black curve) and perpendicular (polarizer transmission axis perpendicular to the dyes maximum absorption direction, perpendicular to the LC director - red curve) absorption of the mixture under a LED lamp.

Table 1 : Calculation of the order parameter from absorbance values recorded from the spectrophotometer

Absorbance	Light source	Value [A.U.]
Parallel	LED	1.73
	Halogen	1.74
Perpendicular	LED	0.27
	Halogen	0.30

Table 2 : Order parameter comparison between LED and halogen light source

Light source	Order Parameter (S)
LED	0.64
Halogen	0.62

The measured value of S is indeed a value expressed for the nematic LC E7.

4.2.2 Orientational order parameter of aligned CNT sheets

Since CNT films have a thickness below 100 nm, we considered a two-dimensional configuration for analyzing our aligned MWCNT sheets. Therefore, in order to calculate the order parameter of the aligned CNT sheets, we can use equation 14, which considers absorbances in the parallel (maximum absorption) and perpendicular (minimum absorption) directions. These quantities are estimated in order to find the maximum absorption from the measurement of absorption as a function of the angle of incident polarization. This was found by rotating the cell around the axis perpendicular to the cell plane, also corresponding to the light propagation direction.

The absorption spectrum parallel to the alignment direction and perpendicular to the alignment direction of the CNT sheets deposited on a glass substrate has been shown in section 4.1 (Figure 30 (b)). In our CNT sheets, the absorption in visible wavelength is uniform unlike the absorption in dye where there is a peak absorption in a specific wavelength. In the case of CNT sheets, we calculated the order parameter at wavelength 520 nm (chosen randomly). Moreover, we repeated the same experiment and calculated the order parameter in a different location of the same sample to evaluate the homogeneity of the alignment. The spots are randomly chosen among regions that looked fairly similar except for point five, deliberately included as an example of disordered area and effects on the order parameter.

Table 3 reports the order parameter at different locations of the CNT sheets. Indeed, the order parameter is not the same for all over the sample. However, the differences in value are very small: the highest order parameter was found is S = ~0.44 and varied down to S = ~0.33. In case of point five, the sample was scratched intentionally to find the lowest order parameter.

Table 3 : Order parameter of CNT sheets in different location in the sample

Points	Order Parameter (S)	Average S without point 5	Average S with point 5
1	0.33	0.39	0.31
2	0.36		
3	0.42		
4	0.44		
5	0.17		

While the maximum order parameter is, indeed, *S* ~0.44, the average overall order parameter of the sample is *S* ~0.39 without taking into consideration the order parameter in point 5. Figure 43 shows the OPM image of single layer CNT sheets. Macroscopically the CNT sheets look homogeneous and highly oriented in one direction. However, locally they are not as shown in Figure 43 (b) an OPM image taken by 50× objective. Therefore, it is not surprising to find differences in values in order parameter within the sample in different points.

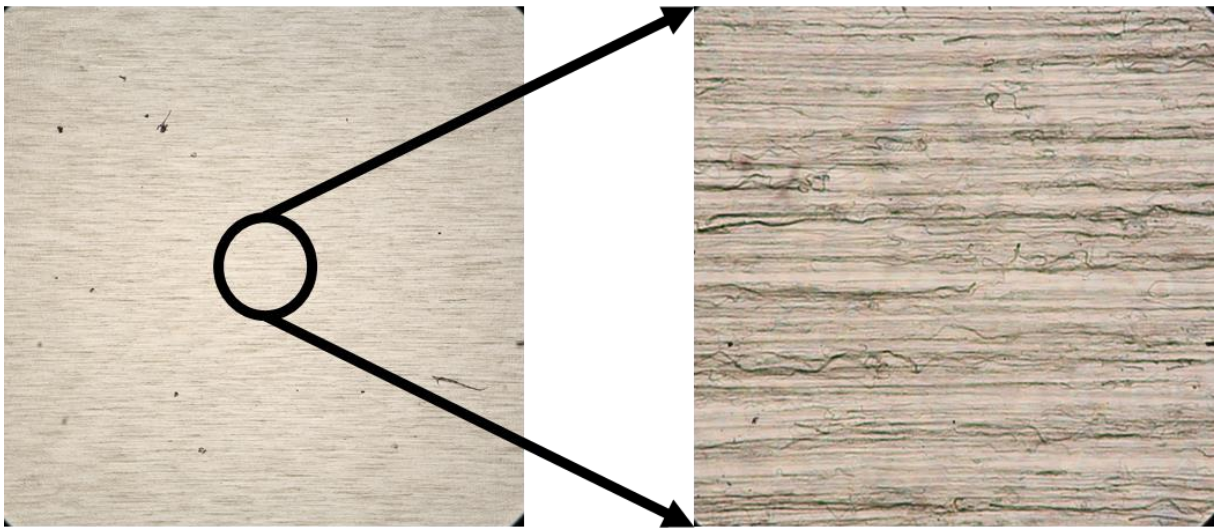

(a) (b)

Figure 43 : POM images of a single layer CNT sheets with (a) 4× and (b) 50× objective

4.3 Adhesion between CNTs and glass surface

The adhesion of the CNTs on the surface of the substrate has been an issue. Since we prepare our samples by depositing free-standing sheets on a glass substrate, we found that the film is not homogenously attached to the surface after the deposition. Moreover, the parts that are attached on surface are not well adhere. We have checked the adhesion of deposited CNT sheets on a glass substrate by using an OPM. While focusing on the CNT sheets on glass substrate, we noticed that some areas of the CNT sheets are not in focus while others are. This means that the parts that are out of focus are the CNTs not lying on the glass surface and/or have weak or no adhesion on the glass surface.

In order to address this issue and to improve the adhesion of CNTs with the substrate's surface, we used ethanol treatment after transferring the suspended CNT sheets to the substrate. We named this treatment "Adhesion Driven by Ethanol to Surface" in short ADES treatment. The mechanism of the ADES treatment is the following:

- **The capillary bridges formed between tubes and surface are expected to be able to pull the nanotubes down on the surface as the evaporation progresses.**
- **We assume ADES treatment force the tubes to lie in the plane of the substrate**
- **Finally, van der Waals attraction forces would keep the nanotubes in place.**

The technique of the ADES treatment is shown by the schematic in Figure 44. Drops of ethanol dropped on the edge of the substrate while tilting the substrate so that the ethanol can flow along the CNT alignment. Then substrate was transferred onto a hot plate and kept at 90°C for 15 mins.

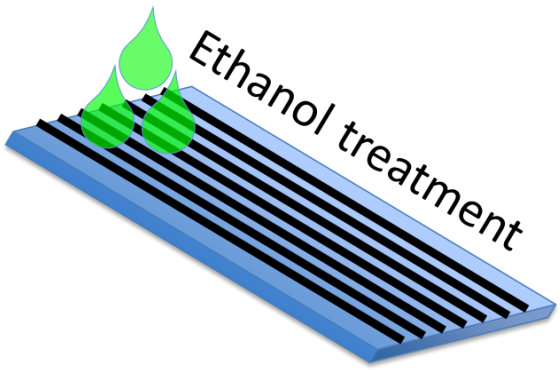

Figure 44 : Schematic of ADES treatment

Figure 45 (a) shows the POM image of the CNT sheets as deposited on a glass substrate. The inset is a zoomed-in section of the out of focus area. The area in the inset shows CNTs with no/weak adhesion to the surface which makes them “float”; that is, they stand out of the plane of the substrate. However, this is an example, there are few other places within the sample having weak adhesion. Figure 45 (b) shows same sample after ADES treatment. We carefully studied the morphology of the sample and we did not observe “floating” CNTs, at least microscopically, all the tubes being in the same focal plane.

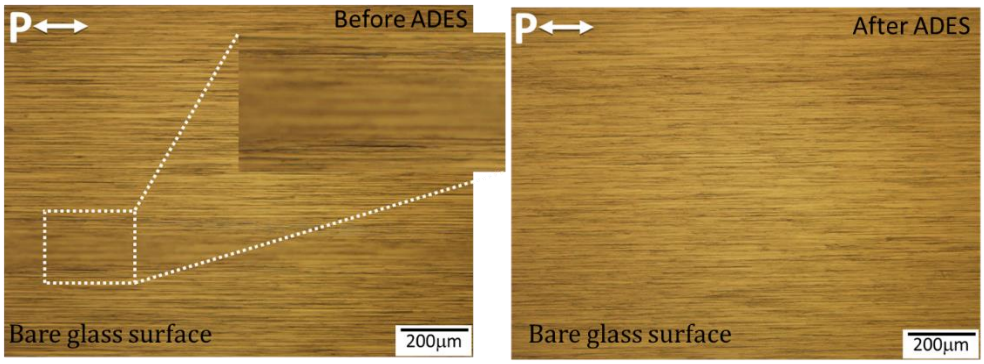

(a) (b)

Figure 45 : Without analyzer POM image (a) Before ADES treatment. The inset shows the CNTs that are out of focus (b) After ADES treatment, the CNTs are in focus.

4.4 Effect of adhesion on order parameter of CNT sheets

We evaluated the performance of ADES treatment by studying the sample with SEM. Figure 46 shows a SEM image (side view) of the sheet on a glass substrate, showing the hairy nature of the surface due to nanotubes sticking out (two blue arrows). We believe the ADES treatment is not enough to push down all the dangling tubes to the substrate. The hairy tubes (perpendicular to the substrate) have dimensions in the order of several micrometres. They can bend horizontally as well vertically reducing the orientational order. Moreover, due to the poor adhesion, the alignment of the CNT sheets is potentially unstable. The waviness reduces the contact area between the substrate and CNTs, which results in a weak adhesion of the overall CNT sheets.

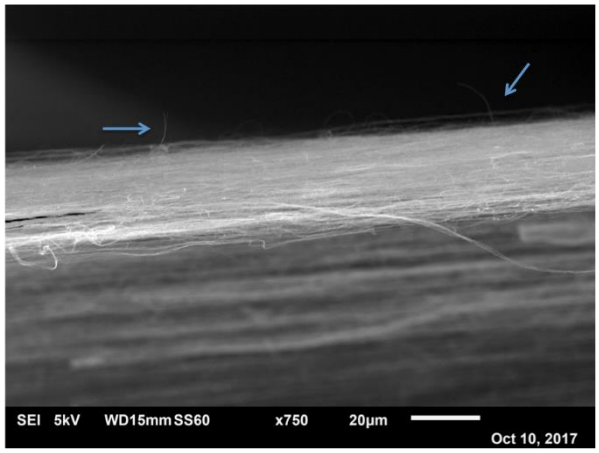

Figure 46 : SEM side image of as deposited CNT sheet showing there are nanotubes outside the main plane (blue arrow)

4.4.1 Polymer surface under the CNT sheets

We studied multiple surfaces in order to assess any improvement of the adhesion due to the surface characteristics and then estimate the order parameter. Thus, we coated the glass surface with three different polymers, separately: PVA, PVP and PMMA. The reason for using PMMA is to create hydrophobic surface in contact with CNTs, deposited with dry, solvent free, process, hoping that CNTs would have higher adhesion preferring hydrophobic than hydrophilic (PVA and PVP) surface since CNTs are hydrophobic. Three different solvents - toluene, ethanol and distilled water, were used in order to dissolve the PMMA, PVP, and PVA polymers, respectively. However, adhesion was still an issue even though we changed the surface as shown in Figure 47. We found the same characteristics as depositing CNT sheets on a bare glass substrate. Some parts of the sheets were out of plane, meaning not attached to the surface or having weak adhesion. Therefore, ADES treatment was indeed a crucial step to improve the adhesion by pushing them to the surface even in presence of a polymer surface.

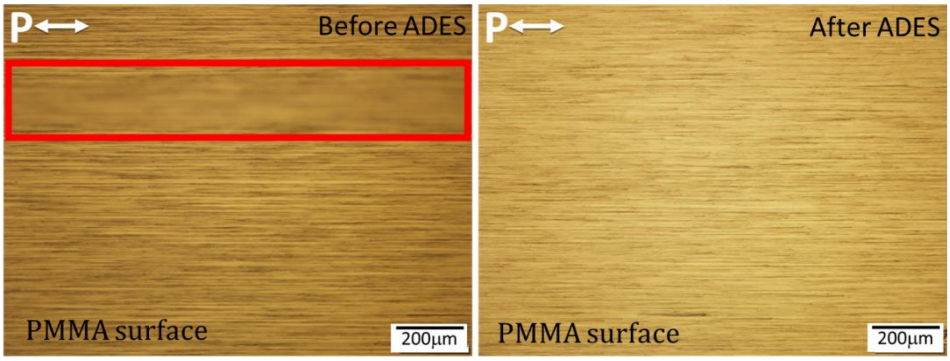

(a) (b)

Figure 47 : POM images of CNT sheets on PMMA surface (a) before ADES treatment. The red box indicates the parts that are not in focus. (b) After ADES treatment. The entire sample is in the same focal plane.

In order to assess the influence of the adhesion on the order parameter, we studied and compared the order parameter of CNT sheets with and without ADES treatment on glass and polymer surfaces. In Figure 48 (a) and (b) we can see how the values and trend change greatly after ADES treatment, all lower than that for the as-deposited sheets, indicating an increase in the disorder of nanotubes. After ADES treatment, the orientational order parameter S decreases for the CNT sheets for all substrates as reflected by the decrease of ΔA. For highlighting the change in S before and after treatment, we point out that on glass the order parameter is S ~0.4, but after ethanol treatment the value decreased to S ~0.32. This indicates that the solvent has induced orientational disorder in the nanotube sheets on the substrates either due to side aggregation or lateral pulling or even a natural curving of the nanotubes when pulled down by the capillary bridges to fit space shorter than their length.

The reason for the slightly higher orientational disorder of as deposited tubes on polymers than on glass can be ascribed to the higher roughness of the polymer surface, which is not followed by the nanotubes, due to a lack of specific attraction forces at the interface. The result is the presence of larger areas with nanotubes at different vertical locations, which suggests that these parts are less stretched, thus less oriented unidirectionally. Therefore, the ADES treatment clearly reduces the degree of alignment with the highest anisotropy values for the nanotubes on glass followed by the tubes on PMMA. Lower values are found for PVP and PVA surfaces, presumably for the larger

infiltration of the solvent into the polymer. The resulting softening of the polymer surface and the subsequent nonuniform evaporation can lead to aggregation of nanotubes, thus disrupting their order. The same trend can be observed in the order parameter always being lower than for the as-deposited nanotubes but different depending on the type of underlying surface. PMMA gives the higher order parameter among the tested polymers, but it is still lower than for the tubes on bare glass. Though the ADES treatment the adhesion was improved, but the order parameter is reduced, which we believe is due to an amplification of the in-plane waviness from the planarization of the vertical disorder.

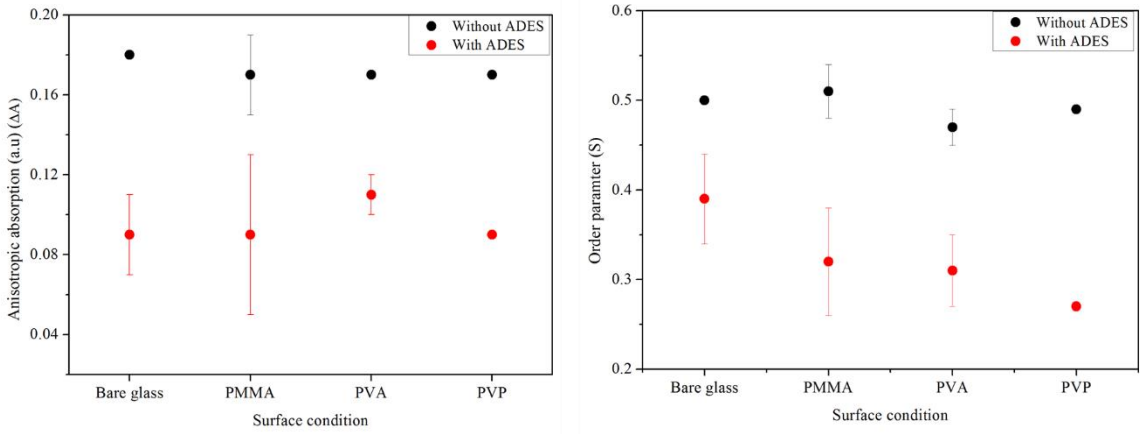

Figure 48 : (a) Optical anisotropy for CNT sheets deposited on bare glass, PMMA, PVA and PVP coated glass substrates before (dots) and after ADES treatment (squares) b) order parameter estimated for the same samples.

4.4.2 Coating a transparent layer on top of CNT sheets

Due to the lack of adhesion, the hairy nature of CNT sheets on a substrate has been a critical issue to focus on for LC displays. Tubes which are out of plane may make connections to the upper substrate, creating a short circuit. Therefore, a transparent layer of aluminium oxide (Al_2O_3)/silicon dioxide (SiO_2) on CNT sheets was used to prevent the short circuit. We have evaluated the order parameter of the CNT sheets substrates with Al_2O_3/SiO_2 coating and compared with the CNT sheets on bare glass substrate and/or polymer surface. Indeed, the CNT sheets with coating layer showed higher order parameter.

A layer of Silicon dioxide (SiO_2) was coated on top of CNT sheets by ALD techniques as mentioned earlier in chapter three section 3.1.5. Initial experimental results suggest that the CNT sheets with SiO_2 coating indicated higher orientation order parameter of aligned CNT sheets. However, the order parameter value before the coating is not present to compare the results after coating, because the coating and the sample were prepared by our collaborator in Korea. Nevertheless, compared to the uncoated CNT sheets measured here, highest order parameter found on the sample coated with SiO_2. For uncoated CNT sheets, the order parameter achieved was ~0.4. The CNT sheets with the SiO_2 coating has the orientational order parameter ~0.6. The sample not only showed high order parameter but also high transmission with large anisotropy compared to the CNT sheets without SiO_2 coating Figure 49.

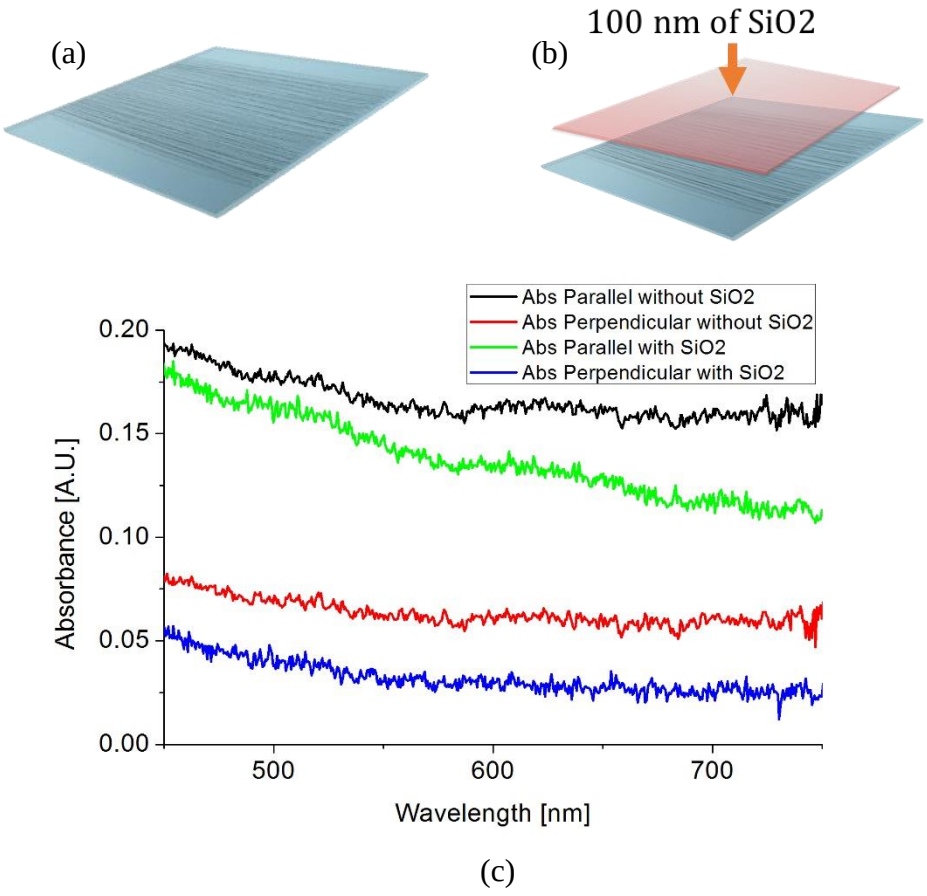

Figure 49 : (a) Scheme of CNT sheets on a glass substrate (b) CNT sheets with 100 nm of SiO_2 coating (c) absorption parallel and perpendicular with and without SiO_2 coating

The increase in order parameter was also found in case of Al_2O_3 coated CNT sheets substrate. The order parameter for 100 nm thick Al_2O_3 substrate was found 0.5 which is higher than non-coating CNT sheets substrate but lower than SiO_2 coated substrate.

Our preliminary results suggest that the orientational order parameter might be possible to improve by coating the CNT sheets with the SiO_2/Al_2O_3. We believe that this is due to the pushing down the tubes to the substrate along the alignment (without bending) of the tubes which are out of the plane. Moreover, the mother of the CNT sheets which is the forest might have a higher degree of alignment, which in return results in higher order parameter in free standing film before coating the SiO_2/Al_2O_3 layer. Since, we do not have the value of the order parameter before coating the CNT sheets, it is difficult to conclude that the coating increased or preserved the order parameter. However, further experiment and evaluation of order parameter on same sample before and after deposition of coating layer is needed in order to understand the mechanism behind the improvement of overall alignment.

4.4.3 A brief summary on orientational order parameter of aligned CNT sheets

The order parameter of free-standing CNT sheets (as pulled from forest) was also evaluated to study the surface influence in the alignment of the tubes. Moreover, we evaluated how the orientational order parameter changes from initial pulled CNTs to the deposited CNT sheets. For this experiment, we prepared free standing CNT sheets by transferring the film on two glass capillaries from the stage. We then calculated the order parameter of the free-standing CNT sheets. Table 4 summarizes the order parameter of CNT sheets on different surfaces including free standing. Indeed, the order parameter of the free-standing film was higher (S = ~0.6) than deposited CNT sheets on bare glass substrate and CNT sheets after ADES treatment. This indicates that the alignment decreases when the free-standing sheets transferred to a glass substrate and decreases further after ADES treatment (S = ~0.4). We believe this is due to the tubes which are not in the plane (dangling around) shift by the ADES treatment which further disturbed the neighboring tubes, thus, decrease the overall alignment. From above mentioned experiments and analysis, we noticed that a polymer surface was also not helpful to preserve the original alignment found in free standing CNT sheets. On the other hand, the highest order parameter is found when the CNT sheets

on a glass substrate are coated with Al_2O_3/SiO_2 however, the origin of the high values in order parameter is not clear to us. Further experiments with improved deposition technique and materials are needed to understand the mechanism.

Table 4: Orientational order parameter of CNT sheets with and without a coating layer

CNT sheets	**Order parameter S (2D)**
Free Standing	0.58
On a glass substrate without ADES	0.50
On a glass substrate with ADES	0.44
On a glass substrate coated with 60 nm thick Al_2O_3	0.40
On a glass substrate coated with 100 nm thick Al_2O_3	0.50
On a glass substrate coated with 100 nm thick SiO_2	0.66

4.5 Interaction of visible light with aligned MWCNT sheets

We observed a change in transmission when the CNT samples were rotated from 0 to 90 degrees in the optical microscope between crossed polarizers. At orientations of the transmission axis of the CNT sheets parallel and perpendicular with respect to the transmission axis of the polarizers, no transmission was observed. However, a maximum in intensity was found when CNT rotated at about 45° as shown in Figure 50 (a). Figure 50 (b) shows the OPM image of single layer CNT sheets under crossed polarizer. We believe that this change in transmission is likely mainly due to the anisotropic absorption, not birefringence. In this section, we will discuss the origin of the maximum in transmission as well as the observed rotation of polarization, experimentally and theoretically.

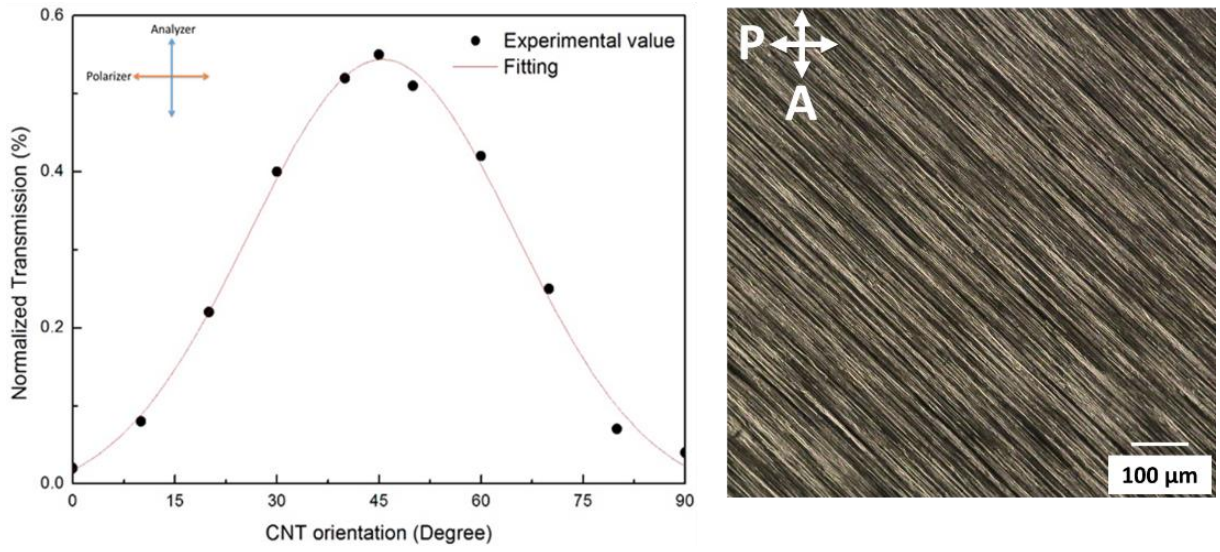

(a) (b)

Figure 50 : (a) Change in transmission between crossed polarizers of CNT sheets as the nanotube orientation direction is rotated. (b) OPM image of CNT sheets between crossed polarizer at 45° to the input polarizer clearly showing transmission

4.5.1 Rotation of polarization

To investigate the output polarization state, we put our sample between two linear polarizers. The top polarizer we will be addressing as analyzer and the bottom one as a polarizer. The polarizer was kept fixed and the analyzer was rotated from -90° to +90° with the step of 10°, in respect to the polarizer transmission axis. To validate the polarizers' condition in the system, a measurement was done without sample with the analyzer rotated -90 to +90 degrees with respect to the polarizer. Maximum intensity is observed when both polarizers are in a parallel configuration which is at 0 degrees in Figure 51 and zero transmission was found when they are in a crossed condition which is -90 and +90 degrees in the x-axis of the graph (Figure 51). The sample was then placed with its CNT absorption axis parallel to the polarizer TA axis followed by rotation of analyzer TA from -90 to +90 degrees. Maximum intensity for this configuration was found when the polarizer and the analyzer are in parallel condition (0 degrees in). Similarly, the peak position of the maximum also was observed when CNT sheets (CNTs absorption axis) were placed perpendicular to the polarizer TA. The same experiment was repeated for CNT sheets (CNTs absorption axis) oriented at 45° to

the polarizer TA. In this configuration, the maximum intensity shifted right to the x-axis (Figure 51), which we calculated ~4° (fitted with Malus' law).

We believe this is due to the anisotropic absorption by CNTs which results in rotation of polarization and only observable when CNT sheets are not parallel or perpendicular to the polarizer TA. The degree of rotation of polarization increases as CNT sheets rotate from 0 to 45 degrees. At 4° the highest ~4° of rotation were observed. However, CNT sheets only rotate the direction of the polarization and do not change the polarization state: this is observed by the extinction of transmittance at identical offsets from both -90° and +90°. This means both that the input light was linearly polarized and that the output polarization remains linear. Thus, in the x-axis of Figure 51, at +90° and -90°, the transmittance is zero as observed in the commercial linear polarizer.

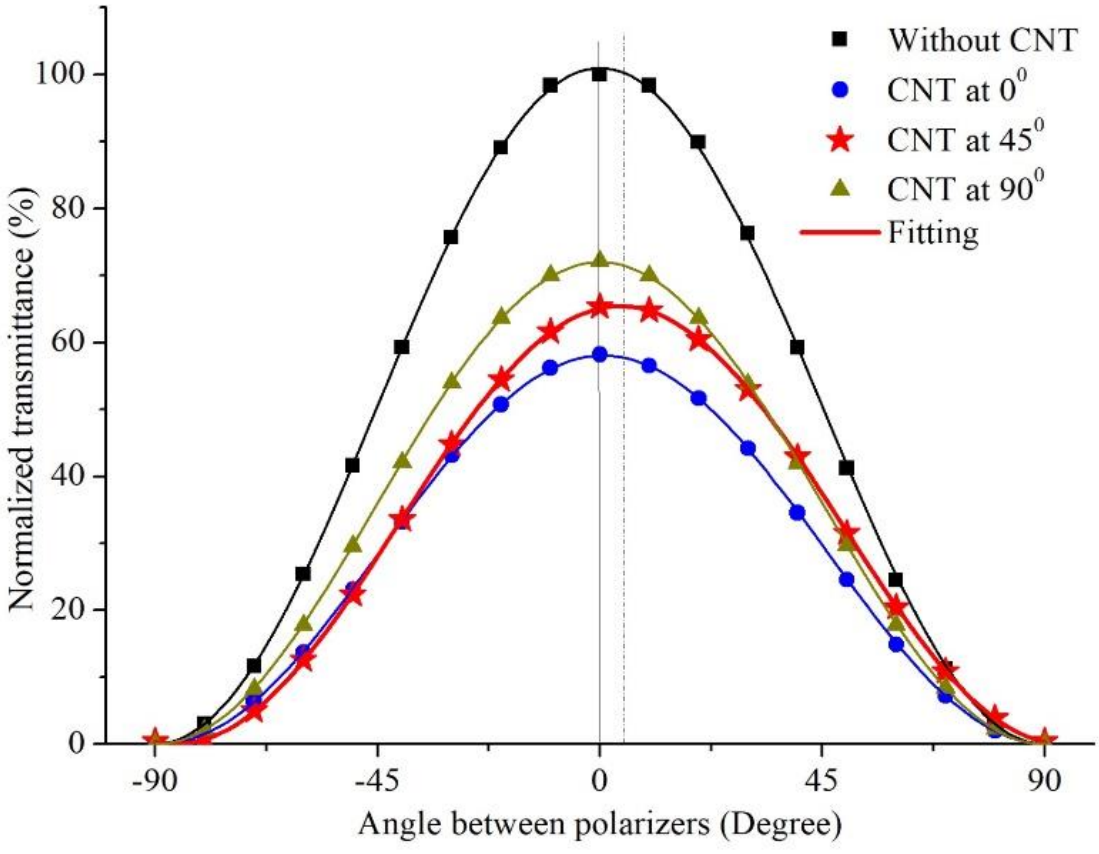

Figure 51 : Transmission from CNT sheets between two polarizers (one is fixed while other was rotating) and observation of rotation of polarization from CNTs at 45°.

The experimental data were fitted with a modified Malus' law:

$$I = I_0 \cos^2(\beta - \omega) \dots\dots\dots (15)$$

where I, I_0, β and ω are the output intensity, initial intensity, angle between polarizers and rotation angle, respectively. To find the maximum angle of rotation of polarization for a single layer of aligned CNTs in sheets we calculated the rotation of polarization other than 45°. We studied other angles such as 0° to 30° and 60° to 90° with a resolution of 10° and 30° to 60° with a resolution of 5°. We found that as we increase the angle between CNT sheets absorption axis and input polarizer transmission axis, the rotation of polarization increases and highest rotation was found at 45°. From 45° to 90°, the rotation of polarization decreases.

4.5.2 Theoretical analysis

To investigate the origin of the rotation of polarization and its relationship with anisotropic absorption, we performed a numerical analysis. Since CNTs absorb in an anisotropic manner, the absorption parallel to the CNT absorption axis and transmission axis is dependent on the attenuation coefficients along the absorption ($A_{\parallel}$) and transmission ($A_{\perp}$) axes. When the angle between input polarized light and CNT absorption axis (θ) = 0° or 90° (as shown in the Figure 52), the transmitted electric fields according to the attenuation coefficient are

$$[\theta = 0^{\circ}]\ \mathrm{E}_{\parallel} = \mathrm{E}_0\sqrt{\mathrm{e}^{-\mathrm{A}_{\parallel}}}$$

$$\text{and } [\theta = 90^{\circ}]\ \ \mathrm{E}_{\perp} = \mathrm{E}_0\sqrt{\mathrm{e}^{-\mathrm{A}_{\perp}}}$$

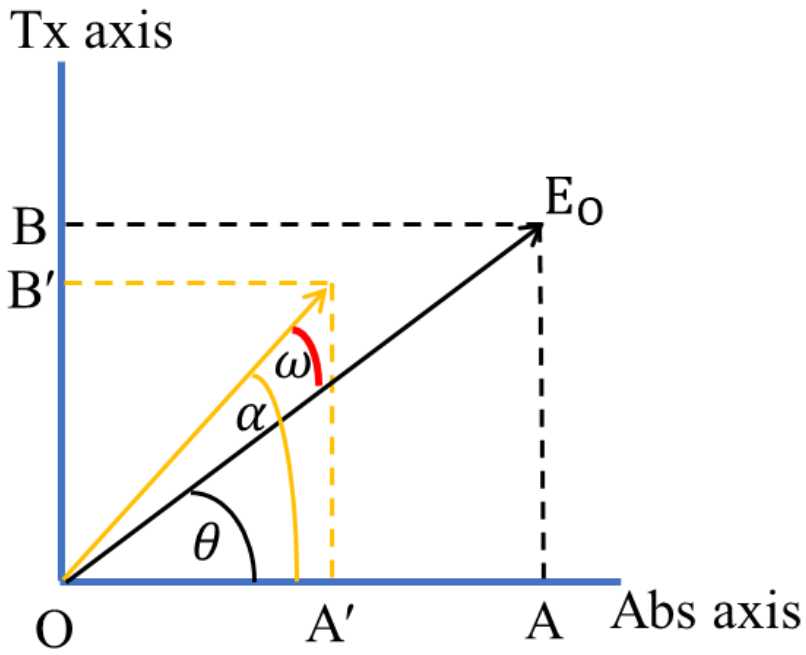

Figure 52 : Rotation of polarization from the geometrical analysis. CNT absorption axis is along CNT transmission axis, input linear polarized light E_o with an angle θ, light coming out from CNT sheets with an angle α and final rotation ω.

Using trigonometric function, we can write the components of the vector:

$$OA = E_O \cos\theta$$

$$OB = E_O \sin\theta$$

When the CNT sheets are rotated at an angle θ, each of these components (OA & OB) will be reduced in strength according to the value of the attenuation coefficient along TA and Abs axis of the CNT sheets. Therefore, for a given angle θ the reduced $OA'$and OB'will be:

$$OA' = OA\sqrt{e^{-A_{\parallel}}} = E_O \cos\theta \sqrt{e^{-A_{\parallel}}}$$

$$OB' = OB\sqrt{e^{-A_{\perp}}} = E_O \sin\theta \sqrt{e^{-A_{\perp}}}$$

From these components, we can extract the angle of the output light polarization.

$$\tan\alpha = \frac{OB'}{OA'} = \frac{E_o \sin\theta \sqrt{e^{-A_\perp}}}{E_o \cos\theta \sqrt{e^{-A_\parallel}}} = \tan\theta \sqrt{\frac{e^{-A_\perp}}{e^{-A_\parallel}}}$$

$$(\alpha) = \tan^{-1}\left(\tan\theta \sqrt{\frac{e^{-A_\perp}}{e^{-A_\parallel}}}\right) \dots\dots\dots (16)$$

The actual rotation of polarization induced by the CNT sheets is then,

$$\text{Rotation angle, } (\omega) = \alpha - \theta \dots\dots\dots (17)$$

We used the intensity $|OA|^2$ and $|OB|^2$ experimetal values that we measured using the spectrophotometer. The analysis predicts indeed a rotation of polarization from our CNT sheets and a dependance on the angle θ.

Figure 53 shows the comparison between theoretical and experimental values of the angle of rotation of polarization. The experimental result at 45° is higher than the theoretical prediction: in the theoretical calculation, we assumed CNTs are perfectly aligned, but this is not the case experimentally. Additionally, in the experiments, the measurements of light transmission in the direction parallel and perpendicular to the tube axis are made by rotating the stage on which the sample is placed. This introduces an ~100 μm shift of the measured spot which introduces an error in the experimental evaluation of $A_\parallel$ & $A_\perp$ used for the theoretical prediction. This could be the origin of the discrepancy between experimental data and theoretical prediction. However, despite this, the theoretical values followed the experimental trend. Therefore, the hypothesis about the origin of rotation of polarization indeed coming from anisotropic absorption is corroborated by the comparison.

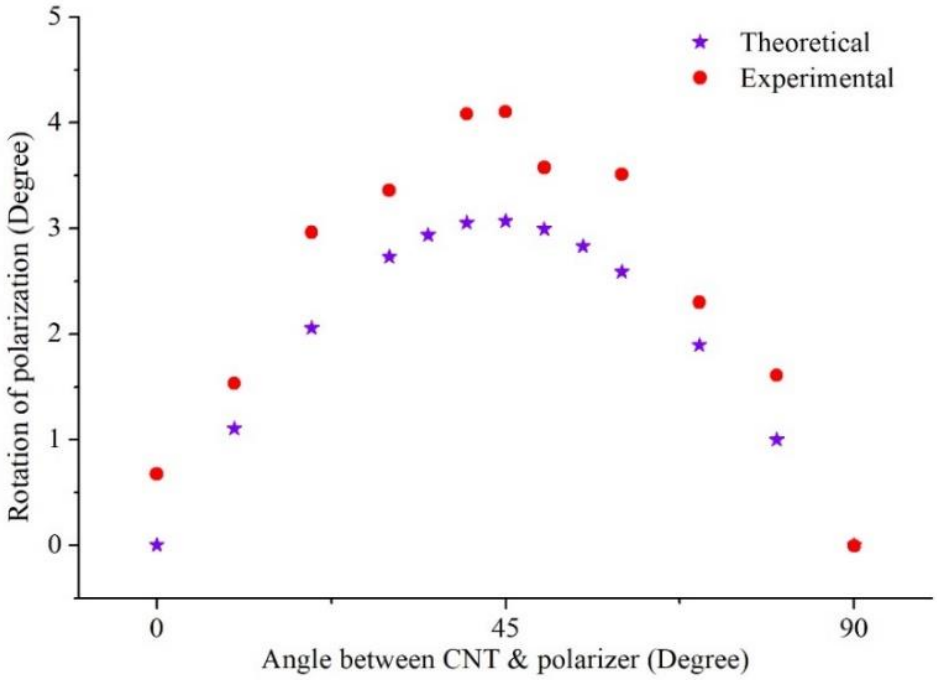

Figure 53 : Rotation of polarization, a comparison between the theoretical prediction value and experimental value.

4.5.3 Rotation of polarization as a function of CNT sheets layer

We studied how the rotation of polarization changes with the CNT sheets thickness. In this case, we increased the layer from one to seven and estimated the rotation of polarization for each layer. Figure 54 shows the rotation of polarization vs CNT sheets layers. As the thickness of the overall layer increases, the value of the rotation of polarization increases as well. The highest rotation of polarization is ~32° found for seven layers of CNT sheets. For each layer, two samples were characterized. For layer one, three, five and seven, rotation of polarization was calculated for multiple locations and the deviation indicated by the error bar.

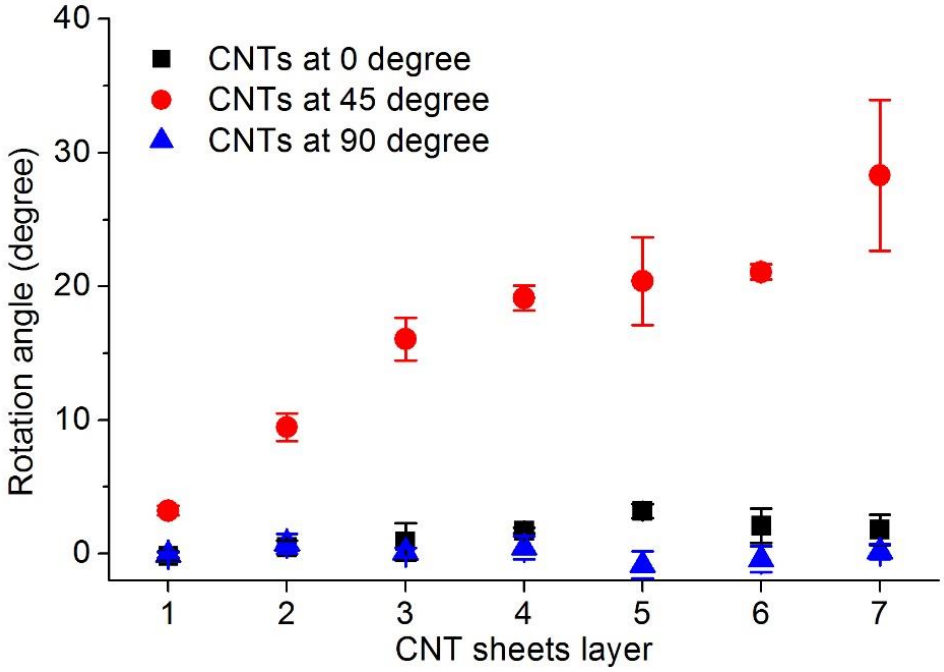

Figure 54 : Rotation of polarization as a function of CNT sheets layer

4.5.4 Rotation of polarization of the samples from batch Two

In the case of batch two, similar behaviour observed. The rotation of polarization increases as CNT sheets layer increase as shown in Figure 55. Until layer five, the increase is linear and from layer five to layer ten the increase has lower growth rate. The same behaviour was observed in the case of samples from batch one. A linear increase from layer one to three and smaller rate of increase for more layers. Also, no rotation of polarization observed when the angle between CNT sheets and polarizer 0° and 90°.

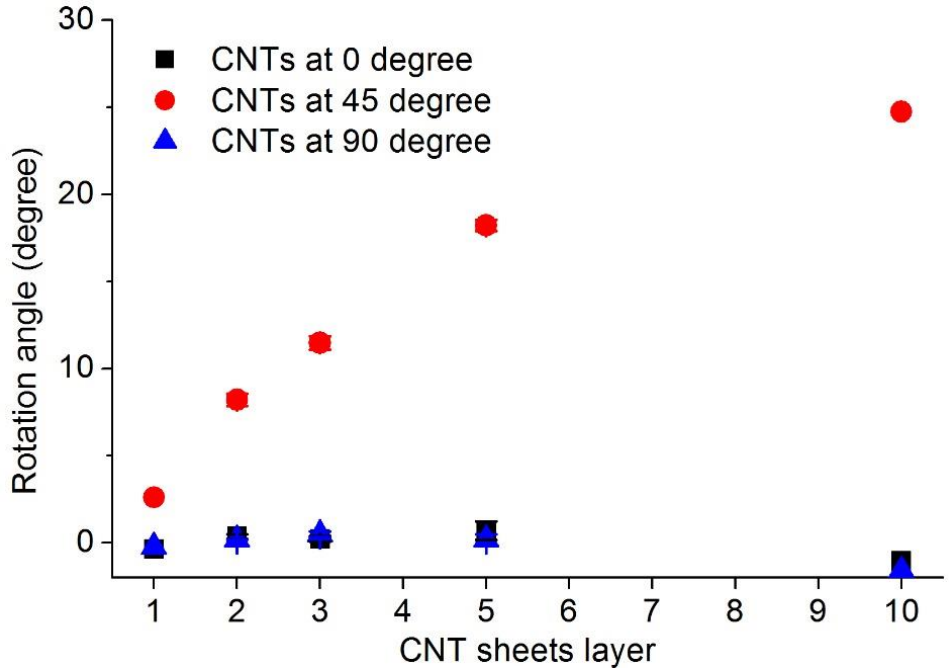

Figure 55 : Rotation of polarization as a function of CNT sheets (batch two) layer

4.5.5 Where does it rotate?

In order to understand the direction of rotation, we used the same setup (setup used for rotation of polarization experiment) with two polarizers in a parallel condition. In our experiment, we know the transmission axis of both polarizers. In the configuration one (Figure 56 (a)), the transmission axis of the CNT sheets made an angle of -45° with the polarizer transmission axis. For the other configuration (Figure 56 (b), we rotated the sample 90° to make the angle +45° between CNT transmission axis and polarizer TA. The schematic in the middle of the Figure 56 represents the reference point between CNTs TA axis and polarizer TA axis. To find the rotated light we rotated the top polarizer (analyzer) clockwise and anticlockwise. For the configuration one (Figure 56 (a)) we had to rotate the analyzer anticlockwise and for configuration two, we rotated the analyzer clockwise to find the maximum intensity. In both cases, the analyzer was needed to rotate towards CNT transmission axis to find the rotated light from CNTs. This means the light polarization is rotated by the CNT sheets toward the CNT transmission axis.

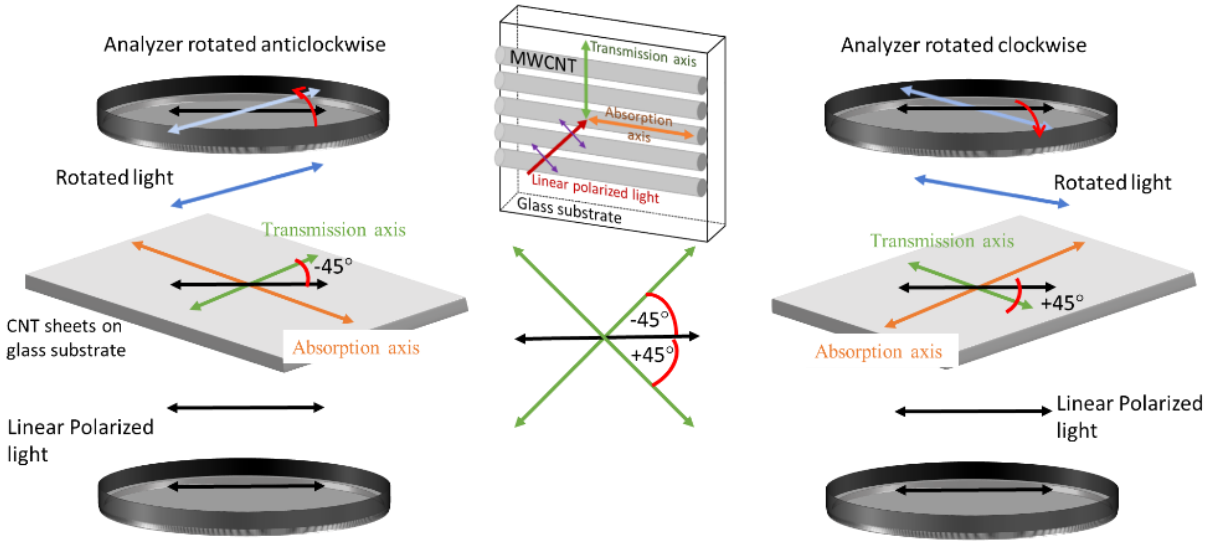

(a) (b)

Figure 56 : Schematic of the setup used to find the direction of rotated linear polarized light coming out from the CNT sheets. The transmission axis of CNT is (a) -45° (b) +45° to the input polarizer

We can find the rotated light by CNT sheets using maximum intensity analysis from the graph showing in Figure 57. We used the same experiment technique which was used to investigate the rotation of polarization by CNT sheets. In this case, we performed the same experiment twice by putting the sample at +45° and at -45° to the input polarizer. The red curve (Figure 57) represents the intensity profile of the tubes forming an angle +45° to the input polarized light. Indeed, the analyzer has to rotate clockwise (positive direction) to find the maximum intensity. On the other hand, when the sample is rotated 90° (the angle between input polarized light and the tube TA -45°), the maximum intensity is found when the analyzer is rotated in opposite direction (anticlockwise). In both cases, the analyzer was rotated towards the CNT transmission axis (see Figure 56 for analyzer and CNT transmission axis reference) which confirm the rotated polarized light is always towards the CNT transmission axis.

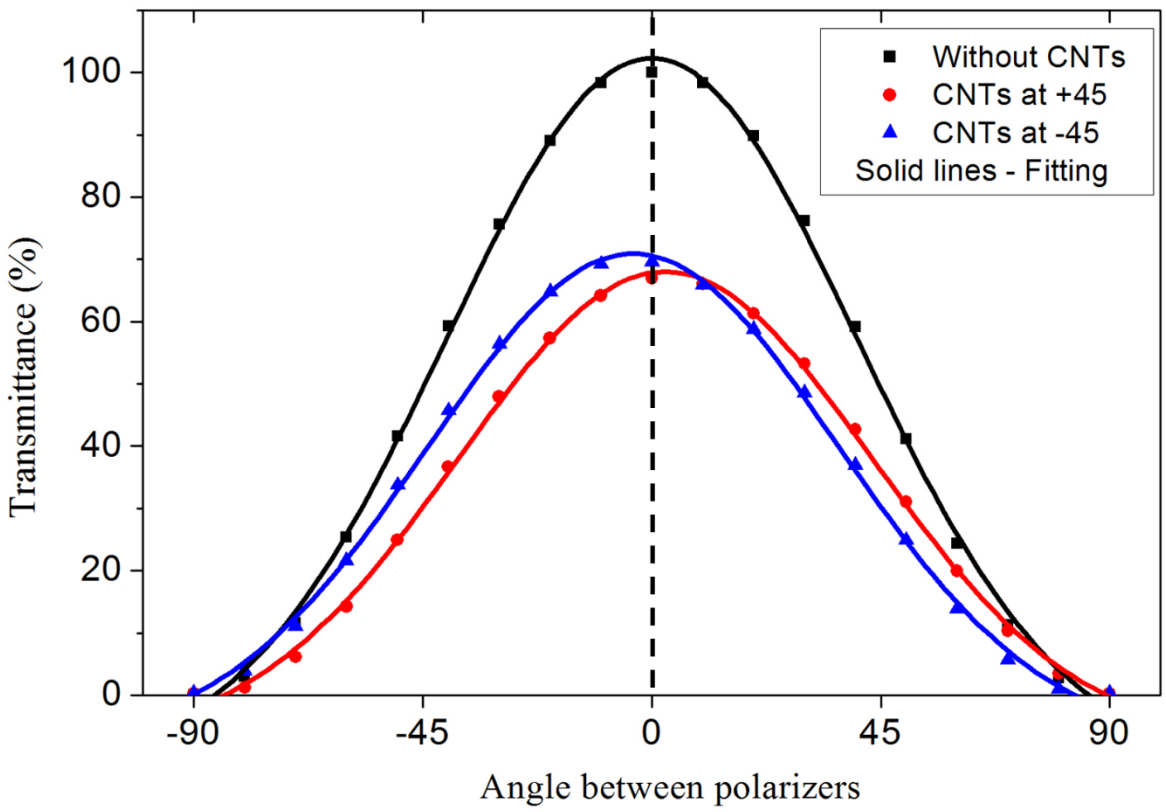

Figure 57 : Transmission from CNT sheets at +45 (red line) and -45 (blue line) to the input polarizer.

4.5.6 Visual confirmation of ROP with LC cells

Figure 58 shows a visual understanding of the rotation of polarization. Here we have used thermotropic nematic liquid crystal (5CB) in a commercial planar LC cell. The cell is then placed between two crossed linear polarizer films, on top of a white light source. The LC cell is placed in a way that the alignment of the LC director is parallel to the bottom polarizer TA. If the input polarized light either parallel or perpendicular to the LC director, the light sees only one refractive index, therefore, the light does not experience birefringence and travel though the sample without any change. The second polarizer on top of the cell which is kept perpendicular to the input polarizer simply blocks any light coming perpendicular to its transmission axis. The idea behind this experiment is to visualize the rotation of polarization by the aligned CNT sheets. To experience the birefringence the LC director must see the incoming light from at an angle other than parallel

or perpendicular to it. We used aligned CNT sheets to make that angle between the input polarized light and the LC director.

In the absence of CNT sheets, the polarized beam coming from the bottom polarizer is transmitted through the LC experiences no change and it is blocked by the second polarizer placed on top of the LC cell. Then a CNT sheet is placed between the LC cell and the bottom polarizer, having the absorption axis of CNTs parallel to the polarizer's transmission axis (middle image). As we have seen earlier, there is no rotation of polarization by the CNT sheets when CNT absorption axis is parallel to the polarizer TA, therefore, the beam will have the same polarization as before and is blocked by the second polarizer as indicated in Figure 58 left image. A scheme is also shown in Figure 58 (a) in order to show the angle between the CNTs, polarizers TA and LC director. In the case of the CNT sheets is placed at a 45° angle with the polarizer's transmission axis (Figure 58 right image), the beam experiences a rotation of ~4°. Therefore, now the angle between the LC director and the linear polarized light coming out from CNT sheets is ~4° which is enough to experience the birefringence from LC and rotates the final polarization and there is light transmission (only the part of CNT sheets) when coming out from the analyzer right image.

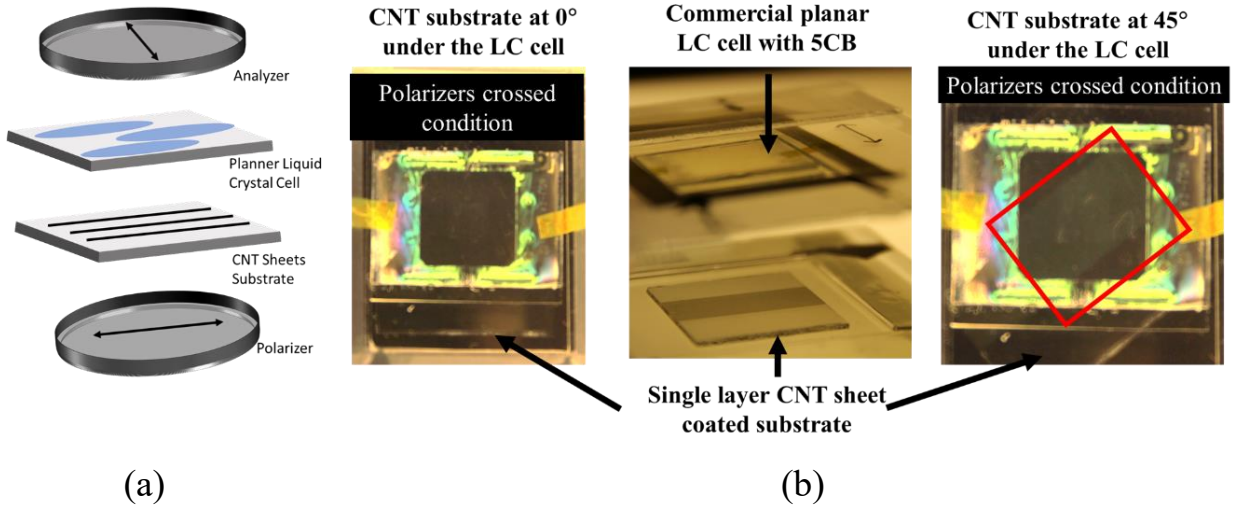

Figure 58 : (a) Scheme of the experimental setup (b) Visual presentation of rotation of polarization by the CNT sheets

A schematic shown in Figure 59 explains the rotation of polarization with liquid crystal cell. The LC optic axis is kept parallel to the polarizer hence light does not experience birefringence while travelling through LC, since the light is sees only one refractive index. However, the linear polarized light has been rotated by the CNT sheets (as we saw earlier, CNTs rotate the polarization of light when they made an angle 45° to the input polarizer) and it is not parallel to the LC optic axis anymore. The rotated linear polarized light made an angle of ~4° with the LC optic axis. Therefore, the linear polarized light sees both refractive indices and experience birefringence. Due to the birefringence, the polarization of the light coming from the LC cell is no longer perpendicular to the analyzer, therefore, we see transmission.

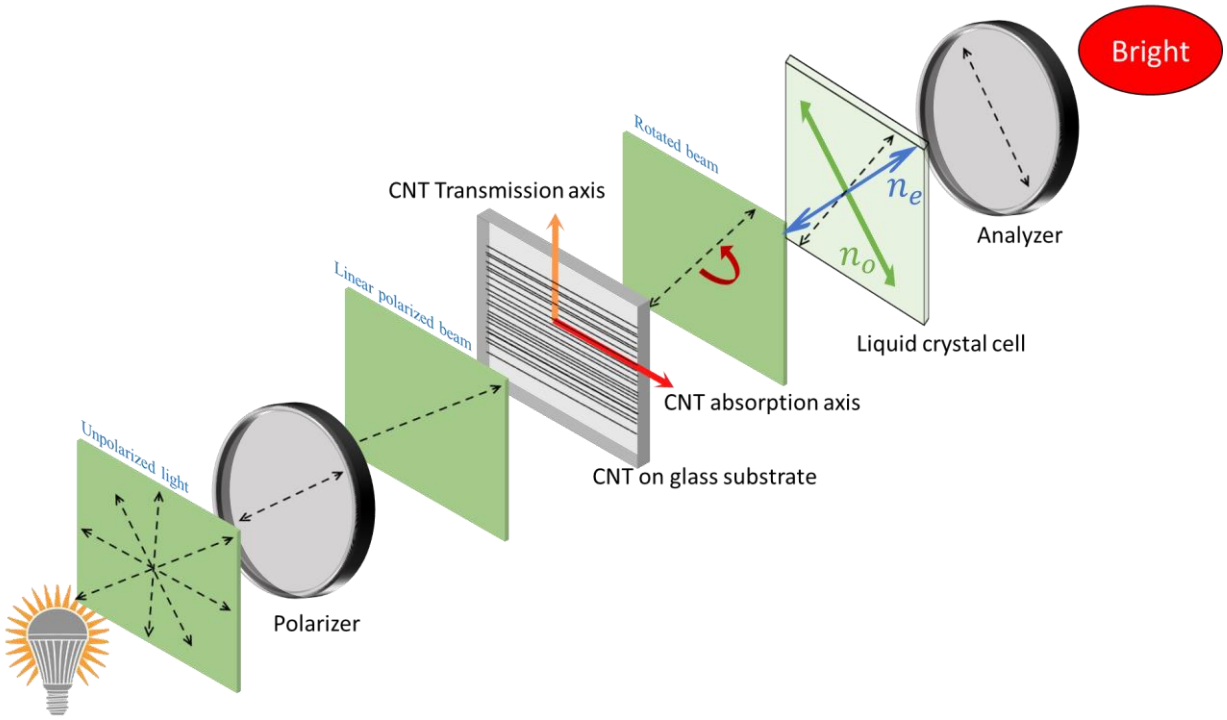

Figure 59 : Scheme of the setup used to visualize the rotation of polarization from the CNT sheets

4.5.7 The dependency of rotation of polarization on the alignment of the CNT sheets

The rotation of polarization was compared with the alignment of the CNT sheets. We calculated the rotation of polarization from our theoretical analysis (equation below) using the absorption values ($A_{\parallel}, A_{\perp}$) obtained experimentally. The same values were used to calculate the order parameter of CNT sheets.

$$(\alpha) = tan^{-1}\left(tan\theta\sqrt{\frac{e^{-A_{\perp}}}{e^{-A_{\parallel}}}}\right) = tan^{-1}\left(tan\theta\sqrt{e^{A_{\parallel}-A_{\perp}}}\right)$$

$$Final\ rotation\ (\omega) = \alpha - \theta$$

Four different locations with four different values of order parameter were chosen and the rotation of polarization was calculated accordingly. The calculated value with the comparison is shown in Table 5. Among the four points, point 4 showed the highest rotation of polarization with the highest value of order parameter. As the order parameter decreases, the rotation of polarization also decreases (point 4 to point 1). The smallest value in the rotation of polarization was found for the lowest order parameter (among four). Thus, the rotation of polarization indeed changes with the order parameter of the CNT sheets. The result suggests that the rotation of polarization can be controlled by controlling the order parameter of the CNT sheets. With a high value of order parameter, a high value in the rotation of polarization can be achieved.

Table 5: Order parameter vs rotation of polarization

Points	Order Parameter	Expected rotation of polarization
1	0.33	2.09
2	0.36	2.62
3	0.42	3.05
4	**0.44**	**3.48**

4.5.8 The dependency of rotation of polarization on the wavelength of light

Here we demonstrated the dependency of rotation of polarization (ROP) of light in three different wavelengths. Three optical filters (blue = 450 nm, green = 520 nm and red = 635 nm) were used separately to produce monochromatic light. The ROP was calculated for each filter. Figure 60 shows the degree of ROP of a single layer CNT sheets for each wavelength. Each black point represents the calculated value of ROP obtained from the local spectrophotometer. The value of the ROP is indeed different from blue to green and green to red wavelength. In case of wavelengths, 450 nm and 635 nm, the ROP values are close to each other (~3.4° and ~3.5° respectively). In the second part of the experiment, the same sample was observed but with photodiode and is represented by red points. The values obtained with photodiode were certainly different from the ones obtained using the spectrophotometer; however, almost same value of ROP was obtained for each wavelength. The small difference in value might be connected to the order parameter since the points that were observed are not in the same location. Therefore, we believe, the ROP is not wavelength dependent. Nevertheless, further investigation with laser sources and in same location (keeping the sample at fixed position) is needed to make sure that there is no influence in visible spectrum.

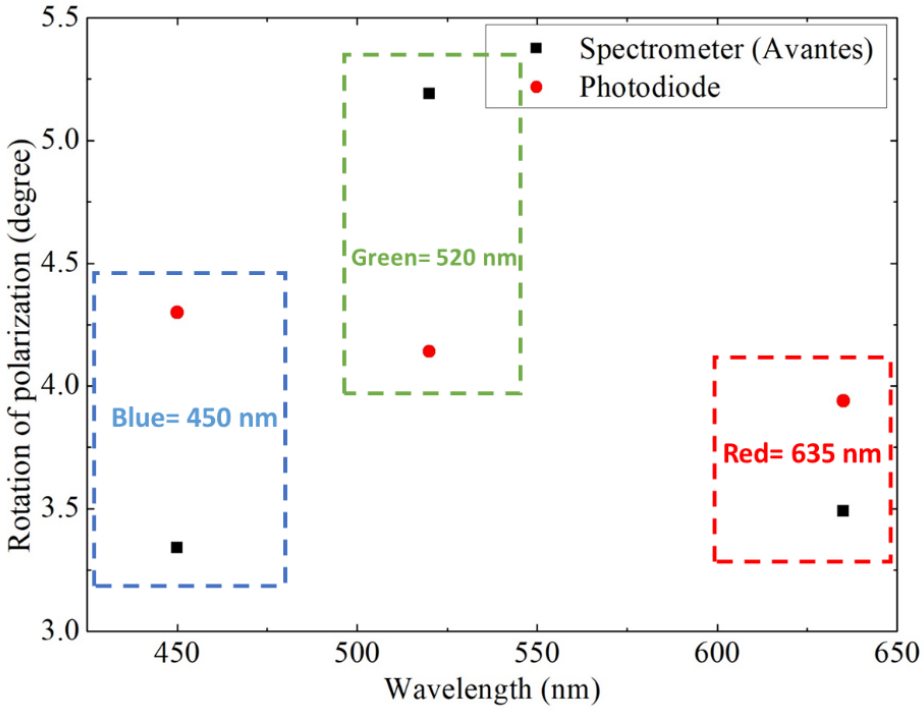

Figure 60 : Dependency of rotation of polarization on wavelength of light

4.6 CNT Polarizer

A CNT is an object with an extremely high anisotropy in dimensions. However, due to their anisotropic absorption, they are expected to be translated microscopically if nanotubes are aligned as in sheets. CNTs are very promising in research for the optical polarizer applications. Optical polarizer in visible length using single wall CNTs embedded in PVA has been reported by Shoji et al [37]. Later in 2009 Ren et al. showed polarizer for longer wavelength (terahertz) using also SWCNTs [38]. The group published another paper in Nano letters in 2012, a terahertz polarizer with 99.9% degree of polarization and ~30 dB extinction ratio [40]. However, Kyoung reported terahertz polarizer made by MWCNTs with better extinction ratio ~ 37dB (0.1 to ~2.0 THz) [39]. The aligned free standing 9 μm thick MWCNTs polarizer was made by drawing CNTs from a CNT forest.

At visible wavelength our aligned CNT sheets have no wavelength dependency, therefore, they are promising achromatic optical polarizers. We compared aligned CNT sheets with a commercial linear polarizer film made with iodine. A typical linear polarizer behaviour between the unpolarized light source and a linear polarizer is plotted in Figure 61. The width of the bell curve represents how good is the polarizer. Additionally, the minimum represents how good it is in terms of blocking light polarized in directions other than the polarizer transmission axis and maximum is how much it transmits the light coming parallel to the transmission axis. We studied from one layer to seven layers of CNT sheets. As the layer of the CNT sheets increases, the shape of the curve gets more bell shape. There is an enhancement in transmission contrast between the transmission axis and ideally full polarization blocking direction.

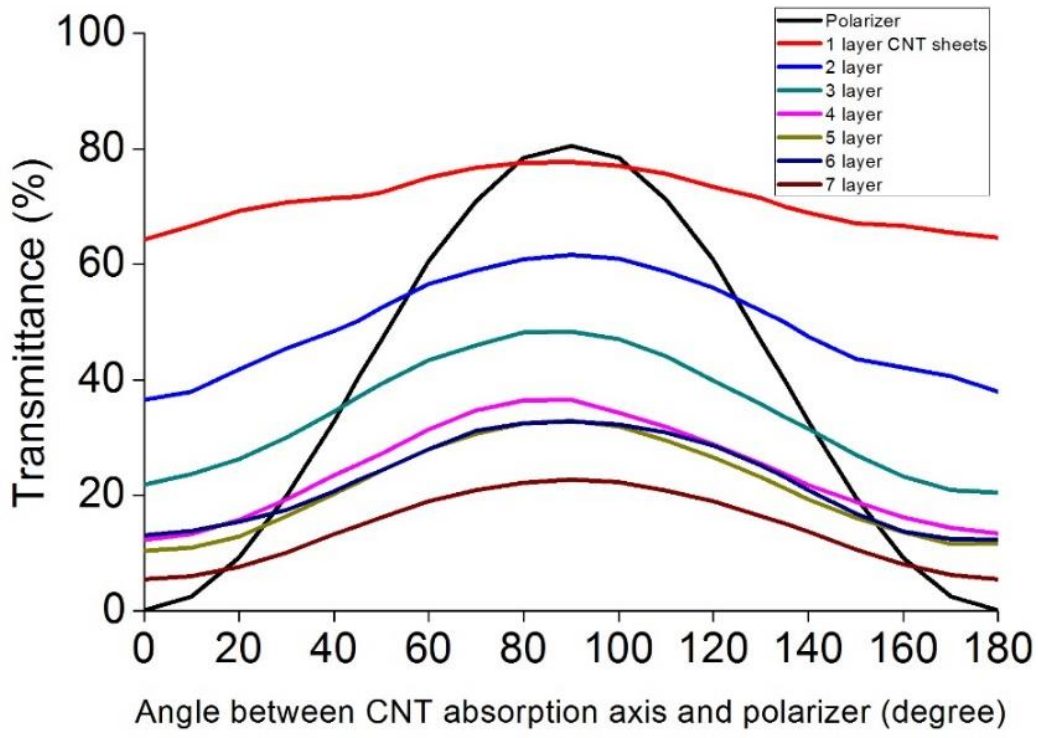

Figure 61 : Transmittance as a function of the angle between CNT sheets and polarizer

To understand how good a polarizer is, it is important to evaluate the degree of polarization (DOP) and extinction ratio. The degree of polarization quantifies what percentage of the light coming out from the polarizer is polarized. For an example, DOP is 100% for light which is perfectly polarized and 0% for unpolarized light. DOP is the ratio of the difference between the maximum and minimum transmission of the polarizer and can be calculated from the equation (18). On the other hand, the extinction ratio is defined by the ratio between maximum and minimum transmission by the polarizer. It defines the efficiency of the polarizer and typically expressed in dB. For a typical sheet polarizer film, the DOP is over 95% and the extinction ratio is 32 dB.

$$\text{Degree Of Polarization}(\%) = \frac{T_{max} - T_{min}}{T_{max} + T_{min}} * 100 \quad \ldots\ldots\ldots (18)$$

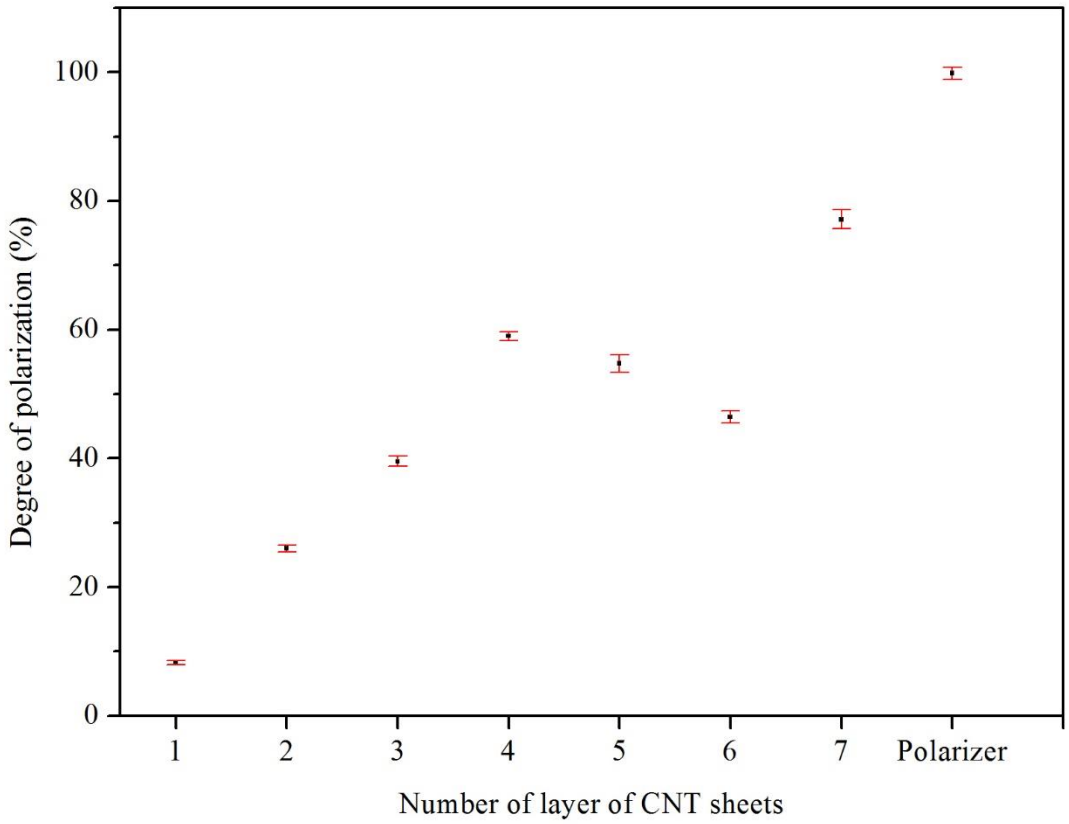

Figure 62 : Degree of polarization as a function of CNT sheets layer and comparison between CNT sheets and a commercial linear polarizer film

Figure 62 shows the degree of polarization as a function of CNT sheets layer. The compared polarizer film has DOP about ~99% while for our CNT sheets substrate with seven layers we achieved 65% of DOP. However, there is a linear growth of DOP from layer one to layer 7 which means certain thickness is needed to achieve a reasonable DOP. It's worth mentioning that the thicknesses of commercial polarizing films can range from tens of micrometers to millimeters, whereas our CNT sheets are less than a micrometer. Figure 63 shows the extinction ratio of CNT sheets and the commercial polarizer film. As mentioned earlier, the polarizer film we used to compare with our CNT sheets has an extinction ratio of ~32 dB. Compared to the polarizer film, CNT sheets have an extinction ratio of ~6 dB calculated from the equation (19). The improvement in extinction ratio is also visible in case of increasing the layer of CNT sheets. Although the ER is

way below the desirable value, we believe there is room for improving the performance in both DOP and extinction ratio for CNT sheets polarizer by improving the order parameter S.

$$\text{Extinction Ratio (dB)} = -10\log_{10}\left(\frac{T_{max}}{T_{min}}\right) \dots\dots\dots (19)$$

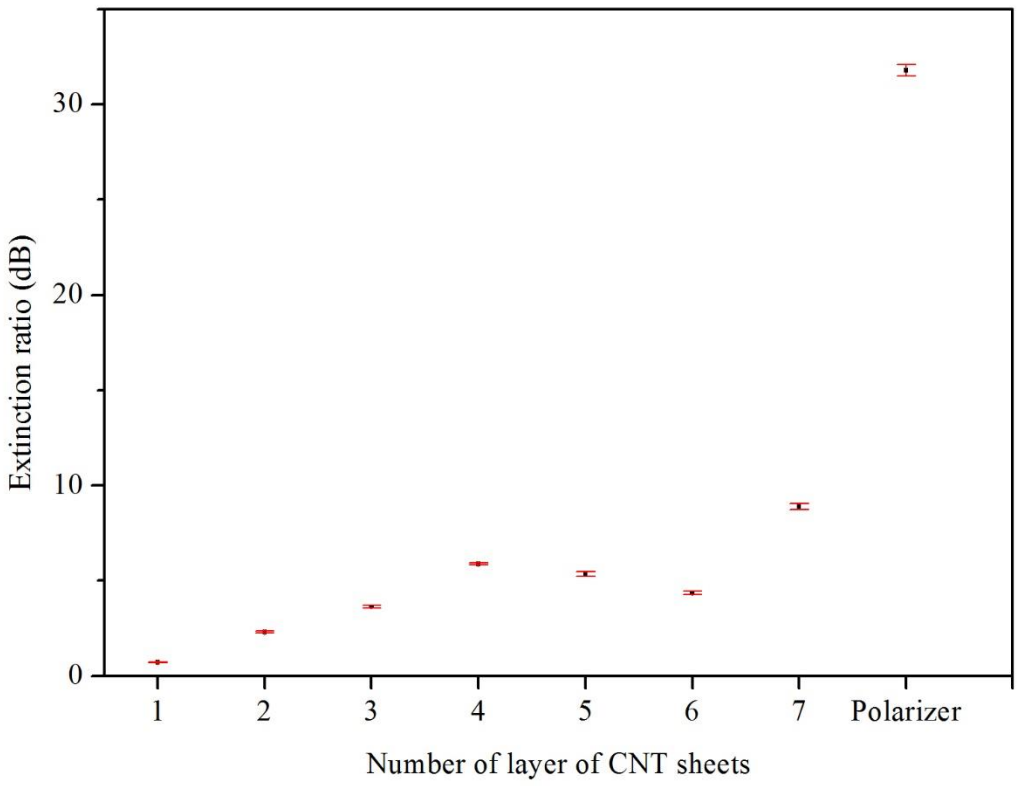

Figure 63 : Extinction ratio as a function of CNT sheets layer and comparison between linear commercial polarizer film.

4.6.1 Order Parameter vs. DOP and Extinction Ratio

We studied the relation between the order parameter and the performance of CNT sheets polarizer. The alignment of CNTs is highly connected to their optical anisotropy. The higher the optical anisotropy the better the polarizer. As we mentioned earlier, within the same sample there is variation in the order parameter. Therefore, we estimate the variation in performance in a typical

sample by performing a measurement in various position (see Figure 64) and calculated DOP and ER for a single layer CNT sheets.

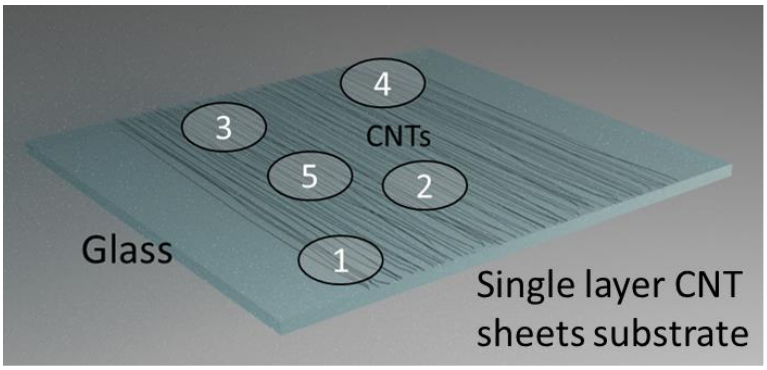

Figure 64 : Schematic of single layer CNT sheets on a glass substrate

Figure 65 shows the relationship between the order parameter, DOP and ER. We observed that the increase in order parameter also on the DOP and ER indicating the key importance of a good CNT alignment. We believe this is due to the improvement in anisotropy. However, this experiment was done in single layer CNT sheet to prove the hypothesis. We assume that a thicker CNT sheets sample with higher order parameter would improve the performance.

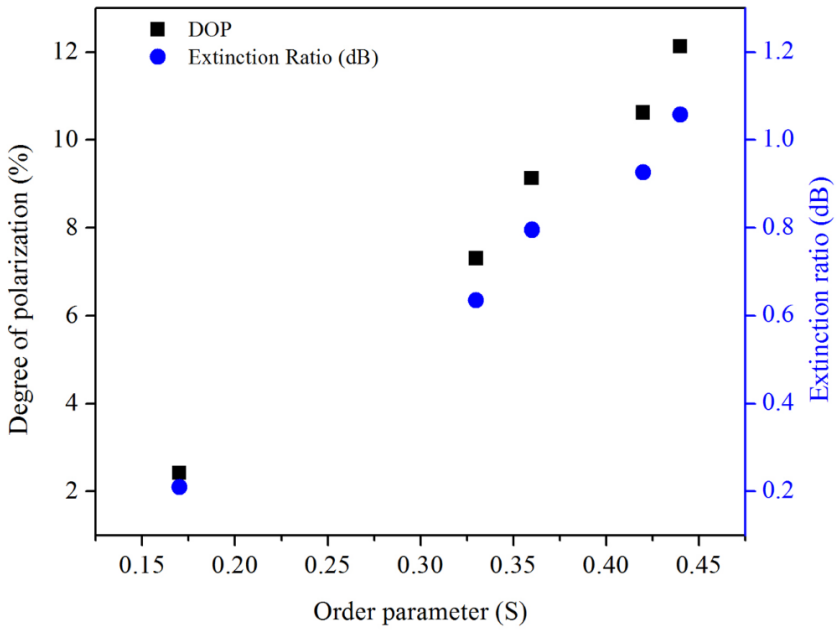

Figure 65 : DOP and ER as a function of the order parameter of single layer CNT sheets.

4.7 CNT sheets as a multifunctional layer for liquid crystal cell

Aligned CNT sheets can be used as a multifunctional layer in the liquid crystal display cell. The idea is transferring the alignment in the CNTs to the liquid crystals. If CNTs are uniformly aligned, then LC can be aligned along the CNTs alignment direction. Additionally, CNTs are highly electrically conductive, thus, can be used as an electrode layer to allow modulation of LC. Furthermore, in section 4.1, we reported the transmission of aligned CNTs. Our aligned CNT sheets can transmit over 85% of light. In a conventional LC display, there are two separate layers used for alignment and transparent electrode layer. Indium tin oxide (ITO) and polyimide (PI) were used as electrode layer and alignment layer respectively. We proposed aligned CNT sheets not only as an alignment layer but also as a transparent electrode layer for LC display devices.

As discussed in section 4.3, the adhesion of CNTs on the glass substrate was an issue. Even though ADES treatment was not enough to push down all the tubes on the surface. Therefore, when the two-glass substrates (with CNT sheets) were sandwiched to make a LC cell, there was a connection of CNTs between the top and the bottom substrate. Due to the connection of the CNTs, there was a short circuit in the cell, thus, applying an electric field for switching LC was not possible. Therefore, we coated a thin transparent dielectric layer on top of CNT sheets to address this issue. Initially, we used SiO_2 as a coating layer later Al_2O_3 used to compare and improve the performance of the cell.

4.7.1 SiO_2 as an insulation layer

In order to increase the adhesion, the substrates were treated with a hexamethyldisilazane (HMDS). HMDS is hydrophobic and we believe it will help the nanotubes to lie on the surface. To induce further flattening of the nanotubes we used ADES treatment. In order to ensure electrical insulation, a layer of SiO_2 was deposited by atomic layer deposition covering the CNT surface. The thickness of the SiO_2 layer was optimized and one with 100nm thickness provided the best results. Finally, two substrates sandwiched and filled with 4-Cyano-4'-pentylbiphenyl (5CB) nematic liquid crystal in capillary action. The schematic of the preparation and configuration of the cell are discussed in chapter three, section 3.1.5.

We studied the alignment of the LC using a polarizing optical microscope with crossed polarizers. Figure 66 shows the alignment of the LC at 45° between crossed polarizers. We compared the alignment of our CNT-based LC cell with commercial LC cell which is typically a rubbed polymer layer. Compared to commercial cells, our CNT-based cell has uniform planar alignment of LC over the sample as shown in the Figure 66 (a). We believe the origin of the unidirectional alignment is from the grooves formed by the CNT sheets.

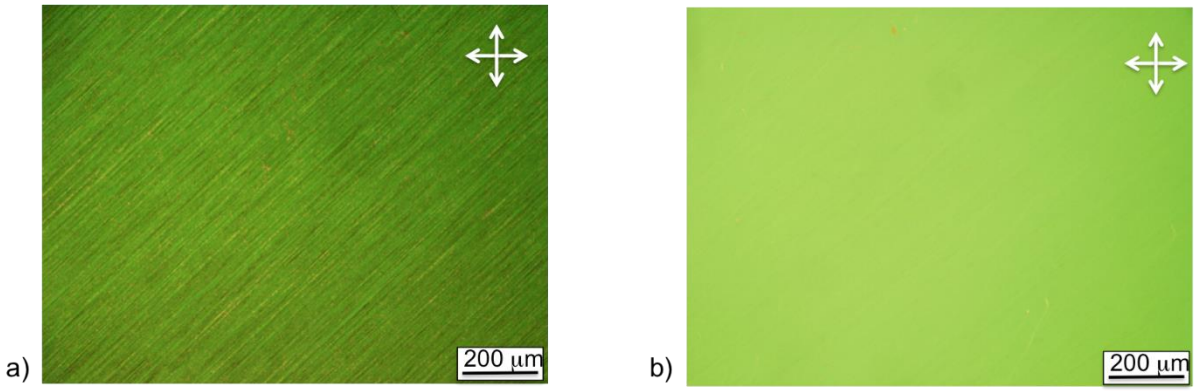

Figure 66 : POM image of 5CB LC in (a) cell made with substrates CNT sheets and SiO_2 with CNT orientation at 45° with respect to the crossed polarizers and (b) in a commercial cell with rubbed polymer from EHC.

4.7.2 Al_2O_3 as an insulation layer

The CNT cell with Al_2O_3 has the same configuration as CNT-SiO_2LC cell discussed earlier. The SiO_2 layer was replaced by Al_2O_3. However, we optimized the thickness of Al_2O_3 at 60 nm which is 40 nm less than SiO_2. A uniform and homogeneous planar LC alignment was also achieved with CNT-Al_2O_3 cell. The POM image demonstrates the alignment of the cell represented in the Figure 67.

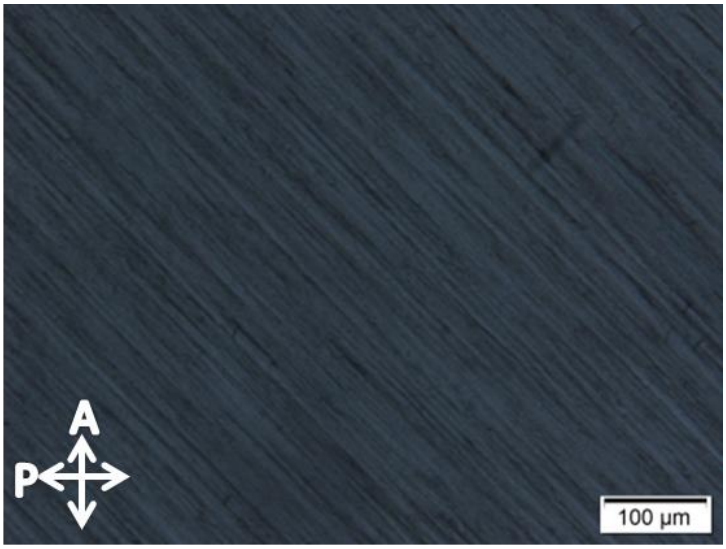

Figure 67 : POM image of alignment of the LC in a CNT-Al_2O_3 cell under crossed polarizers

4.8 Switching of the liquid crystal in CNT sheets based LC cell

We studied the switching behaviour of our proposed CNT based LC cell. The POM image in Figure 68 shows the switching behaviour of the cell. Left image without an electric field and the right image with an electric field. At application of 20 V, 1 kHz alternating current the cell becomes dark and there is no leakage (transmittance) present after the complete switching of LC. This means the electric field is uniform all over the sample. This process is reversible. After removing the electric field, the original alignment of LC was recovered.

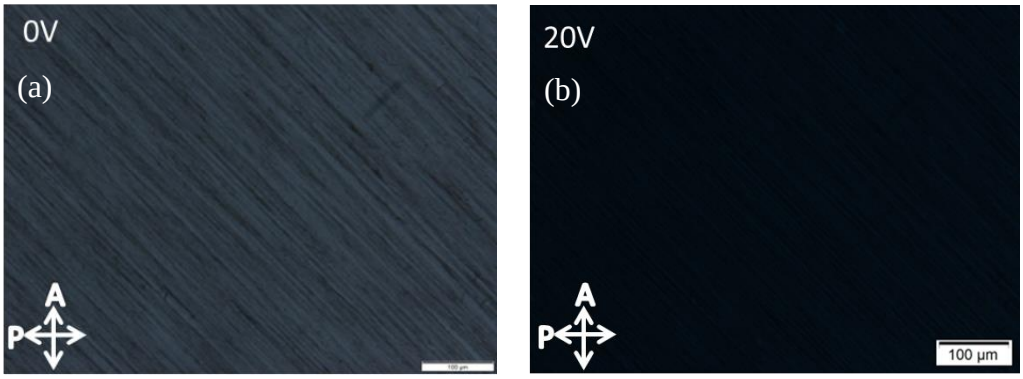

Figure 68 : POM image of the LC in a CNT-Al_2O_3 cell under crossed polarizers. (a) without electric field (b) the cell under the AC electric field

Figure 69 shows the voltage vs transmittance of the LC cell. The cell was placed between crossed polarizers at 45° (highest transmission). The AC field with 1 kHz frequency (square wave) increases amplitude with the resolution of 0.25 V from 0 V until 12 V. As the voltage increases the transmittance decreases and gets stable at zero transmission, indicating that all the LC in the cell align homeotropically. Then we decrease the voltage with the resolution of 0.25 V from 12 V until 0 V and recorded the transmittance. Transmittance vs both increasing (Figure 69 (a)) and decreasing (Figure 69 (b)) voltage is plotted in Figure 69. The decreasing and increasing curves of transmittance with change in voltage coincide with each other; thus, no hysteresis is presence.

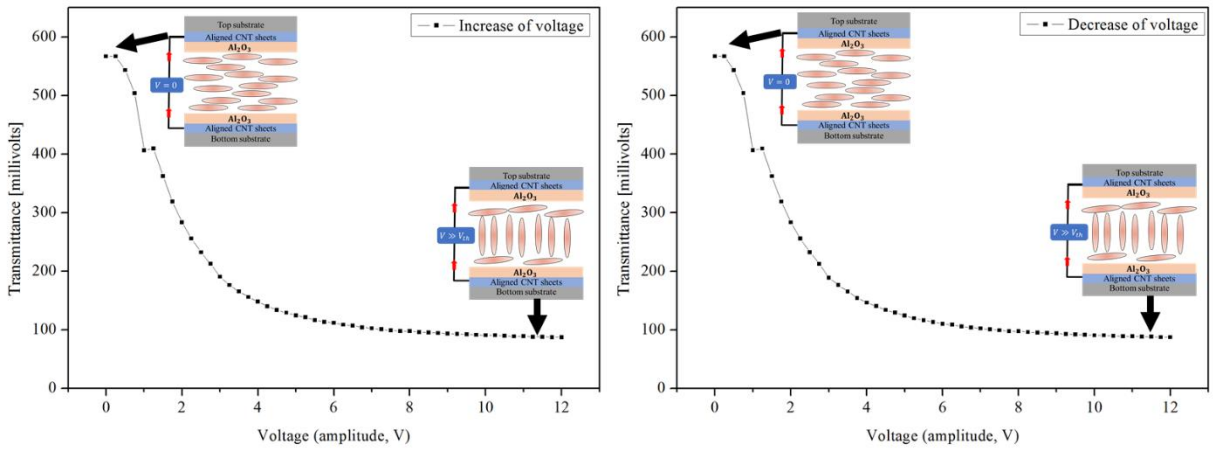

(a) Increasing (b) Decreasing

Figure 69 : Transmittance of CNT-Al_2O_3 LC cell as a function of voltage.

4.8.1 Rise and Decay time

The response time was characterized by studying the rise time and decay time of the LC by applying and removing the electric field respectively. We calculated the time needed to switch the LC (from bright to dark) represent as rise time and time needed for LC going back to initial alignment represent as decay time. For this, we used a voltage above threshold with 1 kHz square wave AC field and recorded the transmission. The duration of the AC voltage (both ON and OFF) was 500 ms was chosen for ensuring saturation of orientation. The Figure 70 shows the transmittance during the voltage on and off in Y-axis and time in X-axis. When the voltage was switched ON, the transmittance changes from bright to dark. We then calculated how much time

was needed for the transmittance to change from bright to dark. We did the same after removing the voltage.

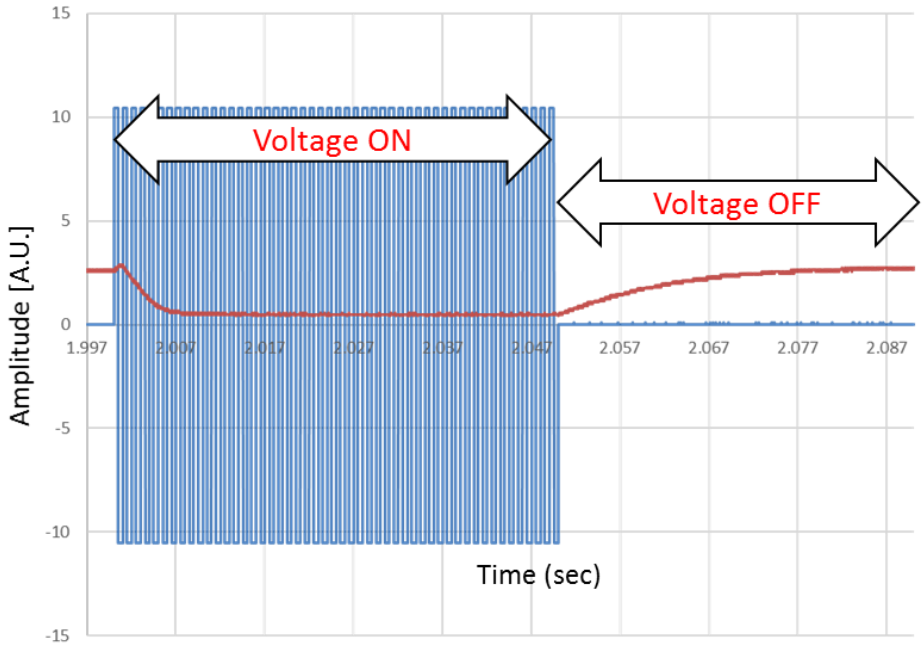

Figure 70 : Applied waveform and optical transmission of the LC cell. Time needed to change is transmittance when the electric field switch ON and OFF.

To compare the performance of our CNT based LC cell we choose a commercial planar LC cell. The commercial LC cell has 10 μm cell gap including planar alignment with polyimide. We characterize the commercial cell in the same way as the CNT based LC cell. The calculated rise and decay times for both cells are represented in the following Table 6. Compared to the commercial LC cell, the rise time is longer in our CNT base LC cell. However, the decay time is lower than a commercial cell. We believe this is due to the anchoring energy of the LC on the Al_2O_3 surface. We assume that the Al_2O_3 surface has strong anchoring energy; therefore, it takes a longer time to switch the liquid crystal parallel to the electric field. Additionally, due to the strong anchoring between LCs and Al_2O_3, as soon as the applied electric field is removed, the LCs are restored to original alignment. This means that one could consider an effective increase of the elastic constant in equation 8: this might be produced through an increase in anchoring strength, although it is not obvious how this can be implemented in the response time. However, we cannot exclude other origin of the decrease of the decay time not clear at the moment.

Table 6: Rise and decay time of commercial and CNT-Al_2O_3 LC cell

Cell name	Voltage ON (rise) (ms)	Voltage OFF (decay) (ms)
10 μm commercial LC cell	5.12	81.94
11μm Al_2O_3	11.74	39.34

4.9 Heating Effect from CNT sheets

We have observed there are small heating effects generated by the CNT sheets when the external voltage is applied in the typical configuration of LC cells as the one used before. We have established this noticing that the application of electric fields on CNT electrodes can induce a phase transition in 5CB LC depending on the temperature of the LC. Fields above the Fredericks threshold results in homeotropic alignment of the LC but this observed effect is not field induced. An increase in electric field or frequency induced a nematic to isotropic transition, which we assume as Joule heating from CNT sheets. Indeed, the external applied voltage difference is across the sample and there is no physical connection between the top and the bottom substrate (see Figure 71 for the electric connections). The Joule heating is, therefore, expected as being induced from the same CNT plane assumed at the same potential.

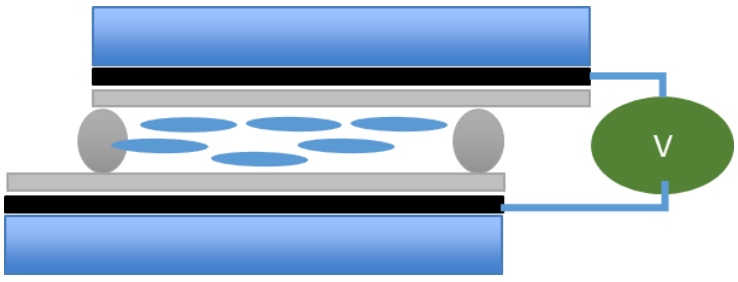

Figure 71 : Schematic of CNT-SiO_2 LC cell with the electrical wire connection

The heating from CNT sheets was confirmed by POM image, see the Figure 72. For example, application of 15 V and 1 kHz, 100 kHz and 10 kHz, tend to align LC normal to the substrate however bringing the LC close to the phase transition after increasing frequency 10 times which

is 100 kHz instead of the realignment of LC, phase transition occurs as shown in Figure 72 (a). After removing voltage, isotropic to nematic transition was observed, which is shown in Figure 72 (b) which confirms the heating generation from CNT sheets.

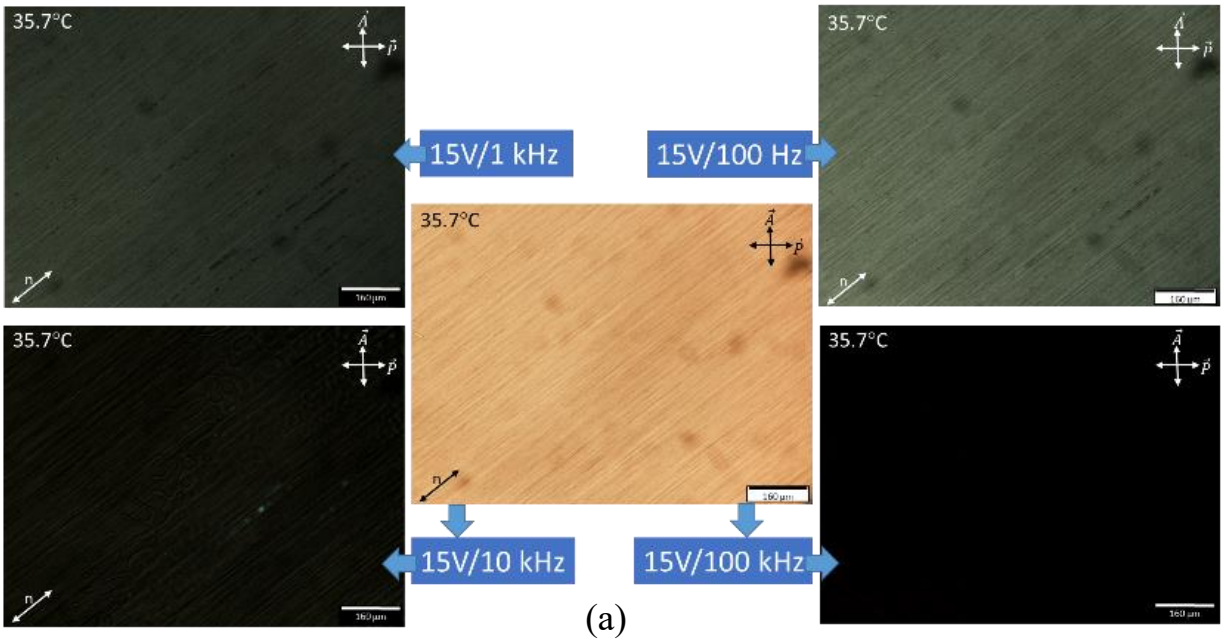

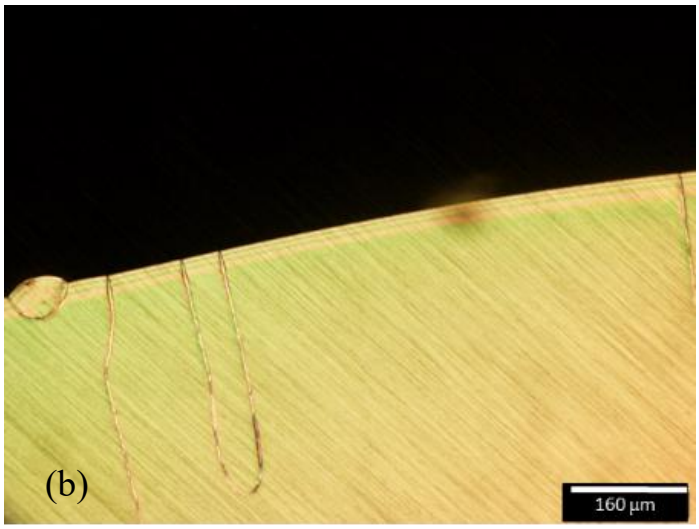

Figure 72 : (a) POM images under application of electric fields (b)Transition I ➔ N obtained switching OFF the electric field at a T= 35.7°C

To investigate the heating effect, the LC was heated first to a temperature 0.3°C lower than the measured nematic-isotropic transition temperature (36°C) and then electric field was applied obtaining a field-induced phase transition. This experiment was then repeated by decreasing the temperature in 0.3°C steps from 36°C to 35°C. It was identified that heat generation is voltage- and frequency-dependent; therefore, voltages of 0 to 50 V (amplitude) at four different frequencies (100 Hz, 1 kHz, 10 kHz and 100 kHz) were applied to the cell. The time needed for inducing the transition was also measured in our study.

4.9.1 Heat Induced by Voltage

At high frequency (100 kHz), a minimum voltage of 10 V was required to induce the N-Iso transition occurring in 7.5 s. On the other hand, at a lower frequency (100 Hz), a voltage of 20 V was required to induce the same effect, but the transition needed a slightly longer period (11 s). The time needed for inducing the transition appears to be connected to the heat transferred to or from the LC. The graphs shown in the Figure 73, demonstrate the time needed for inducing the transition at different voltages for different frequencies (100 Hz, 1 kHz, 10 kHz and 100 kHz). The LC temperature here referred to as background temperature (BT) which was controlled by the external temperature controller for the heating stage. The minimum voltage to induce the N-Iso transition clearly changes with BT. For example, at a frequency of 10 kHz, the minimum voltage needed for the phase transition shifted by at least 5 V for every 0.3°C change in BT, which is not the case for 100 Hz and 1 kHz. In case of 10 V/100 kHz, the N-Iso. transition was induced at every investigated BT, meaning that, with these parameters, more than 1°C was produced.

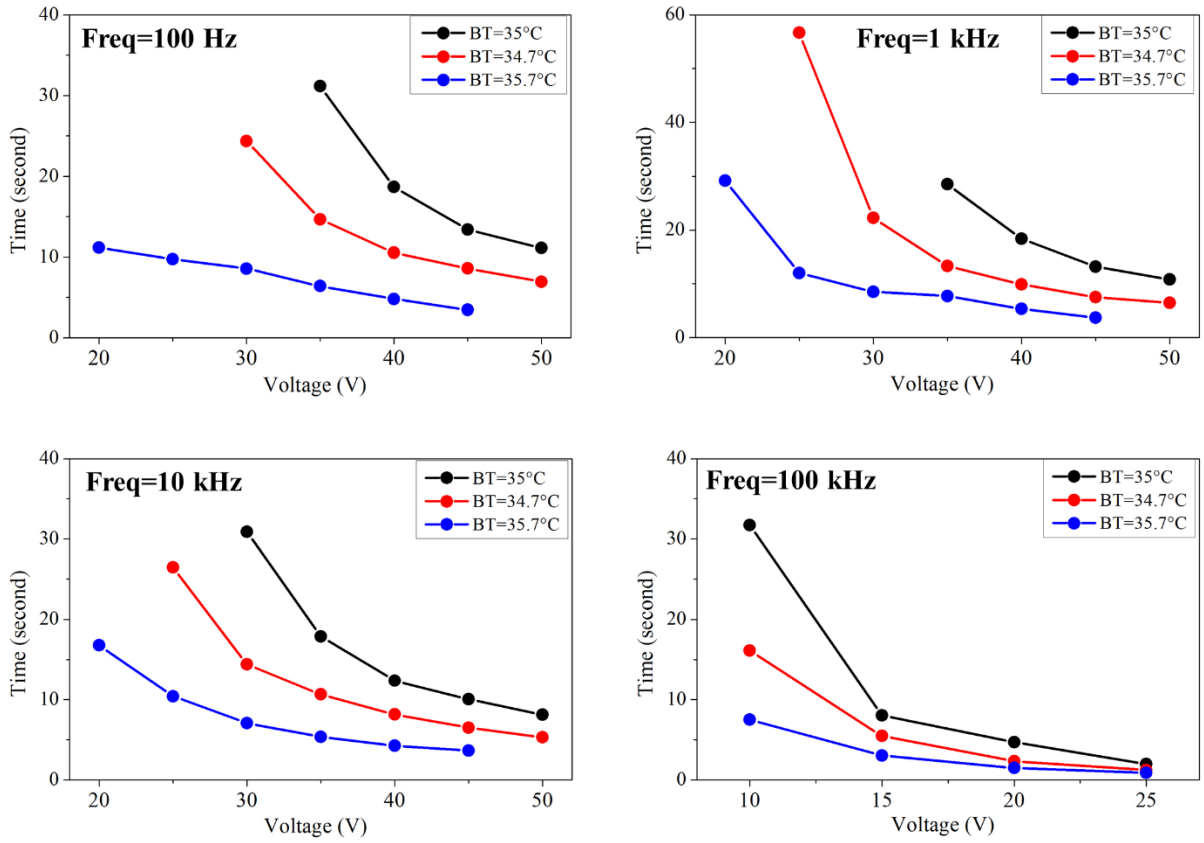

Figure 73 : CNT heat generation as a function of voltage.

4.9.2 Role of Frequency

In the case of BT= 35.7°C phase transition, thus, heat generation started from 20 V at low frequencies (100 Hz) but only 10 V were needed at higher frequencies (100 kHz). At a frequency of 100 kHz, lower voltage and shorter time are needed to induce N-Iso transition compared to other frequencies. The effect from 100 Hz to 10 kHz is similar in terms of voltage and time. The heating effect was also found in a commercial ITO-coated cell (from EHC Co.), but only at high frequencies (100 kHz) and starting from 10 V. The times for obtaining the transition both in heating and cooling were measured and showed here in two different graphs in Figure 74. From cooling, in case of BT= 35°C, the phase transition Iso to nematic takes ~23s upon application of 25V/100 kHz, which indicates the temperature induced by CNT in this configuration is more than 2°C.

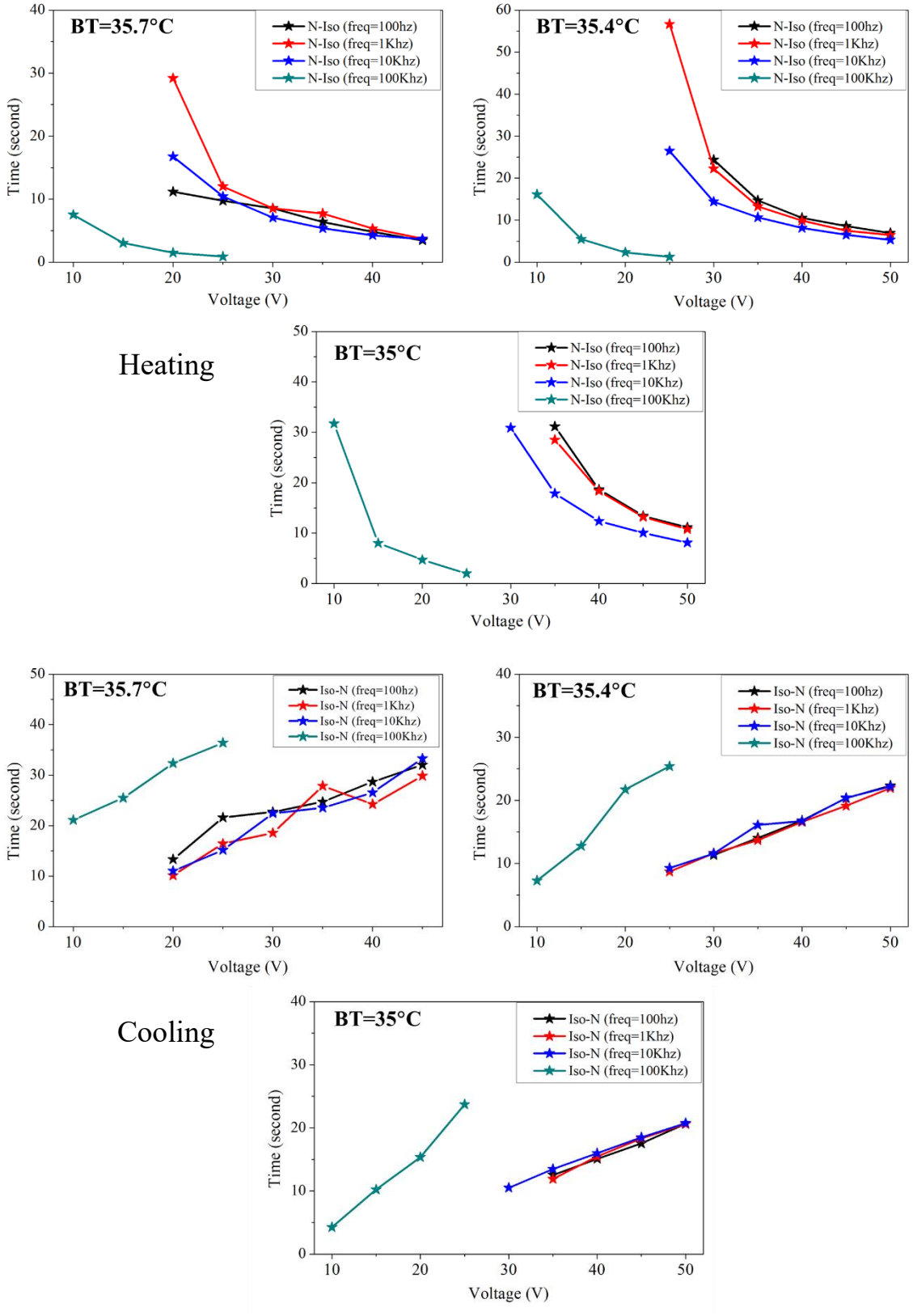

Figure 74 : CNT sheets heat generation as a function of frequency.

Chapter Five

Conclusions

Anisotropic absorption of aligned CNT sheets

We have performed optical investigations at visible wavelength of layers formed by sheets of aligned MWCNTs. Moreover, the optical absorption of CNT sheets along the transmission and absorption directions of aligned CNTs was investigated. The anisotropic transmittance for a single layer CNT sheets was found ~16%. The highest anisotropy found for three layers ~32%. Despite being a very thin layer (in nanometer scale) with some orientational misalignment, an anisotropic response in absorption is clearly visible. In addition, the optical features are quite reproducible indicating that the degree of order is not only fairly similar in all the samples, but also similar for different length scales.

Orientational order parameter and adhesion of CNT sheets on a substrate

The drawing of aligned CNT sheets from vertically aligned CNT forest is simple, yet a stable and good deposition on a substrate presents problems due to lack of uniform and strong adhesion of the CNT sheets. We have investigated polymer-nanotube substrates to improve the adhesion and stability. Slightly lower orientational order was found on polymer films compared to bare glass substrate. CNT sheets either on glass substrate or on polymer surface, all showed lack of perfect flatness and adhesion which could be overcome by using a solvent treatment with ethanol refereed as ADES treatment, as mentioned earlier. Indeed, the ADES treatment increases the flatness and improves the adhesion; however, it decreases the orientational order. The highest order parameter was found for free standing CNT sheets (as pulled from the forest) and the orientational order decreases as deposited on a substrate and decreases further with the ADES treatment. For a single layer of free-standing CNT sheets, the order parameter was calculated S = ~0.6. The order parameter in values further decreases to S = ~0.5 after transferring it to a glass substrate. Finally, our ADES treatment reduces the order parameter to S = ~0.4.

Even if the alignment generally decreased on polymer surface, there is a detectable difference between the types of polymer. We can assess that, among the polymers, PMMA gives better results in terms of order parameter compared to PVA and PVP after the ADES treatment. Despite the reduction in order parameter after ADES treatment, the CNT sheets on the polymer were able to align the liquid crystal as visible in the Figure 75 below for LC (5CB) filled into a sandwiched cell prepared with two PMMA-CNT sheets-coated substrates. In the regions where just polymer is present no unidirectional alignment is observed (no change in the brightness while rotating the cell) confirming the alignment of LCs in only due to the nanotube sheets. Even if the nanotubes were not perfectly ordered, the overall CNT sheets were able to align homogenously the nematic LC. Nevertheless, efforts need to be addressed for improving the adhesion while keeping the orientational order as high as possible.

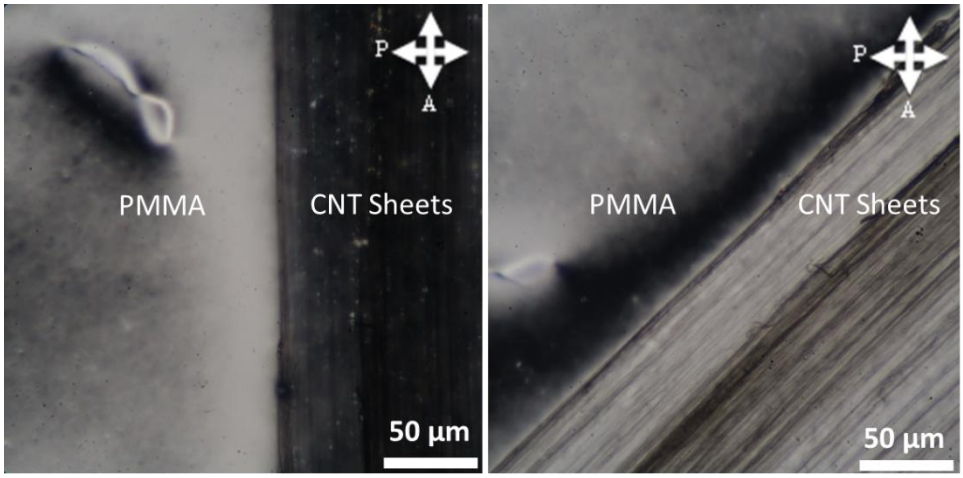

Figure 75: Polarizing optical microscopy images for two angular positions a) 0° and b) 45° with respect to the crossed polarizers. 5CB LC aligns planarly and unidirectionally in the areas with CNTs revealed by the dark and bright appearance of the LC at the two angular positions, while no preferential direction is observed on the bare polymer (PMMA) as expected.

In a separate investigation of CNT sheets coated with transparent insulating layer (SiO_2) showed a higher value in order parameter ~0.66 compared to previous experiment on other bare samples. The origin of higher order parameter is not clear to us yet. Although this indicates that deposited CNTs can have indeed higher order than we typically measured. Nevertheless, at the present stage,

we cannot control the best condition to acquire the high level of alignment. Further experiments are needed to improve the CNT alignment monitoring the order parameter before and after the deposition of SiO_2 and other coating films. This study is needed to investigate the origin and mechanism of improvement in orientational order of aligned CNT sheets.

Rotation of polarization of linearly polarized light from aligned CNT sheets

We have presented experimentally the rotation of polarization induced by the aligned MWCNT sheets. Additionally, our theoretical approach based on anisotropic absorption showed that the rotation of polarization is likely due to the anisotropic absorption of CNT sheets. The rotation of polarization from aligned MWCNT sheets is indeed an interesting, meaningful and one of the main findings of this thesis. The maximum rotation of polarization observed when the angle between CNT sheets and input polarization of light is 45°. No rotation of polarization was observed when CNT sheets are either parallel or perpendicular to the input polarization of the light. For a single layer of aligned CNT sheets, we found experimentally a maximum of ~4° and from our model ~3° of rotation of polarization. An increase in rotation of polarization by aligned CNT sheets was also observed by increasing the thickness of the film by depositing a layer on top of another layer. The highest rotation of polarization found for seven layers is ~32°. We also established the direction of the rotated light. From our experimental results, the rotation occurs towards the CNT transmission axis. We believe that this study will help to integrate and design more efficiently and accurately CNTs in optical devices such as alignment layer and transparent electrodes for LC displays.

Aligned CNT sheets as multifunctional layer for liquid crystal displays

The uniform unidirectional orientation of carbon nanotubes and their density in sheets are capable of aligning liquid crystals. Despite the good alignment of the nanotubes, it is possible to observe by e.g. SEM that several tubes or bundles curl and deviate from the straight direction either in the plane, horizontally as well vertically, resulting in tubes out of the plane that can further deteriorate the alignment or create problems in electro-optic operation of LC cell. We have improved these aspects by enhancing the adhesion of the nanotubes with the substrates and an ethanol treatment that greatly improved the flatness of the sheets. The tubes that still stayed dangling were

immobilized by coating of SiO_2 or Al_2O_3 or polymer. Despite the decent alignment of LC, several defects in LC can be observed by POM associated to particularly bad alignment of CNTs and aggregates from the organic coatings. The CNT sheets are attractive as aligning layer, nevertheless, the quality of the alignment has to be enhanced to limiting the effect of out-of-plane nanotubes, thus, reducing or eliminating the need of covering layers. We could then better explore the other functionalities useful for LC displays.

A single-layer CNT sheet, which was integrated into a nematic LC display cell, not only functions as an aligning layer but also as a transparent electrode layer, simultaneously. We experimentally demonstrated that the unidirectional alignment feature of a CNT sheet passivated by an alumina or SiO_2 thin film could induce LC switching. The electro optic performance was dependent on the type of coating. Alumina showed good performance with successful electro-optical operation, and with fast decay time at room temperature under the application of AC electric fields. We also found that undesirably CNT sheets produce heat establishing the frequency and voltage dependence. The effect, however, was estimated to a couple of degrees, thus, small enough not to influence negatively the LCD performance. These results suggest a bright avenue for the future development of high performance LC display devices and different new types of flexible and stretchable LC displays in particular.

References

1. Jiang, K., Q. Li, and S. Fan, *Nanotechnology: Spinning continuous carbon nanotube yarns.* Nature, 2002. **419**(6909): p. 801-801.
2. Zhang, M., et al., *Strong, Transparent, Multifunctional, Carbon Nanotube Sheets.* Science, 2005. **309**(5738): p. 1215.
3. Kroto, H.W., et al., *C60: Buckminsterfullerene.* Nature, 1985. **318**(6042): p. 162.
4. Iijima, S., *Helical microtubules of graphitic carbon.* Nature, 1991. **354**: p. 56.
5. Geim, A.K. and K.S. Novoselov, *The rise of graphene.* Nature Materials, 2007. **6**: p. 183.
6. Hirsch, A., *The era of carbon allotropes.* Nature Materials, 2010. **9**(11): p. 868.
7. Iijima, S., *Carbon nanotubes: past, present, and future.* Physica B: Condensed Matter, 2002. **323**(1-4): p. 1-5.
8. Iijima, S., *Helical microtubules of graphitic carbon.* Nature, 1991. **354**(6348): p. 56.
9. Iijima, S. and T. Ichihashi, *Single-shell carbon nanotubes of 1-nm diameter.* Nature, 1993. **363**(6430): p. 603.
10. De Volder, M.F., et al., *Carbon nanotubes: present and future commercial applications.* Science, 2013. **339**(6119): p. 535-539.
11. Pan, Z., et al., *Very long carbon nanotubes.* Nature, 1998. **394**(6694): p. 631.
12. Zhu, H., et al., *Direct synthesis of long single-walled carbon nanotube strands.* Science, 2002. **296**(5569): p. 884-886.
13. Hu, L., D.S. Hecht, and G. Gruner, *Carbon nanotube thin films: fabrication, properties, and applications.* Chemical reviews, 2010. **110**(10): p. 5790-5844.
14. Cheung, W., et al., *DNA and carbon nanotubes as medicine.* Advanced Drug Delivery Reviews, 2010. **62**(6): p. 633-649.
15. Hamada, N., S.I. Sawada, and A. Oshiyama, *New one-dimensional conductors: graphitic microtubules.* Physical Review Letters, 1992. **68**(10): p. 1579.
16. Saito, R., et al., *Electronic structure of graphene tubules based on C 60.* Physical Review B, 1992. **46**(3): p. 1804.
17. Wilder, J.W., et al., *Electronic structure of atomically resolved carbon nanotubes.* Nature, 1998. **391**(6662): p. 59.
18. Stavarache, I., et al., *Electrical behavior of multi-walled carbon nanotube network embedded in amorphous silicon nitride.* Nanoscale research letters, 2011. **6**(1): p. 88.
19. Attaf, B., *An Eco-approach to boost the sustainability of carbon nanotube-based composite products.* Research and Innovation in Carbon Nanotube-Based Composites, Word Academic Publishing-Advanced in Materials Sciences and Applications: p. 1-14.
20. Rao, C.N.R., R. Voggu, and A. Govindaraj, *Selective generation of single-walled carbon nanotubes with metallic, semiconducting and other unique electronic properties.* Nanoscale, 2009. **1**(1): p. 96-105.
21. Mubarak, N.M., et al., *An overview on methods for the production of carbon nanotubes.* Journal of Industrial and Engineering Chemistry, 2014. **20**(4): p. 1186-1197.
22. Endo, M., T. Hayashi, and Y.A. Kim, *Large-scale production of carbon nanotubes and their applications.* Pure and Applied Chemistry, 2006. **78**(9): p. 1703-1713.

23. Zhang, Q., et al., *Carbon nanotube mass production: principles and processes.* ChemSusChem, 2011. **4**(7): p. 864-889.
24. Truong, T.K., Y. Lee, and D. Suh, *Multifunctional characterization of carbon nanotube sheets, yarns, and their composites.* Current Applied Physics, 2016. **16**(9): p. 1250-1258.
25. Murakami, Y., et al., *Polarization dependent optical absorption properties of single-walled carbon nanotubes and methodology for the evaluation of their morphology.* Carbon, 2005. **43**(13): p. 2664-2676.
26. Ichida, M., et al., *Anisotropic optical properties of mechanically aligned single-walled carbon nanotubes in polymer.* Applied Physics A, 2004. **78**(8): p. 1117-1120.
27. Hwang, J., et al., *Polarized spectroscopy of aligned single-wall carbon nanotubes.* Physical Review B, 2000. **62**(20): p. R13310.
28. He, X., et al., *Wafer-scale monodomain films of spontaneously aligned single-walled carbon nanotubes.* Nature nanotechnology, 2016. **11**(7): p. 633.
29. Zhu, Y.F., et al., *Alignment of multiwalled carbon nanotubes in bulk epoxy composites via electric field.* Journal of Applied Physics, 2009. **105**(5): p. 054319.
30. Zamora-Ledezma, C., et al., *Conductivity anisotropy of assembled and oriented carbon nanotubes.* Physical Review E, 2011. **84**(6): p. 062701.
31. Thostenson, E.T. and T.-W. Chou, *Aligned multi-walled carbon nanotube-reinforced composites: processing and mechanical characterization.* Journal of Physics D: Applied Physics, 2002. **35**(16): p. L77-L80.
32. Russell, J.M., et al., *Alignment of nematic liquid crystals using carbon nanotube films.* Thin Solid Films, 2006. **509**(1): p. 53-57.
33. Fu, W., et al., *Super-aligned carbon nanotube films as aligning layers and transparent electrodes for liquid crystal displays.* Carbon, 2010. **48**(7): p. 1876-1879.
34. Lee, W.K., et al., *Super-Fast Switching of Twisted Nematic Liquid Crystals on 2D Single Wall Carbon Nanotube Networks.* Advanced Functional Materials, 2011. **21**(20): p. 3843-3850.
35. Lee, H., et al., *Orientational and electro-optical properties of liquid crystal aligned with a directly spinnable carbon nanotube web.* Liquid Crystals, 2015. **42**(3): p. 322-327.
36. Truong, T.K., et al., *Dynamic operation of liquid crystal cell with inherently nanogroove-featured aligned carbon nanotube sheets.* Current Applied Physics, 2019. **19**(2): p. 162-167.
37. Shoji, S., et al., *Optical polarizer made of uniaxially aligned short single-wall carbon nanotubes embedded in a polymer film.* Physical Review B, 2008. **77**(15): p. 153407.
38. Ren, L., et al., *Carbon nanotube terahertz polarizer.* Nano Letters, 2009. **9**(7): p. 2610-2613.
39. Kyoung, J., et al., *A reel-wound carbon nanotube polarizer for terahertz frequencies.* Nano Letters, 2011. **11**(10): p. 4227-4231.
40. Ren, L., et al., *Broadband terahertz polarizers with ideal performance based on aligned carbon nanotube stacks.* Nano Letters, 2012. **12**(2): p. 787-790.
41. He, P. and L. Dai, *Aligned carbon nanotube–DNA electrochemical sensors.* Chemical Communications, 2004(3): p. 348-349.
42. Shimoda, H., et al., *Self-Assembly of Carbon Nanotubes.* Advanced Materials, 2002. **14**(12): p. 899-901.

43. Kim, Y., N. Minami, and S. Kazaoui, *Highly polarized absorption and photoluminescence of stretch-aligned single-wall carbon nanotubes dispersed in gelatin films.* Applied Physics Letters, 2005. **86**(7): p. 073103.
44. Pan, S., et al., *Novel Wearable Energy Devices Based on Aligned Carbon Nanotube Fiber Textiles.* Advanced Energy Materials, 2015. **5**(4): p. 1401438.
45. Lv, T., et al., *Wearable fiber-shaped energy conversion and storage devices based on aligned carbon nanotubes.* Nano Today, 2016. **11**(5): p. 644-660.
46. Yang, Z., et al., *An integrated device for both photoelectric conversion and energy storage based on free-standing and aligned carbon nanotube film.* Journal of Materials Chemistry A, 2013. **1**(3): p. 954-958.
47. Jang, H.S., S.K. Jeon, and S.H. Nahm, *The manufacture of a transparent film heater by spinning multi-walled carbon nanotubes.* Carbon, 2011. **49**(1): p. 111-116.
48. Jung, D., et al., *Transparent film heaters using multi-walled carbon nanotube sheets.* Sensors and Actuators A: Physical, 2013. **199**: p. 176-180.
49. Baughman, R.H., et al., *Carbon Nanotube Actuators.* Science, 1999. **284**(5418): p. 1340-1344.
50. Koziol, K., et al., *High-performance carbon nanotube fiber.* Science, 2007. **318**(5858): p. 1892-1895.
51. Hata, K., et al., *Water-assisted highly efficient synthesis of impurity-free single-walled carbon nanotubes.* Science, 2004. **306**(5700): p. 1362-1364.
52. Futaba, D.N., et al., *Shape-engineerable and highly densely packed single-walled carbon nanotubes and their application as super-capacitor electrodes.* Nature Materials, 2006. **5**(12): p. 987.
53. Wang, X., et al., *Fabrication of ultralong and electrically uniform single-walled carbon nanotubes on clean substrates.* Nano Letters, 2009. **9**(9): p. 3137-3141.
54. Hayamizu, Y., et al., *Integrated three-dimensional microelectromechanical devices from processable carbon nanotube wafers.* Nature Nanotechnology, 2008. **3**(5): p. 289.
55. Poulin, P., B. Vigolo, and P. Launois, *Films and fibers of oriented single wall nanotubes.* Carbon, 2002. **40**(10): p. 1741-1749.
56. Shaver, J., et al., *Magnetic brightening of carbon nanotube photoluminescence through symmetry breaking.* Nano Letters, 2007. **7**(7): p. 1851-1855.
57. Zamora-Ledezma, C., C. Blanc, and E. Anglaret, *Orientational order of single-wall carbon nanotubes in stretch-aligned photoluminescent composite films.* Physical Review B, 2009. **80**(11): p. 113407.
58. Bacsa, W., et al., *Aligned carbon nanotube films: production and optical and electronic properties.* Science, 1995. **268**(5212): p. 845-847.
59. Cui, J., C.P. Daghlian, and U.J. Gibson, *Gold nanoparticle mediated formation of aligned nanotube composite films.* The Journal of Physical Chemistry B, 2005. **109**(23): p. 11456-11460.
60. Li, X., et al., *Langmuir− Blodgett assembly of densely aligned single-walled carbon nanotubes from bulk materials.* Journal of the American Chemical Society, 2007. **129**(16): p. 4890-4891.
61. Cao, Q., et al., *Arrays of single-walled carbon nanotubes with full surface coverage for high-performance electronics.* Nature Nanotechnology, 2013. **8**(3): p. 180.
62. Lynch, M.D. and D.L. Patrick, *Organizing Carbon Nanotubes with Liquid Crystals.* Nano Letters, 2002. **2**(11): p. 1197-1201.

63. Lagerwall, J.P. and G. Scalia, *Carbon nanotubes in liquid crystals.* Journal of Materials Chemistry, 2008. **18**(25): p. 2890-2898.
64. Zamora-Ledezma, C., et al., *Anisotropic thin films of single-wall carbon nanotubes from aligned lyotropic nematic suspensions.* Nano Letters, 2008. **8**(12): p. 4103-4107.
65. Puech, N., et al., *Highly ordered carbon nanotube nematic liquid crystals.* The Journal of Physical Chemistry C, 2011. **115**(8): p. 3272-3278.
66. Hone, J., et al., *Electrical and thermal transport properties of magnetically aligned single wall carbon nanotube films.* Applied Physics Letters, 2000. **77**(5): p. 666-668.
67. Walters, D., et al., *In-plane-aligned membranes of carbon nanotubes.* Chemical Physics Letters, 2001. **338**(1): p. 14-20.
68. Fischer, J.E., et al., *Magnetically aligned single wall carbon nanotube films: Preferred orientation and anisotropic transport properties.* Journal of Applied Physics, 2003. **93**(4): p. 2157-2163.
69. Zaric, S., et al., *Estimation of magnetic susceptibility anisotropy of carbon nanotubes using magnetophotoluminescence.* Nano Letters, 2004. **4**(11): p. 2219-2221.
70. Hopkins, A.R., N.A. Kruk, and R.A. Lipeles, *Macroscopic alignment of single-walled carbon nanotubes (SWNTs).* Surface and Coatings Technology, 2007. **202**(4-7): p. 1282-1286.
71. Beyer, S.T. and K. Walus, *Controlled orientation and alignment in films of single-walled carbon nanotubes using inkjet printing.* Langmuir, 2012. **28**(23): p. 8753-8759.
72. Russell, J.M., et al., *Alignment of nematic liquid crystals using carbon nanotube films.* Thin Solid Films, 2006. **509**(1-2): p. 53-57.
73. Shimoda, H., et al., *Self- assembly of carbon nanotubes.* Advanced Materials, 2002. **14**(12): p. 899-901.
74. Reinitzer, F., *Beiträge zur kenntniss des cholesterins.* Monatshefte für Chemie und verwandte Teile anderer Wissenschaften, 1888. **9**(1): p. 421-441.
75. Kawamoto, H., *The history of liquid-crystal displays.* Proceedings of the IEEE, 2002. **90**(4): p. 460-500.
76. Qiao, X., et al., *Boundary layer viscosity of CNT-doped liquid crystals: effects of phase behavior.* Rheologica Acta, 2013. **52**(10-12): p. 939-947.
77. He, G.S., et al., *Dynamic properties and optical phase conjugation of two-photon pumped ultrashort blue stimulated emission in a chromophore solution.* Physical Review A, 2008. **77**(1).
78. Creagh, L.T. and A.R. Kmetz, *Mechanism of Surface Alignment in Nematic Liquid Crystals.* Molecular Crystals and Liquid Crystals, 1973. **24**(1-2): p. 59-68.
79. Blinov, L.M. and V.G. Chigrinov, *Electrooptic effects in liquid crystal materials*. 2012: Springer Science & Business Media.
80. Nemoto, F., et al., *Anchoring and alignment in a liquid crystal cell: self-alignment of homogeneous nematic.* Soft Matter, 2012. **8**(45): p. 11526-11530.
81. Ishihara, S., et al., *The effect of rubbed polymer films on the liquid crystal alignment.* Liquid Crystals, 1989. **4**(6): p. 669-675.
82. Hoogboom, J., et al., *LCD alignment layers. Controlling nematic domain properties.* Journal of Materials Chemistry, 2006. **16**(14): p. 1305-1314.
83. Mauguin, C., Bull. Soc. Fr. Mineral., 1911. **34**: p. 71-76.
84. Hasegawa, M., *Rubbing Technologies*, in *Alignment Technology and Applications of Liquid Crystal Devices*. 2005, CRC Press. p. 7-54.

85. Berreman, D.W., *Solid Surface Shape and the Alignment of an Adjacent Nematic Liquid Crystal.* Physical Review Letters, 1972. **28**(26): p. 1683-1686.
86. Zhang, L., et al., *Superaligned Carbon Nanotube Grid for High Resolution Transmission Electron Microscopy of Nanomaterials.* Nano Letters, 2008. **8**(8): p. 2564-2569.
87. Shannon, P.J., W.M. Gibbons, and S.T. Sun, *Patterned optical properties in photopolymerized surface-aligned liquid-crystal films.* Nature, 1994. **368**(6471): p. 532-533.
88. Neill, M.O. and S.M. Kelly, *Photoinduced surface alignment for liquid crystal displays.* Journal of Physics D: Applied Physics, 2000. **33**(10): p. R67.
89. Seki, T., *New strategies and implications for the photoalignment of liquid crystalline polymers.* Polym J, 2014. **46**(11): p. 751-768.
90. Hoogboom, J., et al., *Noncontact Liquid-Crystal Alignment by Supramolecular Amplification of Nanogrooves.* Angewandte Chemie International Edition, 2003. **42**(16): p. 1812-1815.
91. Yaroshchuk, O.V., et al. *Liquid crystal alignment on the polymer substrates irradiated by plasma beam*. Eighth International Conference on Nonlinear Optics of Liquid and Photorefractive Crystals, International Society for Optics and Photonics, 2001. Vol. 4418, p. 441808,
92. Yaroshchuk, O.V., et al., *Plasma beam alignment for the large-area substrates: Equipment and process.* Journal of the Society for Information Display, 2005. **13**(4): p. 289-294.
93. Chaudhari, P., et al., *Atomic-beam alignment of inorganic materials for liquid-crystal displays.* Nature, 2001. **411**(6833): p. 56-59.
94. Doyle, J.P., et al., *Ion beam alignment for liquid crystal display fabrication.* Nuclear Instruments and Methods in Physics Research Section B: Beam Interactions with Materials and Atoms, 2003. **206**: p. 467-471.
95. Lee, Y.G., et al., *Homogeneous liquid crystal alignment characteristics on solution-derived HfYGaO films treated with IB irradiation.* Optics Express, 2015. **23**(13): p. 17290-17300.
96. Kang, Y.G., et al., *Superior optical properties of homogeneous liquid crystal alignment on a tin (IV) oxide surface sequentially modulated via ion beam irradiation.* Optics Express, 2010. **18**(21): p. 21594-21602.
97. Jeng, S.C., et al., *Nanoparticles-induced vertical alignment in liquid crystal cell.* Applied Physics Letters, 2007. **91**(6): p. 061112.
98. Hwang, S.J., S.-C. Jeng, and I.-M. Hsieh, *Nanoparticle-doped polyimide for controlling the pretilt angle of liquid crystals devices.* Optics Express, 2010. **18**(16): p. 16507-16512.
99. Lee, H., et al., *Improvement of the relaxation time and the order parameter of nematic liquid crystal using a hybrid alignment mixture of carbon nanotube and polyimide.* Applied Physics Letters, 2014. **104**(19): p. 191601.
100. Dierking, I., et al., *Aligning and Reorienting Carbon Nanotubes with Nematic Liquid Crystals.* Advanced Materials, 2004. **16**(11): p. 865-869.
101. Lagerwall, J., et al., *Nanotube Alignment Using Lyotropic Liquid Crystals.* Advanced Materials, 2007. **19**(3): p. 359-364.
102. Lagerwall, J.P.F. and G. Scalia, *Carbon nanotubes in liquid crystals.* Journal of Materials Chemistry, 2008. **18**(25): p. 2890-2898.
103. Jiang, K., et al., *Superaligned carbon nanotube arrays, films, and yarns: a road to applications.* Advanced Materials, 2011. **23**(9): p. 1154-1161.

104. DeCoste, D.J., S.S. Zumdahl, and S.A. Zumdahl, *Chemistry (AP Edition)*. 2017, Cengage Learning.
105. Wu, S.T., *Design of a liquid crystal based tunable electrooptic filter.* Applied Optics, 1989. **28**(1): p. 48-52.
106. Rinzler, A., et al., *Large-scale purification of single-wall carbon nanotubes: process, product, and characterization.* Applied Physics A: Materials Science & Processing, 1998. **67**(1): p. 29-37.
107. Endo, M., et al., *Nanotechnology:'Buckypaper'from coaxial nanotubes.* Nature, 2005. **433**(7025): p. 476.
108. Wu, Z., et al., *Transparent, conductive carbon nanotube films.* Science, 2004. **305**(5688): p. 1273-1276.
109. Hu, L., D. Hecht, and G. Grüner, *Percolation in transparent and conducting carbon nanotube networks.* Nano Letters, 2004. **4**(12): p. 2513-2517.
110. De Heer, W.A., A. Chatelain, and D. Ugarte, *A carbon nanotube field-emission electron source.* Science, 1995. **270**(5239): p. 1179-1180.
111. Zhang, X., W.J. Goux, and S.K. Manohar, *Synthesis of Polyaniline Nanofibers by "Nanofiber Seeding".* Journal of the American Chemical Society, 2004. **126**(14): p. 4502-4503.
112. Kim, Y., et al., *Langmuir–Blodgett films of single-wall carbon nanotubes: layer-by-layer deposition and in-plane orientation of tubes.* Japanese Journal of Applied Physics, 2003. **42**(12R): p. 7629.
113. Rao, S.G., et al., *Large-scale assembly of carbon nanotubes.* Nature, 2003. **425**: p. 36.
114. Li, Y.L., I.A. Kinloch, and A.H. Windle, *Direct Spinning of Carbon Nanotube Fibers from Chemical Vapor Deposition Synthesis.* Science, 2004. **304**(5668): p. 276-278.
115. Sun, G., Y. Zhang, and L. Zheng, *Fabrication of microscale carbon nanotube fibers.* Journal of Nanomaterials, 2012. **2012**: p. 2.
116. Zhang, M., et al., *Strong, transparent, multifunctional, carbon nanotube sheets.* Science, 2005. **309**(5738): p. 1215-1219.
117. Jiang, K., Q. Li, and S. Fan, *Nanotechnology: Spinning continuous carbon nanotube yarns.* Nature, 2002. **419**(6909): p. 801.
118. Zhang, M., K.R. Atkinson, and R.H. Baughman, *Multifunctional carbon nanotube yarns by downsizing an ancient technology.* Science, 2004. **306**(5700): p. 1358-1361.
119. Atkinson, K.R., et al., *Multifunctional carbon nanotube yarns and transparent sheets: fabrication, properties, and applications.* Physica B: Condensed Matter, 2007. **394**(2): p. 339-343.
120. Lepro, X., M.D. Lima, and R.H. Baughman, *Spinnable carbon nanotube forests grown on thin, flexible metallic substrates.* Carbon, 2010. **48**(12): p. 3621-3627.
121. Ghemes, A., et al., *Fabrication and mechanical properties of carbon nanotube yarns spun from ultra-long multi-walled carbon nanotube arrays.* Carbon, 2012. **50**(12): p. 4579-4587.
122. Huynh, C.P. and S.C. Hawkins, *Understanding the synthesis of directly spinnable carbon nanotube forests.* Carbon, 2010. **48**(4): p. 1105-1115.
123. Kuznetsov, A.A., et al., *Structural model for dry-drawing of sheets and yarns from carbon nanotube forests.* Acs Nano, 2011. **5**(2): p. 985-993.
124. Gray, G.W., K.J. Harrison, and J.A. Nash, *New family of nematic liquid crystals for displays.* Electronics Letters, 1973. **9**(6): p. 130-131.

125. Klein, S., et al., *The influence of suspended nanoparticles on the Frederiks threshold of the nematic host.* Phil. Trans. R. Soc. A, 2013. **371**(1988): p. 20120253.
126. White, D.L. and G.N. Taylor, *New absorptive mode reflective liquid- crystal display device.* Journal of Applied Physics, 1974. **45**(11): p. 4718-4723.
127. Pellatt, M.G., I.H.C. Roe, and J. Constant, *Photostable Anthraquinone Pleochroic Dyes.* Molecular Crystals and Liquid Crystals, 1980. **59**(3-4): p. 299-316.